Winter 1981

Geomorphology and Dynamics of a Sand Wave in Lower Chesapeake Bay, Virginia

Gerardo Miguel Eduardo Perillo
Old Dominion University

GEOMORPHOLOGY AND DYNAMICS OF A SAND WAVE

IN LOWER CHESAPEAKE BAY, VIRGINIA

by

Gerardo Miguel Eduardo Perillo

Bachiller, 1967
Colegio Nacional Julio A. Roca, Argentina
Licenciado en Ciencias Geologicas, 1975
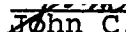Universidad de Buenos Aires, Argentina

A Dissertation Submitted to the Faculty of
Old Dominion University in Partial Fulfillment of
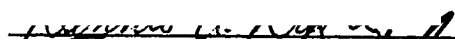the Requirements for the Degree of
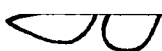
DOCTOR OF PHILOSOPHY

OCEANOGRAPHY

OLD DOMINION UNIVERSITY
December, 1981

Approved by:

John C. Ludwick (Director)

ABSTRACT

GEOMORPHOLOGY AND DYNAMICS OF A SAND WAVE IN LOWER CHESAPEAKE BAY, VIRGINIA

Gerardo Miguel Eduardo Perillo
Old Dominion University, 1981
Director: Dr. John C. Ludwick

A single, more or less isolated, sand wave in a sand wave field recently discovered in the lower Chesapeake Bay, Virginia, was studied intensively for morphology, sedimentology and in terms of dynamic processes. The morphologic investigation consisted of bathymetric surveys of the sand wave field and the specific sand wave. Twenty-five grab samples and four box cores were obtained from different segments of the feature studied. Textural parameters of the samples were determined, and a multivariate technique was utilized to identify subenvironments on the feature. The box cores provided information on the internal structure of the sand wave.

Observations of near-surface currents, and turbulent shear stresses at a level 5 cm above the bottom were made at five stations distributed along the profile of the sand wave. Simultaneously, vertical profiles of density were measured. Time series analysis of the shear stress data at 5 cm above the bed revealed three types of constituents:

(a) long period trends, (b) wave-associated events, and (c) turbulence. The turbulent part of the record was found to be highly reduced in comparison with the other two components. Spectral analysis revealed that the energy of the horizontal component of the flow was smaller than the energy for the vertical component of the flow. Suspended sediments and stable density stratification are known to reduce turbulence, and doubtless have great effect in the present instance; however, the most affected was found to be u and not w as would have been expected.

A decrease in main flow velocity due to the three-dimensional shape of the feature is believed to result in a strong reduction in the horizontal component of the flow, as well as in the shear stress.

In the case of a more-or-less isolated feature, the flow can follow, or partly follow, a path of avoidance around the feature. The integrated results of the study suggest that the sand wave is a "solitary" bedform, originally formed by ebb currents, and presently is in static equilibrium with the circulation pattern.

I do not know what I may appear to the world,

but to myself I seem to have been only like a boy

playing on the sea-shore, and diverting myself

in now and then finding a smoother

pebble or a prettier shell than ordinary,

whilst the great ocean of truth lay all

undiscovered before me.

                    Issac Newton

If I have seen further it is by standing

on the shoulders of giants.

                    Isaac Newton

ACKNOWLEDGEMENTS

During my three years at Old Dominion University, I have received both assistance and guidance, but most importantly the encouragement from professors and friends to carry on through the course of this study.

First, I am deeply grateful to my dissertation director and advisor, Dr. John C. Ludwick. In spite of his busy schedule, he provided me with his advice through lengthy discussions. Above all, Dr. Ludwick provided an important quota of understanding and skillfully oriented me through this study; in sum, he taught me to be a better scientist.

I am also indebted to Dr. Chester E. Grosch. In addition to his continuous support, he was always open to any of the wildest questions on turbulence, spectral analysis and infinity of other subjects that occurred to me. In the most critical moments of the present study, he was there giving ideas and encouragement.

Special thanks go to Dr. Dennis A. Darby, his critiques of the manuscript were helpful. Dr. George F. Oertel assisted by letting me use the box corer

and the Geological Oceanography laboratory for my sediment analysis.

The Consejo Nacional de Investigaciones Cientificas y Tecnicas of the Republica Argentina provided me with financial support in the form of a fellowship. In particular, I would like to thank Mr. Bejamin Fernandez Vines, Fellowship Director, for his unselfish help during the past three years.

I want to express my gratitude to Mr. Thurman E. Gardner, supervisor of the School of Sciences shop, and Mr. Charles Passarell who worked uncountable hours on the construction of the tetrapod. Every time a new problem appeared, they stopped everything they were doing to solve the problem, always with great imagination, skill and sense of humor. I cannot forget Bobby Powell for his help in repairing the data logger.

I would like to extend my appreciation to Dr. Donald Johnson for his helpful commentaries. He also provided the two Geodyne compasses and two small electrical motors for the tetrapod.

During the field work and the initial stages of construction of the tetrapod, John Keating was always present with good humor and desire to work. His help cannot be acknowledged enough. The crew of the R/V LINWOOD HOLTON, Robert Bray, Donald Padget and

Nelson Griffin were attentive and helpful. They were understanding of my lack of English words for the proper navigational terms that always ended in drawing or hand signals.

Thanks must go to Mr. Timothy C. Hendrickson, of the O.D.U. Computer Center, who solved any problem I had with my programs. He always answered with a smile the most extraordinary requests such as punching more than 30,000 cards for my bathymetric charts or desperate increases of memory and core beyond the limits normally assigned to graduate students. My thanks are also extended to the computer operators who were most understanding even when I was occupying both plotters for more than five hours every night.

Mr. Tom Orlowsky, Head of the Tides Branch of the National Oceanographic and Atmospheric Administration, provided the information about tides. Many thanks go to him. Special thanks must go to Dr. Ronald E. Johnson, former Graduate Program Director, and his wife Roberta K. Johnson for their unselfish and continuous help during these three years. I also want to extent my appreciation to Nora Ludwick.

My thanks go to Dr. Carvel H. Blair and Dr. George H. Hecker for their assistance and support, particularly in the administrative part of the last three years.

I greatly appreciate the help of all the graduate students of the Department of Oceanography. My special thanks goes to Mike Jugan, Mike Matyelevich, Mark Byrnes, Jim Todd, Kathy Gingerich, Laurie Kalenak and John Koster, who effectively assisted me during the field work. David Webber and Richard Peralta dived during difficult conditions to check the behavior of the tetrapod during the first field operations.

I want to thank especially:

My Korean friend Im Sang Oh (now Ph.D.) who was constant company during the long nights at work. I engaged him in lengthy discussions on the board, and he assisted me in my fights with the computer.

To Beth Hester, who edited the present manuscript, and offered her warm friendship.

To Dick Phillips and his wife, Kathy, for their support. Dick was always ready to help me during my first steps with the computer and during the calibration of the current meter. His advice was an important contribution.

To Andre Rivamonte, who spent several days of his summer vacations setting up his own microprocessor as a back-up for the data logger. At the same time, he was helping us to repair the data logger.

To Greg Kopanski, David Driver and David Timpy for their willingness to offer assistance and friendship.

To Mimi Lacouture, and Joung Won Kim and his wife, Moon, for helping with the graphs for this research.

Mi profundo agradecimiento a mis padres por haber aceptado y sufrido en silencio estos tres anos lejos del pais. En la misma medida le agradezco a la madre de mi esposa. El soporte moral y espiritual por ellos brindado fue invaluable.

Finally, I wish to dedicate this work to my wife, Cintia. She was present every day with her words of encouragement, with her work during the field trips, but above all with her love and understanding. This work would not have been possible without her unselfish support and company.

My thanks go to Becky Alden, not only for typing my manuscript, but also for doing it under time pressure.

TABLE OF CONTENTS

LIST OF TABLES

LIST OF FIGURES

xii

Chapter 1

INTRODUCTION

1.1 Statement of the Problem

When a fluid moves over a bed of cohesionless sedi-
ments with a velocity greater than the threshold velocity
of the constituent grains, the bed tends to deform by
random erosion and accretion. As a result of these modi-
fications of the bottom layer, bedforms appear which
generate further complexities in flow characteristics.
The most common bedforms are transverse to the flow and
are known generically as "ripples." Several classifica-
tions of these features have been devised, but there is
still no general consensus as to nomenclature (Allen,
1968).

The present study is concerned with large ripples
here designated "sand waves." The physical parameters
of sand waves are: (a) a height greater than 0.6 m; and
(b) a wavelength in excess of 6 m. In marine environments,
subtidal sand waves have been known since the 19th century
(Darwin, 1884; and Cornish, 1901). But as Middleton and
Southard (1978) suggested, the observation and understand-
ing of the bed geometry has been limited by instrumentation

and the unsteadiness of the flow. Only in recent years
with the development of more accurate navigational and
measuring devices, the possibilities of a detailed study
of the morphology and dynamics of subtidal bedforms have
increased. The purpose of this investigation was to study
a particular sand wave in the lower Chesapeake Bay from
morphologic, sedimentologic and dynamic points of view.
To avoid preconceptions, each method has been treated
independently and discussed in different chapters. The
conclusions (Chapter 5) summarize the results of these
methods.

1.2 The Study Area

The sand wave studied is part of a sand wave field
recently discovered in lower Chesapeake Bay, Virginia.
The Bay itself is a coastal plain estuary formed by the
drowning of the Susquehanna River and its tributaries
during the Holocene. The Bay is 314 km long and of
variable width averaging 24 km in the lower reaches. The
entrance between Fishermans Island and Cape Henry is
18 km wide.

A semidiurnal tidal wave is the dominant dynamic
feature of the flow in the estuary. The non-tidal current
calculated by Hilder (1980) was 3.1 cm/s directed 129°
true. The resultant circulation is that of a partially

mixed, moderately stratified estuary. At the mouth the net surface flow is directed toward the ocean, and on the bottom there is a net inflow.

Figure 1 shows the entrance of the Bay and the study area which is limited at the southeast corner by the Chesapeake Bay Bridge Tunnel. The other limits are marked by the parallels 37°01' N and 37°08' N and the meridians 76°04' W and 76°10' W. The total area is approximately 116 km^2.

Chapter 2

BOTTOM MORPHOLOGY

2.1 Objectives

Since man began to navigate, the knowledge of the danger produced by shoals and banks have been an important factor. Therefore, hydrographic surveys were carried out in the vicinities of the coastal navigational routes. Eventually the evolution of navigational and depth recording equipment made possible the study of deeper regions. As a result of these surveys, oceanographers came to realize that the ocean bottom was not flat. As regards sedimentary structures on the bed, descriptions of subtidal sand waves have been common in the literature since the early part of this century.

In the entrance to Chesapeake Bay, sand waves have been described and studied by Ludwick since 1970. A new field was discovered recently in an area outside the common navigational routes. It is the main objective of this chapter to describe the morphologic characteristics and possible evolution of not only this field, but also of a specific sand wave within the field. The results

4

of this analysis have been also utilized to select areas for sediment sampling and flow measurement.

2.2 Methodology

2.2.1 Field Work

The bathymetric study was performed using the R/V LINWOOD HOLTON, operated by the Department of Oceanography, Old Dominion University. The instrumentation on board this 20-m diesel powered vessel included a depth recorder and Loran-C receiver.

The echosounder was composed of a transducer, Raytheon model 7245A, connected to a Survey Depth Recorder model DE-719B of the same Brand. The output was a strip chart. The survey was made on a scale of 0-15.24 m at a chart speed of 5.08 cm/min, unless otherwise specified. The vertical accuracy of the device is thought to be better than 0.30 m. The transducer was calibrated before each day of work using a Check Bar built by J. Keating, marine technologist, Department of Oceanography, Old Dominion University.

The navigational equipment utilized was a Micrologic ML-1000 Loran C-receiver. Loran-C is a radio system based on 3 transmiting stations that send groups of pulses (Group Repeating Invervals, GRI) repeating the same

pattern at specific periods ranging from 40,000 to 99,990 microseconds. The GRI 9960 was the best receiving chain in the study area. The receiver was a small computer that provided approximate latitude and longitude, time difference (TD), range and bearing to a destination, and cross and track. The estimated error in repetitiveness of position location was less than 18.5 m (0.01 nautical mile).

The first task was to define the limits of the sand wave field. For this operation, 15 bathymetric profiles were run along a magnetic North bearing (352° true). Each profile was approximately 11 km in length (6 nautical miles), and separation between them varied from 200 to 1000 m. The general procedure for taking the profiles described here was also employed for the bathymetric study.

With the calculated latitude and longitude of start and end points of the profiles, the first step was to drop a buoy to mark the location of the initial point. Immediately the Loran-C receiver was switched to the TD (time difference) function. In this mode the device displayed X- and Y-TD coordinates with a precision of 0.01 microseconds. The display is updated every 4 seconds, and the function has 21 seconds of recuperation. Latitude, longitude and bearing in degrees true to the end point were entered manually into the receiver.

The profile began as the vessel passed beside the starting buoy at a speed of about 6 knots (1100 RPM) heading due North magnetic. Simultaneously, TD values were taken, and a fix was marked on the strip chart of the depth recorder. After 15 seconds the receiver was turned to the cross and track function, which indicated the deviation of the vessel from the calculated path. Correction for this deviation was imparted to the captain, and the receiver was returned to the TD function. The foregoing procedure was repeated every 2 minutes until the end point of the profile was reached.

Once the sand wave field was delimited from the reconnaissance records, three bathymetric studies were planned. On May 23 and June 13, 1980 the general bathymetry of the field was investigated in two separate field works with profiles ranging from 4.6 to 11 km in length and separated by about 1000 m. The third study was an intensive bathymetric survey made of a particular sand wave on June 12, 1980. Here the profiles were 1500 m in length and were separated by 250 m. Due to the short span of the profiles, fixes were taken at 30 second intervals. Track deviation was not controlled.

2.2.2 Data Reduction

A special chart for each of two scales was constructed for plotting TD values. These charts consisted of two sets

of lines of equal TD drawn on a latitude-longitude grid. The Loran-C grid was adjusted with the recently released Additional Secondary Factors (ASF, U.S. Defense Mapping Agency, J. C. Ludwick, personal communication, 1979).

The water depth corresponding to each fix mark associated with a TD value was read from the bathymetric record. The depths were corrected to mean low water using the observed tide record from the tidal gauge operated by the National Oceanographic and Atmospheric Administration (NOAA) at the first island of the Chesapeake Bay Bridge Tunnel. The gauge was located about 13 km to the south of the geometric center of the study area.

By assuming constant speed of the vessel between fix marks, morphologic features such as the crest of sand waves and prominent ripples were interpolated on the chart, thus providing denser information to elaborate the bathymetric map. The general bathymetric charts were prepared at a contour interval of one meter. A contour interval of 0.5 m was used on the bathymetric chart of the specific sand wave.

2.3 Results

Understanding the characteristics of a single sand wave entails a thorough knowledge of surrounding morphology. In most cases, such a feature is directly related just to

the general bed configuration. This section was divided into three descriptive levels. First, the Tail of the Horseshoe Shoal and its relationship to the lower Bay is introduced. As an intermediate step, the sand wave field is delimited. Finally, a detailed description of the selected sand wave and its immediate neighborhood is presented.

2.3.1 Description of the Horseshoe

The following description of the general bathymetric characteristic of the area over which the sand wave field has developed was based on bathymetric charts prepared by the National Oceanic Survey (NOS) - NOAA (1972) and Goldsmith and Sutton (1977). Several references on the southern part of the area were obtained from bathymetric studies by Ludwick (1979, 1981).

The main morphologic features of the surrounding area are two navigational channels. To the south, Thimble Shoal Channel is the access route to Hampton Roads through the narrows formed between Willoughby Spit and Old Point Comfort. This natural channel has been dredged since 1910, and the estimated filling rate is 242,960 m^3 per year (Ludwick, 1979).

To the north and east, the study area is crossed by the Chesapeake Channel, a wholly natural, wider and

slightly shallower feature than the Thimble Shoal Channel.
This is the route followed by cargo vessels to the north-
ern ports of Chesapeake Bay (Annapolis, Baltimore, etc.).

The sand wave field is distributed over the north-
eastern flank of a large elevated region between the
intersection of the two channels at the Bay mouth and the
coastline of the City of Hampton. This shallow area known
as the Horseshoe (and the Tail of the Horseshoe) has a
minimum depth of three meters and deepens slowly toward
the northeast, that is, toward the Chesapeake Channel.
The inclination is relatively abrupt to the south and
southwest, particularly near the mouth of Hampton Roads.
One inlet-margin shoal (Ludwick, 1979), Thimble Shoal,
marks the southern limit of the shallow area.

Mutually exclusive ebb and flood dominated channels
have been described in the area of the northeast flank of
the Chesapeake Channel (Granat, 1976) and the northern
entrance of the Chesapeake Bay (Ludwick, 1973a). In the
Horseshoe area, ebb dominated channels are far more
developed. One of them, delimited by a 10 m isobath
(NOS-NOAA, 1972), can be traced well inside the study
area (Fig. 1). Flood dominated channels are minor and
not well defined.

2.3.2 General Bathymetry

The bathymetric survey performed on June 13, 1980 is described below. Some references will be made to the data obtained on May 23, 1980 and previous bathymetric profiles made from August 1979 to April 1980 to delimit the sand wave field. The general gradient of the north flank of the Horseshoe, specifically the sector denomi- nated the Tail of the Horseshoe, was toward the northeast. The slope calculated between the shallowest and deepest points on the bathymetric chart (Fig. 2) is $\beta = 0.16°$ (0.28%).

The limits of the sand wave field may be defined by the isobath of 10 m up to a latitude from 27°04'. Northward from this line, 12 m is the limiting isobath. West of meridian 76°10' sand waves were not found, nor were they evident south of the 37°01' parallel. An analysis of the general tendency of the terrain indicated that the flank of the Horseshoe shoal was not a smooth feature. There are elongated mounds or ridges and depressions or channels trending in a south southeast direction.

The first of these ridges was found immediately to the west of the 10 m isobath and formed an angle of about 15° open to the south southeast. Over this ridge the shallowest sand wave crests (up to 6.51 m) were found.

The average depth of the area among sand waves, "flats" (Fig. 5) was on the order of 9 m.

Another ridge was found at the extreme western boundary of the area, parallel of the 76°10' meridian. There, the crests were deeper than the previous ridge (8.31 m), and flats averaged 10 m depth. These two ridges are separated by a channel trending north-south, where bedforms are much smaller. Crests reached 9.95 m in depth, and flats were on the order of 11 m.

All three elongated features incline on a gentle upward gradient to the south and culminate in an almost circular shoal at the southern limit of the area, one of the main features of the Tail of the Horseshoe. There are several areas enclosed by hachure marks (Fig. 2) which indicate depressions, some more than 12 m deep. They are concentrated in the channel sector, and their main axes are more or less parallel to the crest of the sand wave and smaller bedforms.

The crests of the sand waves are disposed transverse the ebb flow. According to the echosounding records (i.e. orientation of the crests was east-west, and they normally presented a linear shape. The crest lengths averaged 800 m, and the maximum length was 2100 m. Separation between crests averaged about 200 m.

Sand wave heights varied in relation to the general features (ridges and channel) with which they were associated. In the area of the ridges, heights averaged 1.7 m, a maximum of 2.1 m. In the channel area, heights were less pronounced and in most cases did not surpass one meter. On the echosounding records (Fig. 5) there was no evidence of smaller bedforms, such as ripples associated with the sand waves. In some situations the sand wave exhibited "catback" features or alternatively, rounded crests, but typical crests were peaked.

Granat (1976) found sand waves only in the southeastern part of the Inner Middle Ground-Nine Foot Shoal. Other sand waves have been described to the north and east toward the mouth of the Chesapeake Bay (Ludwick, 1972; and Wells, 1973). In those studies, in the Chesapeake Channel and on the southwestern flank of Middle Ground, sand waves were not detected. However, ripples (Fig. 3) up to 0.60 m high and less than 10 m in wavelength were observed limited by the 15 m isobath (Fig. 2). In both bathymetric surveys and during the previous bathymetric profiles, the ripples cited above always faced the northwest, up the axis of the Chesapeake Channel.

2.3.3 Sand Wave Bathymetry

Over the small sector within the study area depicted
in Figure 1, an intensive bathymetric study was carried
out on June 12, 1980. Figure 4 is the resulting chart.
The sand wave under investigation is at the center of
the chart and is deliminated by the isobath of 9 m. The
sand wave profile is exhibited in Figure 5. The elongated
crest of the sand wave oriented approximately east-west
was estimated to be 600 m in length, and the minor
axis reached a maximum of 100 m. Maximum relative relief
is 2.1 m at the east end of the bedform, and the calcu-
lated slopes of lee and stoss sides are 4°15' and 1°26',
respectively.

Besides the sand wave, several morphologic features
could be observed in the chart. In the first place the
sand wave was separated from the minor bedforms, to the
north and south, by a relatively flat area circumscribed
by the 10 m isobath on the east and the 9 m isobath on
the other three boundaries. The topography of the areas
described previously as flats is gentle and cam clearly
be distinguished from the sand waves. Two of these
features may be observed on both sides of the main sand
wave in Figure 5.

To the east and west, deeper areas approximately
normal to the direction of the crest of the sand wave

are observed. The sector to the west was part of the
channel described in the previous section. The eastern
deeper area was not so well developed in a longitudinal
form and was not distinguishable in the general bathymetry.

The two sand waves on either side of the main
feature are smaller in height and less well-defined.
Their crests are more sinuous. The three bedforms are
distributed relative to one another over the area in a
peculiar form. They are not situated along the same line,
but rather they are displayed, particularly the northern-
most one. Since the northern sand wave, defined by the
isobath of 9 m, is smaller than the main sand wave, the
western flank of the main sand wave may be more exposed
to ebb flows.

2.4 Discussion and Conclusions

Analysis of the morphologic characteristics depicted
from bathymetric charts revealed that at least the northern
flank of the Horseshoe area is mainly influenced by ebb
currents. This was further estimated by the orientation
of the sand waves that were found since their lee faces
were directed toward the South. Ludwick (1981) has
observed a slow laterial migration to the south of the
Tail of the Horseshoe which might contribute significantly
to the filling of the Thimble Shoal Channel.

The sand wave field has developed on the flank of a
shoal, a relationship which is not an uncommon finding.
Sand waves positioned in this way have been found
associated with linear shoals in the North Sea (Houbolt,
1968) and on several continental shelves around the
western Atlantic (Swift et al., 1978; and Parker et al.,
1978). The sand waves in those areas were considered as
part of a genetic process for those shoals through the
mechanism of hellicoidal flow cells.

On the other hand, several elements in the present
study have suggested that the sand wave field might not
be active presently. The first element is the position
of the main sand wave. From August 1979 to August 1981
at least 18 times the sand wave was located using the
same coordinate and TD values. The only exception was
during the collection of two sediment samples (see
Chapter 3). About 23 weeks separated the bathymetric and
sampling operations. The difference in position was
registered for the western side of the sand wave, which
is exposed to the ebb currents being unshielded by
another bedform nearby.

One of the results of bedload transport is ripples;
they are associated with flows that exceed the critical
shear stress of the bed material. During the field work
in the present study different tidal conditions (i.e.
maximum ebb and flood, etc.) were encountered, within the

sensitivity of the depth recorder (less than 0.30 m):
however, no ripples were observed. The only exception
were the ripples in the Chesapeake Channel which are not
associated with sand waves. Net flood dominance at the
bottom of the channel is suggested, since the steep face
of the ripples was directed northward in all the bathy-
metric profiles of the channel area (Fig. 3).

The last qualitative consideration is the distribu-
tion of channel and flat areas within the field of sand
waves. The concept of "solitary" sand waves has been
introduced here to describe the state of a sand wave in
which further evolution of the sedimentary structure is
mostly independent of adjacent bedforms. This concept
might be applied to several bedforms in the area which
are isolated from the other sand waves by flats. In
particular, the subject sand wave may be considered in
this category.

Excepting the case of the two sediment samples
explained previously, the fact that the sand wave main-
tained the same position throughout the study period may
indicate that migration was not occurring. Another possi-
bility is that the rate of migration was so small as to
be less than the error in the navigational instrument
(18.5 m).

As seen from the bathymetric study, the sand wave field may be in static equilibrium with the ambient flow. The original formation of the field of sand waves may be due to ebb dominated currents, but at this moment most of the flow may be diverted towards the master channels of the area, thereby reducing the current strength over the sand wave. In most studies, sand waves are treated as two dimensional features, that is, the flow is normal to the bedform as is confined to pass over the crest. Since in the present case the crestlength cannot be assumed "infinite," the sand wave must be considered as three dimensional. This would introduce further complications in the analysis of the flow characteristics over the sand wave, since the cross-stream component of the flow has to be taken into account.

During storms, where waves and currents transfer maximum power to the bed, the sand wave field may suffer most of its modifications. Comparison of extremely detailed bathymetric charts from surveys made before and after certain events may indicate the magnitude of the changes produced on the bed morphology, and permit a firmer conclusion as to whether effective activity on the bed configuration is episodic or not. The selection of the events such as tidal currents at the times of equinoctial tides, wind generated currents, high run-off or

waves may define which dynamic elements are the most effective driving force on the area.

Chapter 3

SEDIMENTOLOGY

3.1 Objectives

Sediment texture is a record of the conditions that exist in a sedimentary basin and is the result of the time averaged action of the dynamic components acting on the basin. If the threshold of the material is exceeded by the transporting agent, the grains will be displaced from one point to another. If the agent is strong enough, it may carry the grains outside the area of study. In a unidirectional stream, if the discharge is constant, steady state conditions may hold. Then, sampling at different times may produce similar results. However, when tides and waves are involved, conditions are more complex. Sediment is transported back and forth and interchanged with the surrounding areas. Therefore, when a sand wave in a subtidal environment is sampled, the researcher must bear in mind that the texture will reflect those different conditions and that his work is to separate them.

In the preceding pages, the morphologic description of the northeast side of the Horseshoe area and specifically the sand wave located there have been described.

20

In the present chapter, the textural characteristics of that sand wave will be presented. Samples were obtained with a Shipek sampler and a Box Corer. Textural parameters for these data were analyzed, and a multivariate technique, factor analysis, was utilized to define subenvironments on the sand wave. Box cores provided information on the internal structure of the sand wave.

3.2 Previous Studies

Comparatively little is known about the distribution of sediments in underwater bedforms. Even less is known about the effect of multidirectional currents and waves on those sediments and the internal structures generated by them. Most of the work to date has considered unidirectional flows, mainly in laboratory experiments. The papers of Simons et al. (1965) and Jopling (1965) are examples from a very large list. No studies have been done in flumes that represent an environment dominated by tides; therefore, our knowledge has been based on field data.

The pioneer study of Houbolt (1968) resulted in a detailed description of the sand banks of the North Sea and the first indications of the sand distribution along the profile of a submerged sand wave. Terwindt (1971) found, as did Houbolt, that there was a graded difference

in grain size from trough to crest. On shallower sand waves coarser grains were observed at the crest while sand waves formed in deeper waters not affected by wave action, displayed a reverse distribution.

In the entrance to the Chesapeake Bay, Wells (1973) and Ludwick and Wells (1974) made a detailed study of the sediment characteristics of sand waves along five profiles sampled by divers. They found that migrating sand waves consisted of coarser sediments on the crest. The nearly symmetric (i.e. non-migrating) bedforms exhibited coarser grains in the troughs. Analysis of variance of the data showed that small scale bedforms were not sufficient to obscure the distribution of the statistical parameters in the main structure. Monahan (1979) used an anchored vessel to sample a sand wave in the St. Lawrence estuary, but he was not able to identify a trend in the grain size.

Several authors have addressed the problem of the internal structure of subtidal bedforms. Allen (1980) provided a clear review of some of the prevalent models and compared them with a theoretical scheme that he developed. The most reliable data were obtained by Houbolt (1968) off the Dutch coast; he described foreset bedding that might have been disturbed by sea urchins. Based on the description by Houbolt (1968), McCave (1971) modelled an asymmetric sand wave with two levels; the lower portion was dominated by structures formed by ripples

and burrowing organisms without definitive orientation of the cross bedding. The upper level was formed by foreset bedding and megaripples on the stoss side.

Hine (1977) proposed a model for internal structure for sand waves in an oolite shoal in the Bahamas. The model was based on a previous model of bedform stratification by Harms et al. (1975). Hine described stages of initiation, growth and final equilibrium with specific current, wave and depth conditions. The resulting structure bears a typical lamination known as herringbone cross-bedding.

Shallow subtidal sand waves have been illustrated by Oertel (1973) and Hubbard et al. (1979). These authors observed sand waves in the main channel of tidal inlets with complex planartangential trough cross strata produced by the migration of smaller bedforms across the stoss of the sand wave. The observations attained by Hubbard et al. (1979) clearly showed that complex internal structures are not exclusive of intertidal structures.

Sediments from the entrance of the Chesapeake Bay were studied by Meisburger (1972). His profile along the bridge-tunnel route showed that fine, well-sorted gray sand is the dominant surficial sediment between Fishermans Island and the Thimble Shoals Channel and overlies a gray sandy silt unit. He suggested that the origin of this

sand layer, approximately 36 m thick near Fishermans Island, is from sources outside the Bay area. However, Shideler (1975) proposed a double origin. He suggested that the sand might be a well-winnowed lag sediment derived from erosion of a Pleistocene substrate and an influx of adjacent shelf and littoral sands. Analysis of variance and factor analysis of heavy mineral data obtained from the same samples used by Shideler seemed to support his thesis (Firek et al., 1977).

3.3 Methodology

3.3.1 Field Work

From the bathymetric study described in Chapter 2 several stations were selected as representative of the main morphologic features of the sand wave shown in Figure 6. Samples were taken from the R/V LINWOOD HOLTON with a Shipek sampler and a Box Corer. The Shipek sampler takes a sample of the upper 10 cm of the bed sediments over an area of 412 cm^2. The corer extracts a core of rectangular section (17 by 9 cm) of undisturbed material up to 45 cm long. The following procedure was adopted for the sampling operation. With the geographic coordinates, the captain was able to position the vessel in the general area. He then maneuvered according with the TD values until the desired location was obtained.

Simultaneously, continuous echosounding records were monitored.

From determination of currents, wind direction and strength, one of two methods of sampling was selected: (a) anchored method or (b) moving method.

The anchored method (a) required that currents and/or wind direction form a small angle with the meridian passing over the sand wave since the sand wave crest was oriented approximately east-west. The choice of which side of the bedform (stoss or lee) to be utilized for anchoring was decided at that moment with the available information. Once the anchor was set, the chain was payed out until the vessel was above the opposite flank. As anchor chain was slowly taken in, the feature of interest could be selected with reference to the echosounding information. After selection of the site, the ship stopped and stabilized itself, and the samples were obtained. The instant the sampler struck the bottom, TD values were obtained from the Loran-C receiver, and a fix was marked on the strip chart of the depth recorder.

The moving method (b) was used when current and wind conditions were too rough to proceed as above. This method required accurate positioning on the crest of the sand wave where a buoy was dropped. Immediately afterwards, a bathymetric profile was taken due South, and

buoys were dropped at selected locations. A second profile was taken to insure the proper position of the buoys. The sampling procedure was followed by stopping the ship beside each buoy. Other operations were similar to those described for the previous method. Box cores were obtained by the moving method (b).

Once the sample was on board, visual descriptions of color, grain size, general composition, and biogenic material were made. On many occasions the Shipek sample was relatively undisturbed, and the depth of the top of the reduction zone could be obtained. About 600 g of material were stored in a carton for later study in the laboratory. The cans containing the cores were identified, and descriptions of the surface and bottom characteristics were recorded on board.

3.3.2 Laboratory Work

The size analysis of 28 Shipek samples was made by sieving. Descriptions of the procedures can be obtained from Wells (1973) and Granat (1976). The weights obtained from this analysis were processed with the program GSIZE.FOR (Appendix A), which gives moment and inclusive graphic statistical parameters (Folk, 1974). Several percentages and a plot of the cumulative curve in arithmetic scales were also produced by this program.

The box cores were brought to the laboratory and stored in a refrigerator for two days to reduce the biological activity. After this period, the material was extruded from the cans and transferred to X-ray trays. Each core was photographed, measured and described.

To obtain an X-ray of the internal structure of the material, the core was slabbed down to a longitudinal section 2.54 cm thick. During this procedure, descriptions of significant changes in composition, color, or biogenic material were recorded. With the X-rays for reference, a more detailed sampling of the material was performed.

3.4 Results

Twenty-five of the 28 samples obtained in the sand wave area were studied. Three samples were discarded, because problems with the Loran-C receiver prevented accurate positioning of the vessel. Figure 7 shows the location of the 25 sampling sites. The samples were identified by a letter and number. The letter indicated one of the four morphologic features defined in Figure 5 (C = crest; S = stoss; L = lee; and F = flat).

Two samples that were classified as stoss (S4 and S5) appeared to be on the crest or lee side of the sand wave. This might be due to a possible migration of the sand wave

that might have occurred during the 23 weeks that elapsed between the bathymetric study and sampling. Samples L13 and L29 were classified as lee sediments, because they were obtained in that segment of the sand wave, though very close to the toe. As will be seen below, their characteristics suggested that they could be considered as flat samples.

During the sampling it was clear that sediments obtained from different segments of the sand wave were distinct. Crest samples were pale yellow in color, the coarser material and lack of a reduction zone were also distinctive features. Stoss and lee samples were of finer sediment and pale olive in color. The reduction zone was encountered about 1 to 2 cm from the sample surface. Samples from the flat areas had larger percentages of silt material. The sand size sediment was finer, dark colors were observed (olive), and the oxidation zone was almost nonexistent. In these samples some worms and worm-tubes were observed.

The sand sized material of all samples was mainly composed of clear quartz grains, angular to subangular, subspheric to elongated. Very few shells, in most cases broken fragments of bivalve shells, were present in this size, but they formed more than 80% of the gravel size. Less than 10% of the material was rock fragments, mainly metamorphic.

A standard sieve analysis was performed on all samples including the fragments of shell with a 1/4 ϕ separation between sieves (ϕ = - $\log_2$ grain diameter in mm). Figures 8 and 9 show the histogram representation of the samples. The dominant size was medium sand. Except in one case, all contained less than 10% of the silt-clay fraction (herein called mud). Gravel and very fine sand fractions were almost nonexistent.

Figure 10 displays four cumulative curves, each representing a type of sediment. Assuming that Visher's (1969) division of the cumulative curves is a valid approach, the crest samples could be considered as part of the saltation population. The other three types supplied a larger percentage to the suspension zone. In the suspension population a subdivision is indicated which has never been seen before for the lower Chesapeake Bay. There was very little sediment in the samples between 2.75 ϕ and 3.5 ϕ, in the range of very fine sand. This produced the break observed in the curve, which was marked as the boundary between subpopulations B' and B.

3.4.1 Textural Parameters

Many researchers have tried with varying success to identify environments by using textural parameters. Mason and Folk (1958) and Moiola and Weiser (1968) utilized the

inclusive graphic measures (Folk and Ward, 1957), while Friedman (1961) made use of the statistical moment equations. To date no clear attempt has been made to differentiate subenvironments, specifically, the faces of a sand wave. Except sampling along profiles done by Houbolt (1968), Wells (1973), Ludwick and Wells (1974) and Monahan (1979), no systematic study of a subtidal sand wave has been accomplished.

Inclusive graphic parameters were preferred over the moment type, because the verbal classification introduced by Folk (1974) has been well established. Excluding Kurtosis, which was always greater in the moment method, both systems gave similar results. The analysis of the statistical parameters in the present study was based mainly on maps of the distributions of the parameters and on diagrams which show the relationship between two parameters.

Mean. The phi mean ranged between 1.12ϕ and 2.21ϕ, and averaged $1.61\phi \pm 0.24$. In all but two samples, the mean values occurred in the medium sand size ($1-2\phi$). Table I introduces the average mean value for each of the subenvironments into which the sand wave was divided. Crest samples were the coarsest; and flat the finest, separated by about $0.55\phi \pm 0.16$. Stoss and lee samples possessed approximately the same mean which was similar

to the crest value. This seemed to indicate that the material that constitutes the sand wave was the same, but slightly reworked by the currents and waves.

Figure 11 presents the areal distribution of the mean over the sand wave. Coarser sediments were present along the crestal axis, the sediments became finer on both sides and reached the lowest values on the flats. The sediments from the flats were different depending on the side of the sand wave. Typically, the sediments on the north side were coarser. This may indicate a higher energy activity on the stoss side and protection from what seems to be an ebb dominated environment on the lee side.

Standard deviation. The standard deviation of the sand wave samples ranged from 0.41ϕ to 0.68ϕ. Sixty percent of the samples were in the well sorted category, and the other 40% were moderately well sorted. The overall average standard deviation was $0.5\phi \pm 0.06$. The average for each segment is presented in Table I.

The areal distribution of the standard deviation (Fig. 12) shows the two categories separated by the 0.50ϕ isoline. Moderately well sorted samples were concentrated along the west and south sides of the sand wave, mainly associated with lee and flat areas. Again the shielding produced by the crest showed that sediment downstream of

the ebb current was less reworked and might receive finer particles from erosion of the crest and stoss as well as from settling of suspended material.

Skewness. Skewness measures the deviation of the grain size distribution from the ideal log-normal distribution. The sand wave samples represented almost all the range of skewnesses from strongly fine skewed (4%) to coarse skewed (60%). Only six samples, four of them crest samples, were nearly symmetric.

Generally, lee and stoss sediments tended to be coarse skewed, and flat sediments to be fine skewed. The overall average was -0.079 ± 0.17. Figure 13 exhibits the plan view distribution over the sand wave. Coarsely skewed and nearly symmetrical sediments were observed on the central portions; those finely skewed were dominant on the south side. Specifically, one must note the difference between the flat samples from the northwest of the sand wave and those from the south and northeast parts.

Kurtosis. According to Folk (1974), kurtosis measures the ratio between the degree of sorting of the central portion of the curve and the tails. In other words, it provides the "degree of peakedness" of the curve. In case of a log-normal distribution, kurtosis equals one for the

inclusive graphic measures. For the sand wave, all but one sample (KG = 0.97) had kurtosis larger than one, the maximum was 2.07. This indicated that there was little spread, i.e. the central portion of the curves were better sorted than the tails.

All crest and some stoss and lee samples were meso-kurtic. Some flat samples were leptokirtic, but most were very leptokurtic. Again differences between the north and south side were observed (Fig. 14). The very leptokurtic flat samples were taken from the south and northeast portions of the sand wave. The mesokurtic stoss samples were more similar to the crest samples and formed a continuous band which included the sand wave axis.

3.4.2 Correlation of Textural Parameters

The popular method of correlating two textural para-meters has been only partially effective in discriminating among sands taken from several environments such as beaches, coastal and desert dunes, and rivers (Friedman, 1961, 1967; and Moiola and Weiser, 1968). In the present study, this method was intended as a first approximation to distinguish the sand wave subenvironments. Surprisingly, it has given relatively good separation into three fields. In most of the cases, two fields defined by the crest and flat samples were situated at both extremes of the graphics

(Figs. 15, 16 and 17). At the center of the distributions, stoss and lee samples were found forming a cluster.

Mean versus standard deviation (Fig. 15). Mean particle diameter (M_ϕ) versus phi standard deviation (σ_ϕ) was probably the relationship that best separated the three fields described. Basically, the spreading of the samples was due to the mean. Flat samples were concentrated on the fine side of the plot, including samples L13 and L29. Crest samples tended to aggregate on the coarser side. In the center, lee and stoss samples formed a cluster with small dispersion.

Mean versus skewness (Fig. 16). A very similar pattern was observed when mean was related to skewness; however, the crest samples were more mixed with the central cluster. Together they formed the coarse skewed group. Five out of six samples with a mean finer than 1.8ϕ were fine skewed and spread over a larger range. Again the mean is more important in separating the groups.

Mean versus Kurtosis (Fig. 17). This relationship is rarely seen in the literature, probably due to the complexity in the interrelation between both parameters. It also gives the poorest results for identification of environments.

When plotted for the sand wave, the pattern was similar
to the one shown in Figure 16. The finest sediments tended
to be leptokurtic and very leptokurtic, while all the
samples coarser than 1.8ϕ concentrated in the mesokurtic
range.

3.4.3 Factor Analysis

The standard statistical analysis presented in the
previous section was successful in separating the three
subenvironments on the sand wave. Little can be said
about the general characteristics of each of them, other
than the statistical abstract of each sample given by the
inclusive graphic measures and the group averages provided
in Table I.

Sediment composition in a presently active environment
is a response to several parameters: the source of the
original material, the energy of the transporting agent,
and the composition and reactivity of the material. Factor
analysis has been used to determine and characterize end
points in complex conditions (Imbrie and van Andel, 1964;
Klovan, 1966; Allen et al., 1972; and Miesch, 1976). This
method has been used successfully to differentiate sedi-
mentary environments in lagoon-inlet-beach systems (Klovan,
1966), continental shelves (Drapeau, 1973) and suspended
matter distributions (Nelsen, 1981).

The technique is based on the calculation of eigen-values and corresponding eigenvectors from either a correlation or a covariance matrix (Davis, 1973). The idea is to obtain the smallest possible number of linear independent terms which are combinations of the original variables. Thus, the final result may be interpreted as a function of the initial geological parameters.

Only the Q-mode option was used in the present study. The objective of Q-mode analysis is to interpret the relationship among the samples. The data consisted of the weight percentage of the sediment subdivided into 1ϕ intervals (Table II). All material coarser than -1ϕ was defined as gravel and considered as one class. The same scheme was followed for sizes finer than 4ϕ. The programs and subroutines utilized in the present research were adapted from Davis (1973).

Q-mode results. The eigenvalues are the representation of the factors in this multivariate technique. In this case, the first seven eigenvalues, the percent of variance and the cumulative percent of variance are shown in Table III. The first two factors accounted for more than 99.1% of the grain size variance. The meaning of the original factors may be difficult to extract. Therefore, a rotation technique (Kaiser's varimax) was applied so that the projection of each variable onto the factor axes

are either near the extremities or near the origin. By
this mean, the end members of the sediments may be deduced.
Once the factors are rotated, the factor scores give an
idea of which variables are more important in the composi-
tion of the factors. This is observed in Table IV.

Factor I was the most important since it occupied the
largest share in the total grain size variation: 95.07%.
It represented medium sand (1-2ϕ). This was not surpris-
ing since medium sand was by far the dominant size in all
the samples. Fine and coarse sand were the secondary
components in this factor.

Factor II accounted for about 4% of the information
contained in the grain size data table (Table II). This
factor was formed by the ratio between fine sands and muds
to coarse and medium sands.

Table V presents the loading of each factor in each
sample. In a model where the number of factors is equal
to the number of variables, the communalities of normalized
variables equal 1.0. When the number of factors is less
than the number of variables, the closer the communalities
are to 1.0, the better those factors describe the samples.
In the present case all the samples had communalities
larger than 0.94.

As the input data matrix is transposed, the relation-
ship among the vectors which define each sample can be

determined by applying the correlation method introduced by Imbrie and Purdy (1962). They found that the cosine of the angle between two vectors (cos θ) is a measure of the similarity between both samples. The maximum possible value is 1.0 and is obtained from the correlation of the sample with itself or of two samples alike. A zero cos θ value indicates that there is no correlation between the observations.

The similarity matrix determined for the 25 samples obtained over the sand wave showed high correlations between all samples. The lowest was found between F3 and C46 (0.58). Several samples had the maximum possible or very nearly.

The angle determined in the similarity matrix was in seven dimensions. Since factors I and II had more than 99% of the total information, a plot between them should give an overview of the distribution in a seven-dimensional space. Figure 18 is such a plot. The extreme samples were those with the lower correlation as pointed out before. The maximum similarity was observed in samples L1 and S4 which had a cos θ equal to 1.0. Also a high correlation was noticed between S38 and L40 (0.9998). The lowest overall similarities were seen in the crest and flat samples, values ranging from 0.70 to 0.90.

Factor I represented a more energetic area with coarser material within the small range that characterizes the sediments of the sand wave. As expected, the contrast given by factor II represented the lower energy environment.

The plane view distribution of the factors is given in Figure 12. The relationship between factors I and II was considered. Samples with more than 61% of either factor were assumed to be dominated by such a factor. Samples with 41 to 60% of each of the factors were considered to be mixes of both. The crestal area and the upper part of the stoss and lee side were dominated by factor I, thus defining a relatively high energy zone. Sediments dominated by factor II were mainly distributed on the lower lee and flat areas. Only one sample (F3) on the north side was dominated by factor II. Samples from the stoss and the nothern flat segments of the snad wave were mixed of both factors.

3.4.4 Cores

Four box cores from a profile across the sand wave were obtained. The positions of cores 4, 5, 6, and 7 coincided with the positions of samples S31, S12, C19 and L29, respectively (Fig. 7). Even with the maximum weight

load, penetration of the box cores averaged only 19 cm in the typical medium sand. This size fraction was dominant and uniformly distributed throughout every core.

All four cores exhibited two main layers which were defined principally by color. The upper was olive in color and was normally 5 to 7 cm thick. This layer was dominated by subspheric and subangular to angular clear quartz. About 15% was composed of rock fragments. The bottom layer was dark grey in color indicating a strong reduction zone. The sand was medium to fine-grained, quartz was the dominant mineral and was covered with dark organic matter. A dark brown layer of clayey silt, 0.5 cm thick, was noted on the surface of core 6.

Biological activity was evidently significant in the area, since on the core surfaces concentrations of worm-tubes, small _Mytilus_, and bryozoans were observed. A larger worm tube extruded 5 cm above the surface of core 6. Mud pellets (Oertel, 1973) of ellipsoidal shape with the major axis 1 to 3 cm were observed at different places within the cores. The pellets were formed by dark gray, very fine sand with a large percentage of silt and clay material. All cores displayed a high level of reworking by locomotion of benthic infauna that unfortunately masked most of the primary structure.

Radiographs showed primary structures in two places in core 7 and in one place in core 6. Core 7 which was extracted from the lee side of the sand wave exhibited two different layers containing an apparent foreset bedding. The upper one started 4 cm from the top of the core and was completely within the oxidation zone. The second layer was separated from the former by a 2 mm thick layer of heavy minerals. Core 6 possessed a thin heavy mineral layer with a rippled shape. Two horizontal laminations were also differentiated by X-ray in the upper 4 cm of the core. The described remains of the primary structure did not indicate which process was predominant when the upper layers of the sand wave were formed. In the cores, the bedding was not visually or microscopically apparent.

3.5 Discussion

Meisburger (1972) described a fine gray sand unit in the area where the Chesapeake Bay Bridge-Tunnel is placed. The cumulative curves of three representative samples of that unit are reproduced in Figure 20. Distinct differences between the samples representing the four segments of the sand wave and Meisburger's unit were observed, suggesting no relation between both materials.

According to Shideler, the medium sand composing the northeast flank of the Tail of the Horseshoe may be a

residual deposit from the Pleistocene or early Holocene channel sands of the ancestral York River tributary. After Swift et al. (1971), he classified the sediments as "Palimpset," that is, the sediments are relic deposits partially reworked during the Holocene transgression and are intermediate between modern depostis and unreworked relic ones. Palimpset sediments are not in equilibrium with the modern hydraulic regime. When the information provided by Shideler (1975) was compared to the data obtained in the present study, the results indicate that the sand wave investigated is composed of the same sediment. In the isopleth map of standard deviation presented by Shideler (1975, Fig. 4), only the sand fraction was considered. The material studied here was better sorted, even though the values included the mud and gravel fractions.

The sediments found on the sand wave are presented by their cumulative curves (Fig. 10). In all the curves, a "terrace" between 2.75φ and 3.5φ can be detected. Middleton (1976) proposed three mechanisms to account for the break in a cumulative curve drawn on log-probability paper. They were (1) source of material, (2) mechanical breakage, and (3) hydraulic sorting. In the present case, mechanical breakage did not explain the absence of fine sand material found in the sand wave. Shideler (1975) did not mention a similar break in the cumulative curves for

the sediment of the area; therefore, the apparent source
sediment for the sand wave under study probably contains
fine to very fine sand.

Therefore, the dynamic explanation emerges as the most
appropriate interpretation. Two forms for selection of
the sediment size to be transported are suggested. The
simpler one is to consider the shielding of very fine
material by the medium sand. Shielding is always more
effective when the difference in size of the involved
particles is maximum.

A second process relates the size of the particles
to the energy required to start motion and transport
them effectively. Based on the concept developed by
Visher (1969), the aforementioned breaks in the cumulative
curves were considered as category limits related to
transport mechanism. Visher described three populations:
traction or surface creep (C), saltation subdivided into
subpopulations A and A', and suspension (B). Passega
(1957) defined the term graded suspension as the material
transported in suspension just above the bed such that its
concentration, as well as maximum and median grain size,
decreases with height above the bottom. This term was
later related to the subpopulation A' of Visher (Allen
et al., 1972.). The presence of the terrace on the
cumulative curves (Fig. 10) called for a subdivision of
the suspension population into two subpopulations B

and B'. Subpopulation B' indicates the material which
is in less than the expected proportion in the sample.

The average grain size in millimeters was calculated
for each break in the cumulative curves in Figure 10
(Table VI). The Shields' (1936) parameters for initia-
tion of motion are also shown. Bagnold's (1966)
modification of the Shields' parameters permitted the
estimation of the shear stress values to transport the
material as bedload or suspension load. If not otherwise
indicated, all values corresponded to the lower limit
for each class. When the grain threshold was exceeded,
Bagnold's criterion for suspension indicated that subpopu-
lations B and B' were transported as suspension load
without bedload stage. Material from subpopulation B'
could be transported as suspension by a velocity lower
than that required by subpopulation B. The difference
in velocity for these two subpopulations may be explained
for an increase in the cohesion for finer materials.

The lower limit of the saltation population was well
inside the fine sand class, and the shear stress necessary
to move it could be as low as 1.6 dynes/cm^2. To transport
larger particles, the shear stress must become large and
is rarely achieved except during extreme storm conditions.
In such situations the waves might enhance the bed shear
stress generated by the tidal currents by a factor of

five (Heathershaw, 1981). The conditions needed to transport subpopulation B' occurred normally in this area.

Neither mechanism proposed here acts independently; a combination may be the appropriate solution. That is, the action of relatively weak currents washes out the original fine sand. Then shielding becomes more important as the medium sand percentage increases in proportion to the decrease in fine material.

From this analysis, one might define the sand wave as part of a lag deposit, since the main mechanism for its formation is based on bedload transport of material. The sediment not trapped among grains was carried out of the area as suspension load. Within the sand range, lag deposits tend to be well sorted, since the agent acting over the sediment has enough strength to carry the larger particles. The resulting deposit tends to a larger mean size and becomes coarse skewed.

Based on the sediment itself and the evidence from the cores, the energy required to transport the sediment might be present only during storm conditions. The high degree of bioturbation, delicate worm tubes on the surface of the cores and strong reduction zone seemed to indicate a low energy environment. If large movement of material are present, the reduction zone, also known as the Sulfide System (Fenchel and Riedl, 1970), must be deeper or non-existent in the upper 20 cm. Reineck and Singh (1980)

indicated that anaerobic conditions are associated with the ". . . absence of turbulence or current activities, low rate of deposition and almost no reworking."

Fenchel and Riedl (1970) defined the sharp boundary between the oxidized layer and the reduce zone underneath as the redox-potential discontinuity (RPD), where an abrupt change in conditions occurs. There, reduction processes displace oxidizing processes due to the surplus of organic matter. In still waters, several elements take part in defining the depth of the RPD. Both the amount of organic matter present and the sediment characteristics (Fenchel and Riedl, 1970) are important. Coarse materials if associated with poor sorting tend to deepen the RPD due to the larger pore spaces and permeability of the sediments, allowwing maximum communication with the oxygenated waters above.

With the present knowledge, the question remains unanswered as to how fast the depletion of oxygen occurs from interstitial waters, the phosphates and finally the sulphates in the oxidization of organic matter. The dark color in the sediment appears when the sulfate is reduced to sulfide. This is the last stage of the process. All the stages require stable conditions, otherwise new oxygen is introduced and prolongs the reaction. Not until all the processes can be reproduced under controlled conditions will this system be understood in its entirety (Wong, personal communication, 1981).

The required stability for the development of a strong reduction zone can be further indicated for the sand wave. Biological activity of the proportion observed in the sediment, and the presence of closely spaced dwelling tubes on the surface illustrate that the sand wave was in a low energy environment for an undeterminated period of time previous to the sampling. The depth at which the primary sediment structure occurred was smaller than the depth for the RPD (5.7 cm); this may indicate that the oxidation zone was increased downward by the biological activity.

The results from the textural parameters and Q-mode indicated that three main areas were present in the sand wave. Two extreme areas were represented by samples from the crest and flat, respectively. An intermediate consisted of the combination of stoss and lee samples.

In an environment dominated by tides, the grouping of the samples of the sand wave was expected, especially for the stoss-lee case. The flanks of the bedform were exposed to flood and ebb currents for about the same amount of time. However, a more detailed analysis revealed subtle differences that could be defined as a function of the relative energy represented by the sediment. For instance, if flat sediments were considered alone, the samples to the north side of the sand wave indicated higher energy conditions than those from the south side. A similar comparison could be made between

lee and stoss samples. Inside the range of mean values, stoss material may be more affected by larger dynamic movements than is the lee sediment (Fig. 11).

These examples may indicate that the ebb currents are, on the average, stronger than the flood currents in the lower Chesapeake Bay. This fact has been confirmed by numerous measurements of current profiles (Ludwick, 1973a, b) and by Lagrangian analysis of surface currents (Hilder, 1980).

3.6 Conclusions

From analysis of the sediments, it is concluded that the sand wave might be considered to be in static equilibrium with the currents. Possibly storm conditions can originate enough turbulence to modify the bedform. The fact that the sand wave behaves as a three dimensional body, as described in Chapter 2 and contrary to the results of most studies, suggests that the currents move around this bedform and the mean flow across the crest has values less than the estimated from surface values (Chapter 4). Several factors such as the bioturbated cores, delicate worm tubes and a reduction zone near the surface confirm the concept that at least during the sampling period the environment represented by the sediments was of low energy.

Chapter 4

FLOW DYNAMICS

4.1 Objectives

In most studies of flow dynamics involving sediment
transport, the flow is considered steady. This assumption
introduces a simplification and gives reasonable results
when the flow is studied in a flume or, under certain
circumstances, in alluvial streams. However, it cannot
be applied strictly in marine cases, where waves and tides
are in continuous change. If the wave activity is averaged
out and only the tidal currents are retained, Ludwick
(1972) observed that the value of the shear stress at one
station changes as a function of time.

When the shear stress is calculated by the profile
method, only mean velocities at each level are considered;
therefore, short periods of measurements result in good
approximations of the real value. The calculated shear
stress is the combination of the shear stress due to the
grains and each one of the bedforms present on the area.

Another approach in the calculation of the shear
stress is obtaining the fluctuating horizontal and

49

vertical components of the flow at one level close to the bottom. The perturbation components result in a measure of the turbulent behavior of the flow. The turbulent shear stress is defined by the expression

$$\tau = - \rho \ \overline{uw} \qquad (4.1)$$

where u and w are the fluctuation velocities calculated from

$$u(t) = U(t) - \bar{U}$$

$$w(t) = W(t) - \bar{W}$$

where the overbar indicates time average.

Equation (4.1) approximates the total shear stress for fully turbulent flow since the molecular viscosity of the fluid is neglectable in comparison to the eddy viscosity outside of the viscous layer. Daily and Harleman (1966) illustrated the meaning of equation (4.1) by a simple physical model based on the idea of a mass of fluid transported vertically between layers of different mean velocity. While the parcel of fluid is adjusting to the new layer, the horizontal component in this layer will fluctuate with a velocity larger or smaller than the mean depending on the vertical direction in which the momentum transport occurred.

How much the turbulence may be affected by elements
like suspended sediments, density stratification or the
mean velocity at the measuring level is presently unknown.
Studies in flumes and theoretical approaches have shown
that suspended sediments produce considerable damping in
the turbulence and therefore, they modify the value of the
shear stress. The development of the Reynolds stress
concept was based on fluid with constant density. Either
temporal or spatial variation of the density in the
momentum equations makes the mathematics of the problem
insoluble with contemporary techniques.

In the current chapter, a discussion of the measure-
ments of shear stress at a level of 5 cm above the bottom
is presented. The stations were distributed along the
profile of the sand wave, described in previous chapters.
The method utilized is based on the Reynolds stress idea,
and the influence of several factors such as waves,
material in suspension, and density stratification on
the final results are considered.

4.2 Previous Studies

The analysis of the variation of boundary shear
stress (τ_o) along the profile of a transverse bedform
has been done in many theoretical studies, and with rela-
tively few determinations in flumes. Field measurements

have seldom been obtained. The experiments over a fixed-bed ripple in a flume presented by Raudkivi (1963) gave an idea of the distribution of the shear stress and the pressure along the section of the ripple. Along the upstream face the streamlines become closer together and the dynamic pressure drops. The free flow is then much faster and the gradient of U in the vertical direction $(\partial U/\partial z)$ is larger. Then, the maximum shear stress is observed at the crest.

The slope of the lee face of the ripples considered by Raudkivi were about 25°. Flow separation occurred downstream of the crest, where the main flow broke down into an expanding zone of strong turbulence that was diffused upward into the main part of the flow, and downward toward the boundary (Middleton and Southard, 1978). Protected by the ripple, and eddy developed and backflows were present. The reattachment point of the flow was observed between 5 to 10 ripple heights (H) downstream from the crest. Using birefringent materials mixed in the flow, Karahan and Peterson (1980) also observed this separation.

In the case of marine sand waves, the slopes involved are much smaller than those given for ripples, normally of the order of 10° or less. Benjamin (1959), Smith (1969), and Hsu and Kennedy (1971) differ in their estimates of steepness ratios (H/L) required for separation.

On the average they argue that separation takes place when H/L values are larger than 0.1. Here, L is the wavelength of the sand wave. Taylor and Dyer (1977) also pointed out that separation tends to occur when the crest is sharp and a large slope of avalanche steepness is observed.

Laboratory measurements of shear stress distribution in non-separated flow indicate that the maximum value of τ_0 does not occur at the crest but at a distance upstream of it. Hsu and Kennedy (1971) reported that this happens between 0.07 L and 0.05 L upstream of the crest. Similar results were indicated by Kendall (1970), but the distance was 0.19 L. Benjamin (1959) gave a possible explanation for the lag in shear stress, which he found theoretically to be 0.08 L windward of the crest. His idea was based on the effect of sheltering produced by the crest of the bedform.

Taylor and Dyer (1977) presented a numerical model applied to sand waves, previously developed for an isolated "hill" in a meteorological study (Taylor and Gent, 1974; and Taylor et al., 1976). They considered a periodic lower boundary conformally mapped such that it behaves like a streamline. By doing this, the momentum and continuity equations for the fluid can be linearized in a relatively simple way. Results obtained from this numerical treatment were the fields of mean velocity and

pressure, and shear stress on the bed. The lag occurred 0.05 L on the stoss side.

Relatively few field measurements over sand waves are available. Terwindt (1971) noted currents of 80 cm/sec over the crest and 50 cm/sec over the trough, at about 0.50 m above sand waves in the North Sea. Dyer (1970, 1972) used rotor current meters in a study of gravel waves of the Solent Channel (South of England), where he estimated $\tau_o = 200$ dyn/cm^2 and 50 dyn/cm^2 at the crest and trough, respectively. The various velocity profiles presented along the bedform section were highly affected by ripples and megaripples; however, they were very consistent within the set.

In the Chesapeake Bay entrance, current measurements were made by Ludwick (1973a, b) in his analysis of sediment transport and the morphology of shoals. Granat and Ludwick (1980) resolved the near bottom behavior of the currents associated with a large shoal just north of the study area (Fig. 1). They found that the flow avoided the sedimentary structure. Therefore, the crestal part of the bank may be mainly affected by waves.

Instead of using mean velocities distributed at different levels throughout the boundary layer, the shear stress may be obtained by turbulence measurements of the horizontal and vertical components of the flow. About 25 years ago, Bowden and Fairbairn (1956) made the first

determinations of the Reynolds stress in a marine environment with electromagnetic current meters. Since then, the turbulent structure of the bottom boundary layer have been analyzed in several studies (Bowden, 1962; Bowden et al., 1959; Heathershaw, 1976; Soulsby, 1981; and Soulsby and Dyer, in press).

Heathershaw (1979) made a detailed study of simultaneous records at different levels above the bottom and described the variability of the turbulent structure. Gordon and Witting (1977), as did Heathershaw (1974) and Gordon (1974), found that the momentum transport is highly intermittent and characterized for large "spikes" in the instantaneous shear stress ($\tau(t)$) record.

4.3 Methodology

4.3.1 Instrument Mounting

The tetrapod (Fig. 21) consists of a circular platform of acrylic plastic, 25 cm in diameter, 2.54 cm thick, supported by four transverse aluminum rods, 1.905 cm in diameter and 50 cm long. Affixed to the end of each transverse, a vertical leg of the same material was finished in a point to help the tetrapod penetrate the sediment. An acrylic plate (diameter, 10 cm; thickness, 254 cm) was attached to each foot to limit penetration of each leg to 5 cm. Lead weights (1 kg

per leg) were placed on top of these acrylic plates to provide more stability and penetration. Attached to brass eyes on the platform, three stainless steel rods (diameter, 0.5 cm; length, 60 cm) supported a wooden canopy through which a stainless steel swivel was mounted for connection to the winch cable.

Three instruments were arranged on the platform (Fig. 22). An acrylic box housed the motor and gear system was used for driving the probe support (stainless-steel tube). A lowering mechanism was designed to lower the sensor in three steps to 25, 15 and 5 cm above the bottom.

The other two instruments on the platform were a compass and an inclinometer. The compass is an adaptation of the one used in the GEODYNE Model I current meters. The inclinometer is a B.O.D. bottle. Both were half filled with a jelly prepared according to a recipe by Carruthers (1967). After several tests the preparation that set at warmer temperatures (about 32°C) was chosen. With the tetrapod situated on the bottom, the setting of the gelatine locked the compass with the orientation of the X_+-component of the current meter and also gave the direction and angle of inclination of the platform, which is assumed parallel to the bottom.

The advantage of this method is an accurate instrument at low cost, providing that the user needs only one

reading per station. The gel can be melted by submerging the compass or inclinometer in boiling water. The first time, liquefaction takes about 15 minutes, five to ten minutes on successive times, depending on the water temperature, the elapsed time, and the temperature of the last setting. The gel time depended on the water temperature but was estimated to be 15 minutes at 28°C.

A triangular vane was added to the platform (Fig. 21) to orient the tetrapod with the mean current. The center of mass of the vane is at about 60 cm above the current meter when the probe is at its lowest position (i.e. 5 cm above the bottom).

Several tests were performed before attempting actual measurements. The first tested the strength of the structure by exposing it to waves 0.60 m high at a beach. The instrument was placed at about 2 m offshore at the breakers and the results were satisfactory. Operational tests were conducted in the swimming pool at Old Dominion University, in the Lafayette River, and on the study site itself.

During the first set of measurements, a brass gear in the driving mechanism was damaged and could not be replaced. For this reason only one vertical velocity profile was actually recorded at a single location over the sand wave.

4.3.2 Field Work

Before taking current data, the station sites were determined and marked with buoys. For both days of actual measurements, the positions of the buoys with respect to the sand wave profile are indicated in Figure 23.

Once the buoys were positioned, the R/V HOLTON was anchored about 200 meters from the line of buoys and as close as possible to the crest of the sand wave. On that station, vertical profiles of temperature and salinity were recorded each hour at depth intervals of one-meter using an inductive salinometer.

On board of the R/V ODU I, the following steps were taken at each station:

1. The tetrapod was linked to the boom, while the current meter was connected to the data recording system.

2. With the current meter in the vertical position, the tetrapod was lowered to a level 2 meters below the surface, at which depth the shadow effect of the boat on the currents was considered negligible. Near-surface currents were measured for a period of 256 seconds. The direction of the current was estimated by observing the orientation of the vane as compared with the magnetic compass of the boat. After a period of training, the error using this procedure was estimated to be $\pm 5°$.

3. The tetrapod was raised on board, and the probe
of the electromagnetic current meter was placed in a
horizontal position (Fig. 24); then the structure was
lowered to the bottom. There, measurements were taken
for 1024 seconds.

4. Again the instrument was brought up and secured
on board. The compass and inclinometer were exchanged for
a set containing liquid jelly. The boat moved to the
next station by simultaneously retrieving one anchor line
and paying out the other. Once on station, steps 1 through
4 were repeated.

A variation of the above was carried out on August 12,
1981. After the near surface currents were measured, the
current meter was lowered to the bottom in the uppermost
vertical position. There the instrument recorded data for
256 seconds at each level (25, 15 and 5 cm) above the
bottom.

4.3.3 Data Acquisition System

The instrument was an electromagnetic current meter
and the data logger system (Fig. 25). The sensor was a
Marsh-McBirney Model 523 electromagnetic current meter,
originally designed for laboratory use. The diameter of
the sensor was 1.27 cm. The entire instrument can be
described as a transducer with 30 meters of waterproof,

shielded cable and a portable case that houses a signal processor. The transducer used two pairs of orthogonally-disposed electrodes which sense the water flow in a plane normal to the probe axis. The flow was resolved into its two components by the orthogonal pairs of electrodes, and in addition to being recorded was visualized on the panel meters on board.

The output was an analog signal in volt units. The maximum output was 1 volt which corresponds to a velocity of 10 ft/sec (304.8 cm/sec). The instrument offered a selection of three time constants (0.2, 1.0 and 5.0 seconds). The time constant (t_o) acted as a low pass filter by averaging the input signal over the time t_o. The current meter was calibrated before and after the experiments in a circular flume at Marsh-McBirney, Inc., Gaithersburg, Maryland. Repeated checks against hot-wire anemometers were performed in a rotating tank built by R. B. Philips in the Department of Oceanography, Old Dominion University. In all cases, the current meter had a linear response. The estimated rms error of the instrument was 0.91 cm/s.

The data logger was an InterOcean Model 680 Digital Recorder. Data were entered in four channels in the following pattern: channels 1 and 3 recorded component X; channels 2 and 4 recorded component Y. The instrument recorded data for 256-second period. The values were

monitored in the field by comparing the meter readings with a digital voltmeter connected to the recorder input. Both current meter and digital recorder had their own power supply.

4.3.4 Selection of the Parameters

The characteristics of the instrumentation dictated the selection of the parameters to be used during the experiment. The first consideration was the sampling interval (Δt) selected as 0.25 seconds which corresponded to a Nyquist frequency, f_N , of

$$f_N = \frac{1}{2 \, \Delta t} = 2.0 \text{ Hz}$$

The time constant of the current meters was selected such that the cutoff frequency was smaller than the Nyquist frequency. The value used was $t_o = 1.0$ seconds. The spectral window of the gauge, f_w, was found by taking one hundredth of the spectral power function ($H(f_w)$). Thus

$$10^{-2} = H(f_w) = \frac{1}{1 + 4\pi^2 \, f_w^2 \, t_o^2}$$

$$f_w = 1.5836 \text{ Hz} .$$

Therefore, the spectral window was 0.0 to 1.58 Hz.

4.3.5 Data Reduction

The data on the cassette tape were transferred to a
DECsystem-10 computer using an InterOcean Digital Cassette
Reader Model 696. The resulting disk file was edited for
noise introduced into the system by the recorder. This
noise appeared sporadically as anomalous characters that
replace one of the digits (normally the last one) in a
data word. On other occasions, the channels in one group
were switched. All these problems were easily detected
when a listing of the file is analyzed. The editing was
simple but had to be done individually with a text editor.

Only the observations obtained with the probe in the
vertical position $(\hat{U}_i, \hat{V}_i)$ (near-surface and profile)
were coreected by rotating the reference axis through an
angle α, such that the time average of the cross-stream
component becomes identically zero $(V \equiv 0.0)$. The
angle α was calculated

$$\alpha = \tan^{-1} (\tilde{V}/\tilde{U})$$

where $\tilde{U}$ and $\tilde{V}$ are the unrotated mean of the observa-
tions and

$$U_i = \hat{U}_i \cos \alpha + \hat{V}_i \sin \alpha$$

$$V_i = \hat{V}_i \cos \alpha - U_i \sin \alpha$$

U_i and V_i are the new variables after the rotation of coordinates. In all cases $i = 1, 2, 3,..., 1024$.

4.4 Results and Discussion

Measurements of velocities at five stations along the profile of the sand wave were taken on August 12 and 14, 1981. Each record consisted of two sets of observations. With the current meter in the vertical position, the streamwise $(U(t))$ and cross-stream $(V(t))$ components of flow, 2 m below the surface, were recorded for a total of 256 seconds. In the second set, the current meters was used in the horizontal position. This method gave values of the horizontal $(U(t))$ and vertical $(W(t))$ components of flow at 5 cm above the surface of the sand wave. Table VII is a summary of the 18 records that were collected.

For clear denotation each record will be identified by two numbers separated by a dash, for instance, 3-07 indicates a record obtained at station 3 during the seventh interation through the four stations. An interation consists of a set of records taken successively at stations 1 through 4 or vice versa (Fig. 23). Records P1-02 and P1-03 were obtained on the same day (August 12) and only station P1 was occupied.

The presentation of the results is divided into three sections: (1) surface currents, (2) density profiles, and (3) time series analysis.

4.4.1 Surface Currents

Ludwick (1973a, b) analyzed the data from 24 tidal current stations on the north side of the Chesapeake Bay entrance. His findings indicated that tidal currents were of a reversing nature. The directions of ebb and flood were not exactly opposed, but formed an obtuse angle, which averaged approximately 158° and usually opened to the North. The rotation of the current vectors formed greatly elongated ellipses with a mean traverse period of 12.58 hr. During the turning time, Ludwick (1973a) never observed them to decrease to zero speed.

Granat (1976) described eight near surface tidal current stations over and adjacent to Inner Middle Ground-Nine Foot Shoal, located 10 km due Northeast of the present area (Fig. 1). In all cases the currents were reversing. As in the data described by Ludwick, the current vectors did not point in opposite direction, but formed an angle, typically open to the North.

From February to October 1979, Hilder (1980) made studies of surface circulation across the present research area. Hilder's work clearly demonstrated the rotary nature

of the tides in an area which is evidently less affected by bottom features and the orifice flow than is the northern part of the bay entrance. In the area studied by Hilder the surface currents formed an ellipse with the major axis directed northwest-southeast. The ratio between the major and minor axis of the tidal ellipse was 1.36.

In the present study the measurements obtained over the sand wave were not taken to analyze the behavior of the tidal currents, but to serve as collateral information in the calculation of parameters measured near the bottom. However, the characteristics of these values calls for a brief description. The rotary nature of the tidal current was clearly observed during the second day of observations. Table VIII is a synthesis of the surface current values and orientation. The velocity vectors are represented in Fig. 26. Tidal records of height above mean low water (Fig. 27) were obtained from the tide gage operated by NOAA at the first island of the Chesapeake Bay Bridge-Tunnel.

The following description refers to the data obtained on August 14, 1981 and reference will be made to the vectors in Table VIII. Current data represented by vectors were obtained at the end of maximum flood, and the tidal rotation was typically clockwise. During maximum ebb the orientation of the current vectors fluctuated in

a 30° sector between 146° and 176°. A complete rotation between vectors 2 and 16 occurred in 8 hours 42 minutes.

Correlation of near-maximum ebb current with the time of low water seemed to indicate that maximum ebb occurred at the beginning of the rising segment of the tide. This suggested that the tidal wave is mostly a progressive wave in the area. This analysis may suggest that the currents would also fluctuate inside a small sector during high water.

A second observation of the tidal curve confirmed the tide's diurnal inequality. Only one measurement was taken at the lowest tide: the record P1-03 on August 12 revealed that the maximum surface currents observed were almost 3 m/sec. This was about five times greater than the maximum surface currents measured two days later. Maximum forecasted velocities for the area were about 2 m/s during spring tides. The experiments were performed two and four days after the date of forecasted neap tide.

The average value of the surface current was 34.01 cm/sec. Considering an average depth (h = 9 m) in the sand wave area, the estimated Reynolds number was approximately 3×10^6. Therefore, the flow might be considered as fully turbulent even with the assumption of a flat bottom. Complex bed configurations can induce fully turbulent flow even at lower Reynolds numbers.

4.4.2 Density Profiles

For future use in calculating the shear stress, values of salinity and temperature were converted into units of σ_t , defined as

$$\sigma_t = 1000 \ (\rho - 1)$$

where ρ is the density of the water depending on temperature and salinity alone. Profiles of σ_t for both days of measurement with their starting times are displayed in Figure 28. Minimum densities were always found at the surface, ranging from 12 to 15 σ_t units. In all cases maximum values, up to seven σ_t units larger, corresponded to the bottom 1 m.

An evolution of the density at the study area may be observed in the graphic for August 14. The profiles obtained between 0757 and about 1100 showed a smooth general trend and no definite indication of a pycnocline. The pycnocline developed in the afternoon profiles and also appeared in both profiles on August 12. In general, the steep change in density was about 3 σ_t units at mid-depths between 3 and 6 meters. In the last three profiles, the pycnocline became more difficult to define.

Analysis of the temperature and salinity profiles (not shown here) indicated that both contributed to the changes in density. The surface temperatures ranged

from 24.5 to 29.2°C, the bottom temperatures were more stable, 23.3 to 24.8°C. The salinity gradients were the inverse of those for temperature with variations of the same order. Maximum salinities up to 29 %o were found at the bottom in the second profile on August 12.

An interesting feature of the surface density was noticed in the data. The surface values were gradually reduced from almost 14.4 at 0854 to 12.5 at 1658. Figure 29 exhibits the hourly distribution of salinity and temperature at the surface, 4 m and 9 m . Both surface curves showed variation from the initial conditions, specifically the temperature which might explain the density change. In most cases the salinity decreased with the increments of temperature, consequently the densities also decreased. Since these data were obtained in summer, the formation of the pycnocline in the afternoon hours might be produced by heating in the surface layer. The data were not collected long enough to extract any conclusions about the behavior of salinity and temperature in relation to tidal conditions, nor could these observations be extrapolated to other periods or locations in the bay.

4.4.3 Time Series Analysis

The first step in the analysis of the data obtained with the current meter in horizontal position was to plot

U(t) and W(t) as a function of time. Figures 30
through 41 are six examples from records separated in
time and position over the sand wave. When these plots
were examined, three distinct components were identified:
(1) long period trends, (2) wave period phenomena, and
(3) turbulence.

Long period trends. The long period trends were
evident mainly in the U-component of the flow. In W(t)
they were observed only after a detailed inspection of
the graphics. Therefore, the discussion of this informa-
tion will refer almost exclusively to the U(t) plots.
The analysis of the trends indicated that these flow
structures have certain periodicity that varied from
station to station from three minutes to an estimated 20
minutes. The latter value could not be confirmed since
the record length was only 17.27 minutes. The velocity
amplitude of these phenomena approached 30 cm/s. In
some cases the amplitude was not constant but was diminish-
ing with time, indicating that these long period trends
were generated by a temporary flow structure.

In half of the records the long period trends masked
any steady flow that might have been present (Figs. 30,
32 and 34). The remaining records displayed those trends
associated with a steady flow current (Figs. 36, 38

and 40). The range of velocities for the steady currents was between -9 and 22 cm/s.

On several occasions during the field experiments, negative values for the current in the U-component of the flow were observed on the panel meters on board. After the first indications of those negative values, an additional precaution was taken. Originally, the tetrapod was lowered to the bottom with the power to the current meter turned off to prolong the charge of the batteries. However, as a result of the problematic readings, the panel meters were monitored while paying out line slowly. A rough profile of the current was observed but not recorded, since there were no provisions for accurately determining the distance of the instrument above the bottom.

In particular, stations 1-04 and 3-08 were checked carefully. Visibility into the water surface was approximately 2.5 m, and it was seen that the current meter was oriented with the flow and indicated positive values. As the descent continued, the indicated velocity of the flow decreased slowly with depth to a point about a meter above the bed. Then, the gradient of velocity increased reaching 0.0 cm/s about 20 or 30 cm above the bed. From this level until such time when the tetrapod was positioned on the surface of the sand wave, the flow values were observed to be negative. When this was noted, the tetrapod was

hoisted about two meters above the bed and lowered again,
and the same results were obtained.

An explanation of these observations was sought in an
analysis of both cases. Flow separation over the sand wave
was ruled out primarily because the tetrapod was situated
on the side of the feature from which the current was
approaching. Another form of separation may be due to
the ripples formed on the surface of the sand wave; how-
ever, their presence was not confirmable.

In accordance with a tentative classification of wave
periods presented by Kinsman (1965), the long period trends
noted in the present study were between the upper limit
of infragravity waves and the lower limit of the long
period waves. To the present author's knowledge, this
phenomenon has not been described previously in the
entrance area of the Chesapeake Bay. Bowden and Proudman
(1949) found similar perturbations in the River Mersey,
and they attributed them to the passage of large eddies
or internal waves. In the present area, the density
profiles indicated a two layer structure separated at
about 4 meters, which may establish the conditions for
the generation of internal waves. Further explanation
is beyond the scope of this research. The author suggests
this as a possible theme for future investigation.

Autocorrelations of U and W separately and their crosscorrelation made use of the Blackman-Tukey Method (Bendat and Piersol, 1971; and Grosch, 1981). Figures 42 through 50 are examples of the results. The autocorrelation of U for records 1-08 and 2-07 exhibited the dominance of a sinusoidal component with a period of 12 to 15 seconds and with slow fall-off as the length of the lag increases. In the autocorrelation of W, the wave component was much less noticeable, but remained important in the crosscorrelation.

On the other hand, the autocorrelation from record P1-03 was not influenced by periodic structures in the flow. The autocorrelation of W for all three examples (Figs. 43, 46 and 49) indicated no effect of periodic forms. The presence of a mean current is most noticeable in Figure 42, since the autocorrelation is very high even after 200 lags. The steady flow is less visible in Figs. 45 and 46.

The velocities obtained with the probe in the horizontal position were subjected to spectral analysis by the Fast Fourier Transform method (FFT), using the program NWFFT.FOR by Dr. Chester E. Grosch. Figures 51, 52 and 53 show the spectra of U and W for the three selected records (P1-03, 4-04, and 2-07). In all the spectra, the peak frequency or the second largest peak occurred at approximately 0.016 Hz. The frequency interval (Δt) for

the spectra was also 0.016 Hz; therefore, the actual peak was included in the first Δf. However, the resolution was too coarse to detect the actual frequency for the long period trends. Although the method permits the use of a smaller Δf, the variance in the output would be too large to be meaningful for the number of data points used.

Wave period phenomena. Spectral analysis techniques were also applied to the determination of periods of the wave components in the records. In the spectra of records 4-04 through 3-06 (Table VII), the peak energy in the wave range was found at $f_1 = 0.078$ Hz (i.e. Fig. 52). This higher energy started shifting towards smaller periods in record 2-06 and was clearly established from record 1-06 to record 1-08 at $f_2 = 0.094$ Hz (i.e. Fig. 53).

During the sampling period on August 14, there were no visible indications that waves were arriving in the area. Therefore, no data referring to direction, height or wave period were recorded. However, from data such as the difference in arrival time (Δt_A) and the energy of the estimated peak frequencies from spectra analysis, characteristic wave parameters may be computed (Table IX). Small amplitude waves, traveling in shallow water with local depth equal to the average depth of the sand wave (h = 9 m), were assumed for the calculations. Because the large, well defined periods were clearly separated

from the other frequencies, it was further assumed that the waves were not generated locally.

If the minimum Δt_A were considered to be the time difference between the times of records 4-04 and 1-06 (Table VII), the minimum travel distance D was calculated to be about 1000 km. This indicated that the current meter registered swell generated somewhere in the middle of the Atlantic Ocean beyond the continental shelf, East to Southeast of the mouth of the Chesapeake Bay. The calculated height and wave steepness (H/L) were too small and could not be detected in the field by visual observation.

In the laboratory, waves generated with a unique frequency give rise to coherences between their horizontal and vertical velocity components from 0.8 to 1.0, respectively. In the study area, the calculated coherences for the indicated frequencies produced mean values of 0.44 and 0.43, respectively. However, the peak coherence was found at station 2-04 (0.91) and at 1-04 (0.73) for f_1, and at 2-08 (0.73 for f_2. Coherences larger than 0.75 were found at frequencies on either side of the ones depicted here. Generally, they were related to peaks of energy in the U component, but this was not always true for the W component.

Theoretical determinations have demonstrated that the thickness of a wave boundary layer (δ_ω) (Lukasik and Grosch, 1963) is defined as

$$\delta_\omega = \frac{3}{m} = 3 \left(\frac{\omega}{2\nu}\right)^{-\frac{1}{2}}$$

where ω is the angular frequency = $2\pi f$, and ν is the fluid kinematic viscosity, taken there as $0.01 \text{ cm}^2/\text{sec}$. Estimations of δ_ω for both frequencies (Table IX) produced results a tenth of the height (5 cm) at which the current observation was made. On the other hand, Jonsson and Carlsen (1976) estimated a boundary layer 6 cm thick, by using obstacles that created equivalent sand roughness of 2 to 6 cm.

The waves have provided most of the energy in the spectra; therefore, determining the thickness of the wave boundary layer becomes an important factor. Lukasik and Grosch (1963) and Johns (1975) showed that the gradient of horizontal velocity inside the boundary layer changes slopes depending on the value of the phase angle. At certain values, the gradient even becomes negative, thus generating a negative shear stress at the same level. Although careful theoretical (Kajiura, 1968; and Johns, 1970, 1975) and experimental studies (Jonsson and Carlsen, 1976) have been performed on the boundary layer generated by oscillatory flows, the effect of ripples has not yet been defined (Davies and Wilkinson, 1977).

Turbulence. One of the basic objectives of this study was to determine the distribution of boundary shear stress along the profile of the selected sand wave.

The spectra (Figs. 51 through 53) indicated clearly that the energy present in the turbulence frequencies inside the inertial subrange was 2 to 3 orders of magnitude smaller than the energy observed in the long period trends or at wind waves frequencies. Therefore, analysis of the turbulent part of the flow has to take into account effects of the low frequency structures. For instance, the values obtained from the original records (Table X) indicated that half the calculated shear stresses were negative. When the data were filtered at 0.7 Hz, the tangential stress became extremely small (i.e. 0.00008 dyn/cm^2), much lower than the error of the instrumentation.

The values obtained from the vertical velocity profile were utilized to estimate the shear stress. The calculations were made using the following equations: the von Karman-Prandtl equation

$$\frac{\bar{U}(z)}{u_*} = \frac{1}{K} \ln\left(\frac{z}{z_o}\right) \tag{4.2}$$

where $\bar{U}(z)$ is the time averaged velocity at the height z above the bottom, u_* is the shear velocity = $(\tau_o/\rho)^{\frac{1}{2}}$ and z_o is the roughness length. Alternatively, a velocity defect equation (Daily and Harleman, 1966) were

also used,

$$\frac{\bar{U}_B - \bar{U}(z)}{u_*} = - 5.6 \text{ log } (\frac{z}{\sigma}) + 2.5 \qquad (4.3)$$

where $\bar{U}_B$ is the mean velocity at the top of the boundary layer of thickness δ. In the present study, δ was considered as the water depth = 8.34 m. Expression (4-3) is applied when $z/\delta < 0.15$.

Figures 54 and 55 show the measured mean velocities and the estimated profile. Table XI is a summary of the parameter estimated with expression (4.2) and (4.3). The estimated boundary shear stresses were low but were consistent with the free flow velocity. Unfortunately, they could not be compared with the results obtained by the Reynolds stress method because, as will be seen later, the turbulence was damped and the value of turbulent shear stress for the same station was not representative of the flow conditions.

The data measured with the current meter in the horizontal position were filtered with a low-pass filter. The low frequency signal was subtracted from the original data to obtain the high frequency information. The filter was a smoothed moving average with half-power frequency $(f_{\frac{1}{2}})$ equal to 0.2 Hz. The selection of the half-power frequency was based on the natural break observed in the slope of most of the spectrum curves. The rms and τ

calculated from this information are included in Table XII. The values for τ were very small; only 6 were positive.

The removal of the long period component in U left short periods structures (Figs. 56, 59 and 62). The autocorrelation of W also showed a wave component whose period is three seconds and which was previously masked by other longer period waves (Figs. 57, 60 and 63). Obviously the crosscorrelation was highly dominated by these structures. In all cases the total correlation at each lag was near zero (Figs. 58, 61 and 64). These periodic structures were observed in the spectra (Figs. 51 through 53) as secondary peaks at 0.3 Hz.

A troublesome result was the occurrence of $\tau < 0$ in so many cases. A similar result was also observed but not explained by McLean and Smith (1979) and Soulsby (1981). In the theoretical derivation of the Reynolds stress, the product, uw, is averaged over a long period of time and is negative. This result is not invariably true (Phillips, 1980). The resulting shear stress is mathematically oriented with the flow by multiplying it by -1.

To obtain negative value of τ, several conditions may occur individually or in combination. Based on semi-quantitative statistical analysis, Gordon and Witting (1977) have calculated that a minimum sampling time of 4.5 hours is required to reduce the error of the estimate

to a value as small as 10% when predicting the real shear stress. Their results were predicted on the existence of steady conditions which can only be achieved in carefully controlled laboratory experiments. Shorter durations, as predicted by these authors, may produce as much as 50% error.

In the present study steady conditions did not exist. The rotation of the tidal current was almost continuous, even during time of maximum ebb. Observed long period trends and swell were also an important factor in the unsteadiness of the flow pattern.

On the other hand, Soulsby (1980) estimated that a record length of 12 minutes would produce a relatively good estimate of the shear stress in tidal conditions. To analyze this claim, shear stress values were calculated for each record as an average over the first 12 minutes, and also over the last 12 minutes (about 7 minutes were common to both). An analysis of variance was performed with each 12 minutes set of data and the total record as treatments. No significant differences were found among the means at $p = 0.9$.

To explore time variations in the calculated quantity of interest, instantaneous shear stress was plotted as function of time (Figs. 65 through 70). Two main elements were distinctive. First, in most records the value of

$\tau(t)$ was almost zero and varied from positive to negative and vice versa in very short periods, usually less than 1 second. Intermittent large spikes, directed either positively or negatively, were the second distinctive feature of the records. Heathershaw (1974), Gordon (1974), Gordon and Witting (1977) and Chung (1979) have associated these structures with large-scale "bursts" similar to those found in laboratory studies (Corino and Brodkey, 1969; Kim et al., 1971; and Rao et al., 1971.

In measurements in a wind tunnel, Lu and Willmarth (1973) found that the frequency distribution of τ had long tails and a sharp peak at $\tau = 0$. Heathershaw (1979) showed similar results for tidal current data. The frequencies (%) of τ, included with $\pm$ three standard deviations ($\pm 3\sigma$) about the mean are shown in Table XIII. Also the extreme number of standard deviations on either side of the mean ($+\sigma$ and $-\sigma$), between which all the values are concentrated, are shown in the table. In Fig. 71, the percentage frequency distribution of τ for some of the records are shown. More than 80% of the data was concentrated between $\pm$ one standard deviation. The distribution also showed a peaked form which was always skewed contrary to the sign of the mean. Extreme spreading was found in records 3-04 and 4-05.

Events defined as the sum of all $\tau(t)$ between two successive zero crossings were considered for their

contribution to the final shear stress. Table XIV
exhibits the distribution of the events per record: posi-
tive, negative and total. The number of events per record
ranges from 1210 to 1639, with an average of 1484. The
total length of the record was 17.27 minutes. The absolute
values were taken into account to calculate the total sum.
Most values ranged between 70 and 1000 dyn/cm^2, but three
records were distinct. Specifically, record P1-03 repre-
sented the largest amount of energy by far. Very strong
velocities were obtained at the surface for this record,
as mentioned before.

The average shear stress per event was also dominated
by record P1-03. When the absolute value of the
means of the positive and negative events were compared,
it was found that the sign of the larger value was the
same as that of the Reynolds shear stress. The number of
events that contribute to the final shear stress are shown
in Figure 72. Four events alone contribute more than 8%
to τ. The major concentration was in the class interval
0-1%, actually 99.63% of all events.

Gordon and Witting (1977) analyzed individual events
and found that in a determined 1.5 hours record, 12 events
contributed to 90% of the total shear stress. The mean
duration, calculated by the same authors, was nine seconds.

In the present case, the value of τ was a result of the small events. Contrary to what Gordon and Witting (1977) have found, the large spikes were not an important contribution to the value of τ. Events that contributed more than 1%, either positive or negative, averaged 33.04 dyn/cm^2, but in time those spikes averaged only 2.33 seconds. The latter indicated that larger spikes were only present during very short periods of time. For instance, Figure 73 exhibits the longest spike with a contribution greater than 1%.

In his analysis of the turbulent structure of the bottom boundary layer in the Irish Sea and Menai Strait, Heathershaw (1979) inserted a classification of the product uw based on the sign of perturbation velocities u and w as follows:

$$u < 0, \quad w > 0 \qquad \text{Ejection}$$
$$u > 0, \quad w < 0 \qquad \text{Sweep (Inrush)}$$
$$u > 0, \quad w > 0 \qquad \text{Outward interaction}$$
$$u < 0, \quad w < 0 \qquad \text{Inward Interaction}$$

In all turbulent studies of boundary layers involving "bursting" phenomena, ejection and sweep or inrush made the largest contributions to the final value of the shear stress. The interactions were less important. In the above classification, the first two forms of momentum transport resulted in a positive shear stress. To achieve this,

u and w must be "out of phase," that is, with an opposite sign (Fig. 77).

The analysis of distribution and characteristics of the spikes (Figs. 73 through 77) indicated results different from those obtained by the above researchers. In most cases over the sand wave, the spikes were formed by "in phase" contributions of the perturbation velocities. Therefore, they would be classified in the Heathershaw scheme as interactions, either outward or inward.

Figures 73 through 77 depict some of the largest spikes in percent contribution to τ expanded to show detail. In all cases there was a maximum value of τ that stood out, associated with minor peaks. In particular, how the process is building up to form the larger spike four seconds later than the zero crossing is shown in Figure 73. Afterward, an immediate reduction required slightly more than one second to achieve zero. Actually, the prominent spikes in each event were very short; few surpassed one second in duration.

The values of u and w did not maintain a uniform sign during an entire event but instead switched intermittently and almost simultaneously with great coherence. Figure 74 shows one of the few exceptions in which $|u|$ is usually greater than $|w|$. In the other figures, the common feature is the relation $|w| > |u|$, which indicates

that the origin of the spikes is produced by an increment in the modulus of the vertical component of the flow.

The Kolmogoroff spectrum law (Hinze, 1975) states that in the inertial subrange, turbulent energy is proportional to $f^{-5/3}$. A line with such slope was compared with the spectra from all the records of the present study. In most cases the upper limit of the range was defined at 0.7 Hz (Figs. 51 through 53). The most striking feature of the spectra at frequencies larger than 0.2 Hz was the relation between the amount of energy present in W and U. Record 3-08 was the only one in which the energy contained in U was larger for all frequencies. In the other records the difference in energy was usually about one order of magnitude. Numerous studies of flows near the bottom boundary layer (i.e. Bowden, 1962; and Heathershaw, 1976, 1979) have shown that the energy in the U component of the flow is always larger than the energy of the vertical component. In the present study, the energy relationship was reversed.

The observed energy reduction indicated that the turbulent part of the flow, specifically the U component, may have been damped. At least two possible causes for reduction in turbulent level can be pointed out: (1) suspended sediment; and (2) a vertical gradient in the density structure of the flow.

Vanoni (1946) suggested that the turbulence is damped by the sediment in suspension. In particular, the effect should be more evident in the vertical component of the flow since this component has to maintain the suspension against the downward action of gravity. Yalin (1977) attacked the problem by considering the effect of the length of the eddy dimensions, but his idea is similar in content to Vanoni's since they are related by the eddy diffusion coefficient. Recently, Adams and Weatherly (1981) have calculated substantial reductions in the turbulent kinetic energy due to suspended sediment. To achieve their result, a drastic reduction of the fluctuation components is proposed.

Heathershaw (1979) followed Wimbusch and Munk's (1971) idea based on the Richardson number (Ri) concept to estimate the concentration of suspended material required to modify the turbulent structure of the bottom boundary layer. In this way he obtained

$$C \leq Ri \ [\frac{\rho_s \ \rho \ u_*^3}{g \ w_s \ K \ z (\rho_s - \rho)}]$$

where C is the concentration of suspended sediment, Ri is the Richardson number, ρ_s is the particle density and w_s is the settling velocity of the particles. For a critical Ri = 0.25, which corresponds to the upper limit for turbulence to be maintained (Schlichting, 1968),

Heathershaw's calculations yielded a concentration of 130 mg/l for u_* = 2 cm/sec. The mean u_* for the present work was 0.33 cm/sec. For a particular size (i.e. 0.01 cm) the expression given by Heathershaw (1979) resulted in a concentration smaller than 8.2 mg/l at 5 cm above the bed.

Unfortunately, the concentration of suspended solids was not sampled during the present measurements. However, in samples obtained by Oertel, Byrnes and Gingerich (personal communication, 1981) the maximum concentration was about 67 mg/l, 1 m above the bottom in the area of the shoals just South of Fishermans Island (Fig. 1). In general, they found values between 10 and 50 mg/l. During the sampling flow velocities at the same level were of the order of 20 to 40 cm/sec. If the minimum values were similar for the study area, the concentration at 5 cm should be larger than the necessary to damp the turbulence.

In coastal areas and estuaries concentration of suspended sediments are in most cases greater than the estimated value of 8.2 mg/l. The determination of this concentration, as pointed out by Heathershaw (1979) were based upon the assumption of a constant stress layer and logarithmic velocitiy profiles. But these assumptions are not present at all times during tidal flow. Therefore, further analysis have to be made of this problem before this result may be extrapolated to other situations.

Phillips (1980) described the effect of a vertical density gradient on turbulence by considering the effect of buoyancy on fluid elements. If the density distribution is statistically unstable, a water particle moving upward will have greater buoyancy than those moving downward. On the contrary, when the density distribution is statistically stable, rising elements are less buoyant.

The Richardson number is defined as the ratio of buoyancy forces to inertial forces:

$$Ri = \frac{(-g/\rho_o)(\partial\rho/\partial z)}{(\partial U/\partial z)^2}$$

where ρ_o is the mean density of the water column; g, the acceleration of gravity. Pond and Pickard (1978) indicated that when $Ri < 0$ the turbulence might be enhanced by the density gradient. However, if $Ri > 0$, the turbulence tends to decrease in intensity. Phillips (1980) suggested that when $Ri > 1$, turbulence is unable to maintain itself, because the rate of energy loss from the turbulence working against the buoyancy gradient exceeds the rate of which turbulence is generated by the mean flow.

All values of Ri calculated from density and mean velocity data, excluding one, were larger than 1.0. The data corresponding to record P1-03 gave $Ri = 0.05$ which indicated nearly neutral conditions.

Up to this point, the proposed processes of turbulence reduction acted on the vertical component of the flow. However, the observed results especially from the spectra showed that the horizontal component has suffered the largest reduction.

Based on the drag coefficient C_{100} calculated by Ludwick (1975) for the Chesapeake Bay entrance, the drag coefficient C_5 may be estimated, assuming that the velocity profile is logarithmic. The mean C_5 equalled 0.609. The quadratic shear stress law may be written as:

$$\tau_o = \rho \, C_5 \, \bar{U}_5^2 \qquad (4.4)$$

where $\bar{U}_5$ is the time averaged velocity at 5 cm above the bottom. Under the assumption that the level of measurement was within the constant stress layer (Townsend, 1976), equations (4.1) and (4.4) can be equated, to yield

$$- \overline{uw} = C_5 \, \bar{U}_5^2 \qquad (4.5)$$

There are many examples of variability in the drag coefficient (Sternberg, 1968; Ludwick, 1975; and Heathershaw and Simpson, 1978). However, if as a first approximation, C_5 is assumed constant for a particular flow condition and bed configuration, changes in the mean velocity will produce large variations in the turbulence.

In particular, one can assume that the most affected should be u since it is more closely related to the mean flow.

4.5 Conclusions

The following items summarize the results obtained from study of the flow measurements and density profiles described in the present chapter:

1. Surface currents at the site of the sand wave ranged in velocity from 7.13 to 282.17 cm/s. Tidal currents were of rotating type and were related to changes in elevation of the surface of the water as if they were formed by a quasi-progressive wave.

2. Density profiles were stably stratified; with a pycnocline formed in the afternoon hours.

3. Time series analysis of data taken at 5 cm above the surface of the sand wave revealed three types of constituents: (a) long period trends, (b) wave period phenomena, and (c) turbulence.

(a) Long period trends were observed almost exclusively in the U(t) component. No explanation was sought for them, but it is possible to draw the weak inference that they may be produced by internal waves since density conditions were appropriate for development of internal waves.

(b) Waves were the second element in prominence
in the records. Spectral analysis data of two
periods (12.82 and 10.94 seconds) were helpful in
determination of the wave parameters. The phenomena
was found to be waves generated at least 1000 km
south to southeast and the entrance to the Chesapeake
Bay. Wave height and wave steepness were too small
to be observed during the field experiment.

(c) The turbulent part of the flow was found
to be highly damped, although it preserved the slope
in power versus frequency corresponding to the
inertial subrange of the spectra. In all cases but
one, the energy of U was smaller than the energy
of W. Two possible explanations for this have been
suggested by Heathershaw (1979) but in most cases
the explanations resulted in the damping of the
vertical component rather than the horizontal compo-
nent of the flow.

A third explanation was considered by calculating
a value for the drag coefficient (C_5) for use with
the mean velocity measured at 5 cm above the bed.
The resulting comparison indicated that the mean
velocity would strongly affect the intensity of the
turbulence. That is, a reduction in $\bar{U}_5$ resulted
in a strong reduction in uw, mainly in u.

4. The plots of the instantaneous shear stress showed two types of events. The dominant events, which may define τ, had values very close to zero. The second component was few large spikes, which contributed more than 1% to the value of τ, but their duration was too small to have a decisive influence in $|\tau|$.

An analysis of the behavior of u and w during the events, showed that in most situations w was the driving force that generated the spikes.

Finally, the research described in this chapter shows that measurements of turbulent flow in open waters with highly stable density structures and large concentration of suspended sediment may result in the reduction of turbulence. Under these conditions, the profile methods for determination of the shear stress of the boundary which uses mean values is statistically more reliable. For unsteady conditions, records of fluctuating velocities can not be long enough to retain a statistically significant number of large spikes; unfortunately, these features seem to be a normal characteristic of geostrophic flows near a boundary.

Chapter 5

SUMMARY AND CONCLUSIONS

A sand wave in lower Chesapeake Bay was studied for morphology and sedimentology, as well as in terms of dynamic processes. From the bathymetric analysis, it was observed that the feature is part of a sand wave field developed on the northeast flank of a shallow area known as the Horseshoe. On the flank of the shoal (Horseshoe), a ridge and channel system was observed. These structures are two elongated elevations separated by a depression trending in a south-southeast direction. In the ebb dominated channel the sand waves are smaller than those observed atop the ridges. All sand waves in the field present their lee faces to the south-southeast, which indicates a net direction of migration related to ebb currents. On the other hand, the constant position of the sand wave with time, the absence of ripples, and the presence of flats between sand waves indicate that migration is not presently occurring or is too small to be detected.

Several bedforms in the area, including the subject sand wave, are in effect "solitary" sand waves.

92

This concept has been introduced to describe the state of a sand wave on which further evolution tends to be independent of the adjacent bedforms.

The sediments that form the sand wave are medium sands. Sediments representing relatively high energy were found on the crest; progressively finer material was observed down the flanks. The lee and flat sediments of the southern side were finer and poorly sorted compared to those of the stoss side and the northern flat.

Although medium sands are indicative of relatively high energy environments, the high bioturbation found in the box cores and the reduction zone encountered in both the samples and cores define a low energy environment where there is little or no reworking. The channel sands described by Shideler (1975) can not be transported by the present hydraulic regime. It is probable that only fine material, mostly transported in suspension and represented by subpopulation B' (Fig. 10), is continually introduced and eliminated from the system (the sand wave) by the currents. From a velocity profile obtained at maximum flood (P1-02), the calculated shear stress was about 0.14 dyn/cm^2. This value was consistent with the measured low free stream velocity, but was not large enough to exceed the threshold of any grain sizes found in the sand wave.

Both flow measurements and vertical profiles of density over the sand wave were obtained during the present study. Rotary surface currents due primarily to tidal action ranged in velocity from 7.13 to 282.17 cm/s. As a result of the measurements of the Reynolds stresses, the turbulence was found to be damped. The lower frequency components of the flow were far more important than the high frequencies. These low frequency components were defined as (a) long period trends, and (b) waves-associated events. The long period trends are probably generated by internal waves. The waves were swell-generated in an area at least 1000 km east to southeast of the entrance to Chesapeake Bay.

From the spectral analysis of the velocity records, the upper limit of turbulence was defined at 0.7 Hz. The energy contained at higher frequencies was two to three orders of magnitude smaller than the energy present in the low frequencies. As a result of the low level of turbulence, the shear stresses calculated by the Reynolds stress method were very small and, in most cases, negative. In plots of the instantaneous shear stress as a function of time, two types of events were found. The dominant events had mean values very close to zero. The other events consisted of large spikes with peak values up to 119 dyn/cm^2; however, their duration was too small to have a decisive influence on $|\tau|$.

From the detailed analysis of several large spikes, an explanation for the negative value of τ was sought. In most cases, perturbation velocities u and w were of the same sign and switched intermittently and almost simultaneously during the entire event. With few exceptions, $|w|$ was always larger than $|u|$ in these events. The coherent behavior and the similarity in sign suggest that the effect of elements in the wave range of frequencies is the driving mechanism.

The most striking feature of the spectral analysis is that the turbulence due to the horizontal component of the flow is highly reduced. Although the concentration of suspended sediments and the density stability are high, their damping effect on the turbulence would be expected to act mainly on the vertical component. The low mean velocity seems to be the main factor reducing the turbulence.

From the integration of the bathymetry, sedimentology, and flow measurements, it is concluded that the shape of the feature studied plays an important role on the local circulation pattern and the resulting mean velocity associated over the sand wave. If the sand wave were a long two-dimensional body transverse to the flow, both theoretical and experimental estimates would predict that the shear stress could increase up the stoss side, and reach a maximum some distance upcurrent from the crest.

Since crest length cannot be assumed to be infinite in this area, the sand wave is believed to behave as a three-dimensional structure, and flow avoidance must thus be taken into account.

Evidently, dynamic conditions over the sand wave field are affected by two types of avoidance. First, the main currents generated by the tide flow mainly into the Chesapeake Channel. Second, the remaining currents, which move over the sand wave field, are also diverted into minor channels of the kind described in the section on general bathymetry of the area. These two avoidance processes reduce considerably the strength of the mean current atop the sand wave. Based on the foregoing, the sand wave is concluded to be a feature in static equilibrium with the environment, at least during calm weather. Shear stresses large enough to exceed the threshold of the sediment may be found during extreme conditions such as storms.

Two approaches are proposed for future study of the area. First, the potential flow field on the sand wave should be analyzed theoretically. The sand wave should be assumed to be a three dimensional body, and the flow field should be taken to be rotary. The second approach may be viewed as a complementary study. Field measurements of vertical current profiles of several locations on the sand wave and the areas around it should be made,

specifically, at both lateral ends of the feature. Comparisons of bathymetric surveys performed at different times could provide valuable information on the evolution of the sand wave.

TABLES

TABLE I

Averages of Inclusive Graphic Parameters.

Parameter	Overall	Crest	Stoss	Lee	Flat
Mean $(M_\emptyset)$	1.61	1.35	1.56	1.52	1.91
Standard Deviation $(\sigma_\emptyset)$	0.50	0.48	0.49	0.49	0.54
Skewness	-0.08	-0.09	-0.18	-0.16	0.10
Kurtosis	1.24	1.04	1.12	1.08	1.62
Median $(Md_\emptyset)$	1.62	1.35	1.55	1.53	1.95
Longest Grain (mm)	3.02	3.40	3.10	2.93	2.71

TABLE II

Frequency weight percent material in Phi grain-size fraction.

Samples	Gravel >-1 ∅	V. Coarse -1-0 ∅	Variables Sand Coarse 0-1 ∅	Medium 1-2 ∅	Fine 2-3 ∅	V. Fine 3-4 ∅	Mud <4 ∅
L1	0.09	0.75	15.13	69.00	12.67	0.64	1.71
F2	0.12	0.18	1.04	59.46	25.85	4.34	9.01
F3	0.21	0.42	0.88	34.50	31.83	8.45	23.73
S4	0.01	0.87	15.03	69.13	12.65	0.63	1.67
S5	0.80	0.92	16.12	68.67	11.01	0.63	1.86
L6	0.05	0.47	17.49	71.39	9.03	0.25	1.32
C7	0.16	1.47	18.99	65.57	10.46	1.10	2.26
S8	0.05	0.85	9.91	63.83	21.97	1.16	2.23
S12	0.13	0.92	13.95	68.84	13.55	0.56	2.06
L13	0.27	0.37	2.72	43.41	29.36	7.72	16.16
F17	0.48	0.37	7.20	67.33	20.89	1.07	2.67
S18	0.17	0.54	9.02	69.70	17.62	0.77	2.18
C19	0.09	0.42	14.17	70.17	11.71	1.11	2.33
F20	0.12	0.41	2.18	55.03	34.32	2.86	5.08
L29	0.12	0.37	5.18	57.28	24.60	4.16	8.28
C30	0.08	0.29	12.68	77.65	8.06	0.16	1.07
S31	0.26	0.72	11.61	70.87	13.90	0.61	2.03
S32	0.11	0.65	13.38	72.89	11.37	0.28	1.31
F37	0.43	1.30	5.66	61.08	26.01	2.13	3.39
S38	0.08	0.71	13.44	68.84	13.97	0.88	2.08
C39	0.06	0.61	31.81	62.85	3.42	0.22	1.03
L40	0.28	0.55	13.58	67.46	13.34	1.54	3.23
L45	0.09	0.62	10.33	73.30	13.10	1.21	1.34
C46	0.00	1.00	35.92	61.27	0.99	0.01	0.80
S47	0.27	1.23	11.01	72.67	12.20	0.87	1.76

TABLE III

Eigenvalues, variance (%) and cumulative variance (%) for the
first seven vectors - Q-mode factor analysis

Vector	Eigenvalue	Variance (%)	Cumulative Variance (%)
1	23.7668	95.0671	95.0671
2	1.0193	4.0772	99.1443
3	0.1732	0.6929	99.8372
4	0.0392	0.1568	99.9940
5	0.0009	0.0038	99.9978
6	0.0004	0.0018	99.9995
7	0.0001	0.0005	100.0000

TABLE IV

Rotated factor scores - Q-mode factor analysis.

Variables	Factors I	II
Gravel	0.0390	0.2534
V. Coarse sand	0.8786	0.0120
Coarse sand	30.2904	-18.2911
Medium sand	70.2462	18.5845
Fine sand	-12.6937	43.0368
V. Fine sand	- 4.8013	8.9474
Mud	-10.9974	20.5312

TABLE V

Rotated factor matrix - Q-mode factor analysis

Samples	Factor I	Factor II	Communa- lity
L1	0.8398	0.5429	0.999
F2	0.6250	0.7782	0.996
F3	0.2812	0.9362	0.955
S4	0.8397	0.5430	0.999
S5	0.8518	0.5236	0.999
L6	0.8691	0.4942	0.999
C7	0.8604	0.5070	0.997
S8	0.7485	0.6596	0.995
S12	0.8294	0.5584	0.999
L13	0.4603	0.8814	0.988
F17	0.7490	0.6584	0.994
S18	0.7847	0.6165	0.995
C19	0.8398	0.5422	0.999
F20	0.5591	0.8184	0.982
L29	0.6549	0.7556	0.999
C30	0.8589	0.5045	0.992
S31	0.8198	0.5705	0.997
S32	0.8439	0.5343	0.997
F37	0.6834	0.7247	0.992
S38	0.8245	0.5655	0.999
C39	0.9181	0.3511	0.966
L40	0.8231	0.5677	0.999
L45	0.8218	0.5647	0.994
C46	0.9272	0.2968	0.947
S47	0.8284	0.5557	0.995

TABLE VI

Values for Shields criterion (θ_b) for the threshold of sediment motion and Bagnold's criterion (θ_s) for the threshold of suspension. τ_b and τ_s are the corresponding critical shear stresses. Grain sizes are the lower limit of population, except in Suspension B' which is the upper limit.

Population	Grain Size (mm)	θ_b	τ_b (dyn/cm^2)	θ_s	τ_s (dyn/cm^2)
Traction (C)	1.10	0.036	6.40	0.72	128.07
Saltation (A')	0.45	0.034	2.47	0.29	21.10
Graded Suspension (A)	0.21	0.047	1.60	0.10	3.40
Suspension (B')	0.09	-	-	0.092	1.34
Suspension (B)	0.09	-	-	>0.092	>1.34

TABLE VII

Summary of records obtained at 5 cm above the surface of the
sand wave.

Record	Station	Day	Time (1)	Azimuth (°True)	Slope Azimuth (°True)	Slope (°)	Density (g/cm³)
P1-02	P1	8/12/81	0904	188	045	7.43	1.018
P1-03	P1	8/12/81	1246	008	045	8.65	1.019
4-04	4	8/14/81	0821	038	000	1.25	1.018
3-04	3	8/14/81	0850	348	135	1.25	1.018
2-04	2	8/14/81	0934	013	270	11.07	1.017
1-04	1	8/14/81	1004	138	110	13.45	1.017
2-05	2	8/14/81	1041	038	160	8.65	1.018
3-05	3	8/14/81	1108	133	000	9.87	1.018
4-05	4	8/14/81	1147	158	090	2.49	1.018
3-06	3	8/14/81	1217	053	000	6.20	1.018
2-06	2	8/14/81	1342	258	135	2.49	1.018
1-06	1	8/14/81	1414	253	180	12.27	1.018
2-07	2	8/14/81	1457	268	180	9.87	1.018
3-07	3	8/14/81	1529	253	225	2.49	1.018
4-07	4	8/14/81	1621	298	-	0.00	1.018
3-08	3	8/14/81	1649	268	315	1.25	1.018
2-08	2	8/14/81	1726	293	135	3.73	1.018
1-08	1	8/14/81	1752	298	315	4.97	1.018

(1) Eastern Standard Time.

TABLE VIII

Summary of the velocity components and other parameters at 2 m below the surface.

Record	Vector (1)	$\bar{U}$ (cm/s)	$\sqrt{\bar{u}^2}$ (cm/s)	$\sqrt{\bar{v}^2}$ (cm/s)	Azimuth (2)	Time (3)
P1-02	–	7.13	3.63	3.27	159.02	0900
P1-03	–	282.17	15.74	11.28	290.87	1200
4-04	1	14.46	2.28	1.57	296.25	0814
3-04	2	18.87	3.08	1.40	311.45	0914
2-04	3	17.88	2.87	3.28	354.20	0925
1-04	4	14.34	2.33	2.06	040.15	1029
2-05	5	16.32	2.01	2.07	090.14	1038
3-05	6	26.59	1.68	1.09	118.02	1133
4-05	7	33.31	1.53	1.03	157.65	1138
3-06	8	50.23	1.40	1.08	146.24	1242
2-06	9	52.98	1.17	0.96	175.82	1342
1-06	10	58.00	1.95	1.37	148.49	1441
2-07	11	58.94	0.82	0.79	158.00	1449
3-07	12	42.78	0.91	1.01	167.71	1555
4-07	13	41.83	1.67	1.22	202.35	1605
3-08	14	29.25	1.27	1.85	248.50	1713
2-08	15	31.00	2.16	2.54	250.13	1719
1-08	16	37.38	2.34	1.87	314.16	1756

(1) Numbers correspond to vectors and marks in Figs. 26 and 27.
(2) Azimuth = Observed angle + Rotation angle (α). *Magnetic.
(3) Eastern Standard Time.

TABLE IX

Calculated wave parameters.

Frequency (Hz)	Period (sec)	L (1) (m)	Height (cm)	H/L_4(2) (10^{-4})	δ_ω(3) (cm)
0.078	12.82	115.4	3.38	2.9	C.61
0.094	10.64	94.7	3.44	3.6	0.55

(1) Local wavelenght

(2) Wave steepness

(3) Wave-boundary layer thickness

TABLE X

Summary of velocities and shear stress determined at 5 cm
above the bottom. Unfiltered data.

Record	$\bar{U}$ (cm/s)	$\bar{W}$ (cm/s)	$\sqrt{\overline{u'^2}}$ (cm/s)	$\sqrt{\overline{w'^2}}$ (cm/s)	τ (dyn/cm^2)
P1-02	1.09	-0.33	2.27	0.63	- 1.003
P1-03	14.71	-2.33	10.12	8.44	- 21.255
4-04	6.27	-1.38	7.95	1.16	7.433
3-04	3.64	-0.34	2.20	0.95	- 0.434
2-04	- 2.27	-1.57	1.93	0.55	- 0.775
1-04	- 1.83	-1.36	1.90	0.73	- 0.735
2-05	7.52	-1.23	7.83	0.88	2.553
3-05	23.68	-2.08	2.10	0.56	0.453
4-05	19.64	-1.17	1.99	0.65	- 0.047
3-06	12.00	-0.95	2.78	0.74	0.271
2-06	0.37	-0.49	2.68	2.84	- 1.589
1-06	4.93	0.01	3.78	4.25	- 2.252
2-07	0.30	-0.47	2.07	1.51	0.164
3-07	18.56	-2.99	3.97	1.50	1.232
4-07	0.47	-0.58	3.89	1.44	0.777
3-08	- 7.34	-0.61	1.39	0.42	0.035
2-08	10.81	0.07	3.35	0.65	- 0.887
1-08	23.66	-1.01	3.97	0.59	0.906

TABLE XI

Parameters calculated from equations (4-2) and (4-3)
for vertical velocity profile measured at station Pl

Parameters	Equation	
	(4-2)	(4-3)
u_* (cm/sec)	0.36	0.37
τ_0 (dyn/cm^2)	0.13	0.14
z_0 (cm)	0.17	--
$\bar{U}_0$ (cm/sec)	--	8.52
Coefficient of Correlation (R^2)	0.86	0.86

TABLE XII

Root-mean squares (rms), shear stress and shear velocity for
the measurements at 5 cm above the bottom. Data filtered at
$f_{\frac{1}{2}} = 0.2$ Hz.

Record	$\sqrt{\bar{u}^2}$ (cm/s)	$\sqrt{\bar{w}^2}$ (cm/s)	$\bar{\tau}$ (dyn/cm²)	$\dfrac{\sqrt{\bar{u}^2}}{\sqrt{\bar{w}^2}}$	u_* (cm/s)
P1-02	0.26	0.21	− 0.022	1.24	0.15
P1-03	1.61	4.32	− 4.854	0.37	2.13
4-04	1.22	4.13	0.032	0.30	0.18
3-04	0.42	0.73	0.192	0.58	0.43
2-04	0.20	0.16	− 0.008	1.25	0.09
1-04	0.26	0.25	− 0.014	1.04	0.12
2-05	0.42	0.27	0.024	1.56	0.15
3-05	0.51	0.24	0.031	1.71	0.17
4-05	0.36	0.37	− 0.036	0.97	0.19
3-06	0.32	0.35	− 0.013	0.91	0.11
2-06	0.51	1.56	− 0.360	0.33	0.59
1-06	0.70	2.29	− 0.793	0.31	0.88
2-07	0.34	0.76	− 0.014	0.45	0.12
3-07	0.52	0.71	− 0.007	0.73	0.08
4-07	0.44	0.73	− 0.084	0.60	0.29
3-08	0.21	0.16	− 0.005	1.31	0.07
2-03	0.33	0.22	− 0.006	1.50	0.08
1-08	0.42	0.26	0.023	1.62	0.15

TABLE XIII

Frequency percent distribution of $\tau(t)$ as a function of its
standard deviation (σ).

Record	$\bar{\tau}$ (dyn/cm^2)	σ (dyn/cm^2)	$+1\sigma$ (%)	$+2\sigma$ (%)	$+3\sigma$ (%)	$-\sigma$ (1)	$+\sigma$ (2)
P1-02	-0.022	0.083	90.55	97.06	98.57	19	8
P1-03	-4.854	9.41	88.06	95.61	98.04	13	9
4-04	0.032	0.33	96.92	98.63	99.19	4	26
3-04	0.192	1.66	97.67	98.77	99.07	2	27
2-04	-0.008	0.04	86.02	96.18	98.42	14	15
1-04	-0.014	0.10	91.40	97.07	98.52	15	17
2-05	0.024	0.13	85.29	95.34	97.85	12	17
3-05	0.031	0.14	88.77	96.71	98.62	19	14
4-05	-0.036	0.76	99.44	99.70	99.78	47	2
3-06	-0.013	0.12	83.50	95.14	98.17	11	13
2-06	-0.360	0.93	85.35	95.18	98.04	14	4
1-06	-0.793	1.90	86.03	95.63	98.90	17	7
2-07	-0.014	0.27	81.09	94.46	98.15	7	14
3-07	-0.007	0.56	90.77	97.34	98.75	20	19
4-07	-0.084	0.48	90.17	96.56	98.42	21	10
3-08	-0.005	0.04	83.33	96.36	98.36	9	14
2-08	-0.006	0.07	79.44	93.75	98.04	7	7
1-08	0.023	0.12	84.18	95.18	97.90	11	10

(1) Extreme number of standard deviation to the left of the mean.

(2) Extreme number of standard deviation to the right of the mean.

TABLE XIV

Distribution of events, defined as the sum of all $\zeta(t)$ between two succesive zero crossings, according to their sign.

Record	TOTAL			POSITIVE			NEGATIVE		
	Number of events	Sum (dyn/cm^2)	Mean (dyn/cm^2)	Number of events	Sum (dyn/cm^2)	Mean (dyn/cm^2)	Number of events	Sum (dyn/cm^2)	Mean (dyn/cm^2)
P1-02	1401	147.54	0.11	700	30.14	0.04	701	-117.40	-0.17
P1-03	1417	22155.52	15.64	708	1402.09	1.98	709	-20753.43	-29.27
4-04	1228	245.76	0.20	614	174.50	0.28	614	-71.26	-0.12
3-04	1539	953.81	0.62	770	858.82	1.12	769	-94.69	-0.12
2-04	1632	90.66	0.06	816	27.71	0.03	816	-62.95	-0.08
1-04	1567	159.79	0.10	784	52.68	0.07	783	-107.11	-0.14
2-05	1306	261.47	0.20	653	173.26	0.27	653	-88.21	-0.14
3-05	1565	275.94	0.18	782	199.13	0.25	783	-76.81	-0.10
4-05	1627	314.17	0.19	813	85.60	0.11	814	-228.57	-0.28
3-06	1603	279.39	0.17	801	111.59	0.14	802	-164.80	-0.28
2-06	1213	1772.05	1.46	606	325.71	0.54	607	-1446.34	-2.38
1-06	1607	4502.37	2.80	803	617.26	0.77	804	-3885.11	-4.83
2-07	1639	652.42	0.40	820	298.91	0.36	819	-353.51	-0.43
3-07	1531	934.92	0.61	765	454.17	0.59	766	-480.75	-0.63
4-07	1572	815.41	0.52	786	240.06	0.31	786	-575.35	-0.73
3-08	1210	70.01	0.06	605	27.73	0.05	605	-42.28	-0.07
2-08	1505	186.00	0.12	752	80.15	0.11	753	-105.85	-0.14
1-08	1551	284.55	0.18	775	189.05	0.24	776	-95.50	-0.12
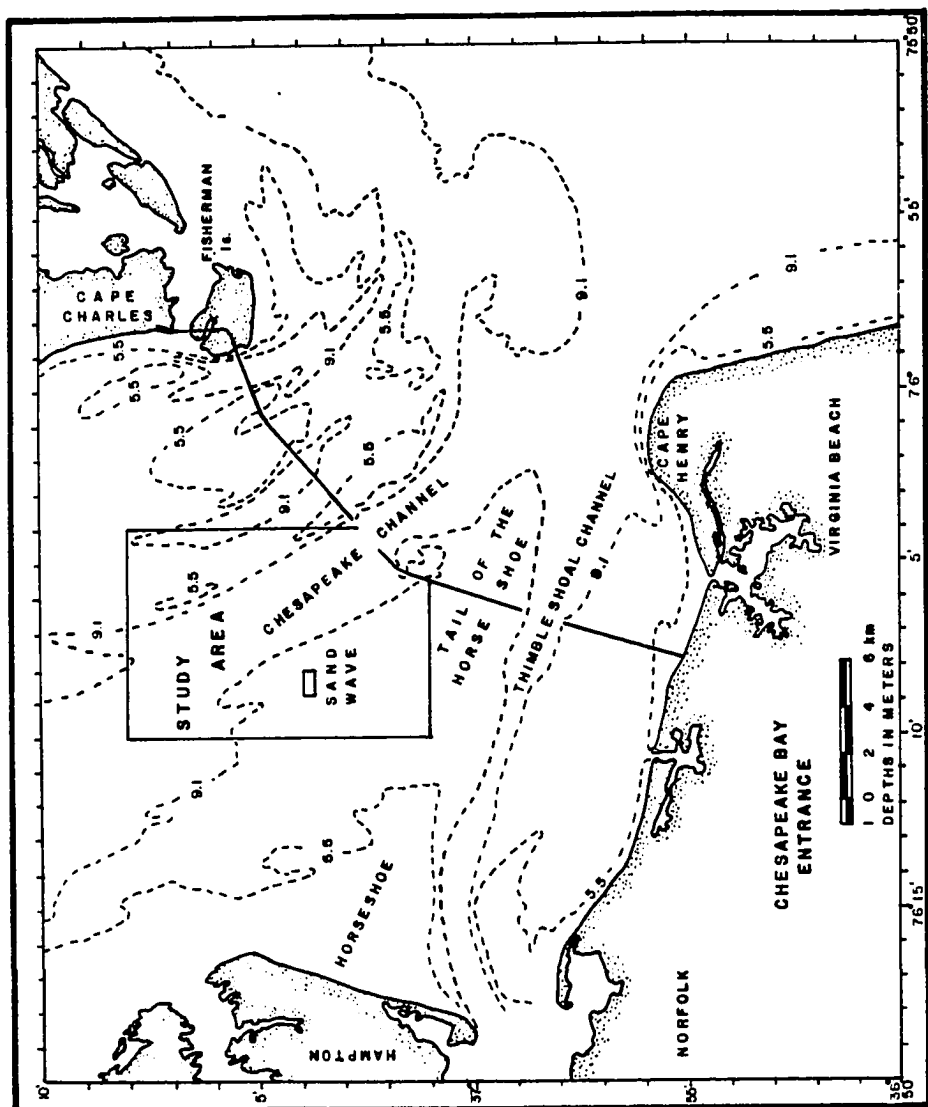
Fig. 1. Index map of general study area.

Fig. 2. Bathymetric chart of the sand wave field on
         the northern flank of the Horseshoe. The
         arrow points to the studied sand wave.

GENERAL BATHYMETRY
LOWER CHESAPEAKE BAY
JUNE 13, 1980

CHANNEL

RIDGE

RIDGE

RIPPLES

RIPPLES

DEPTH IN METERS
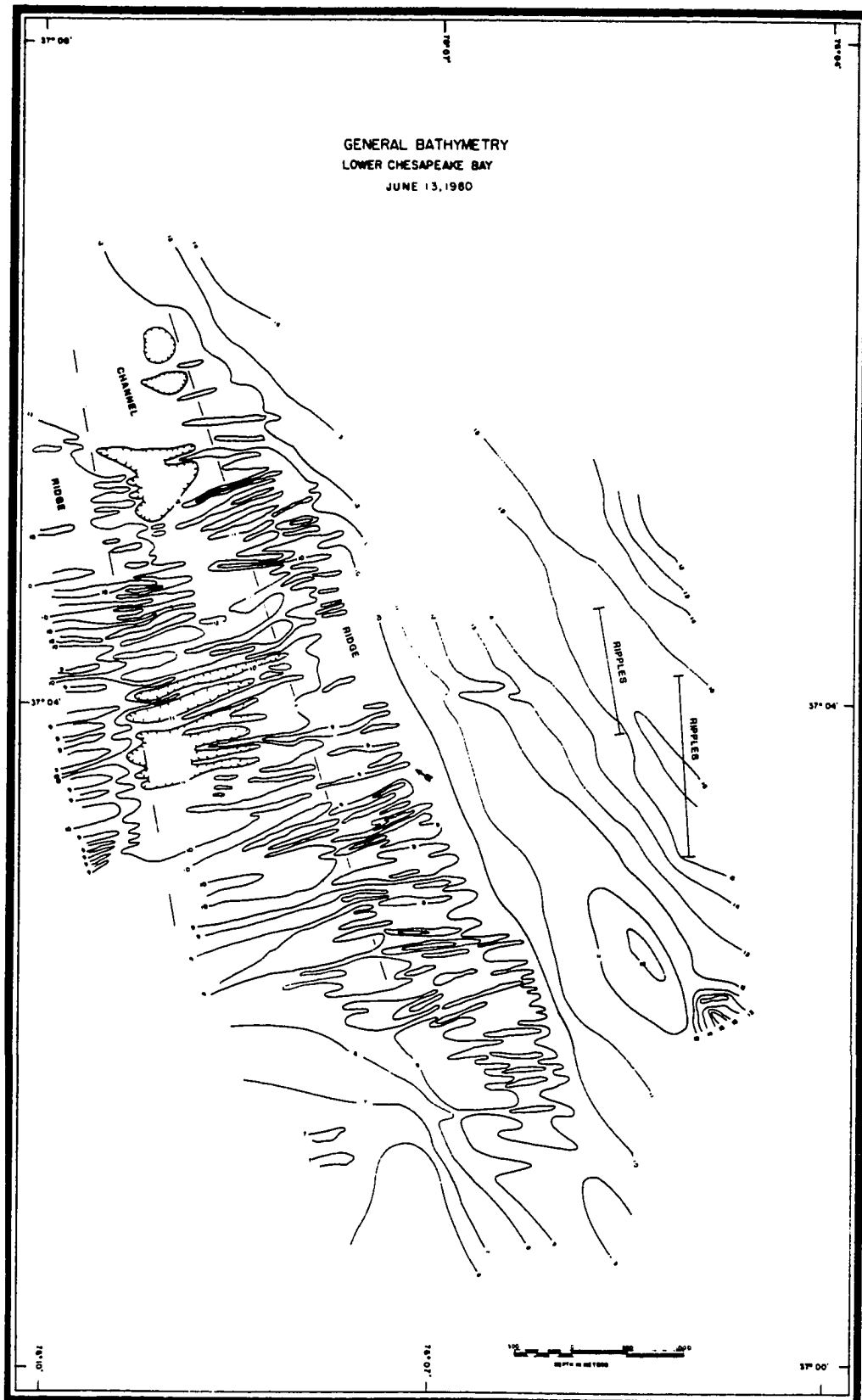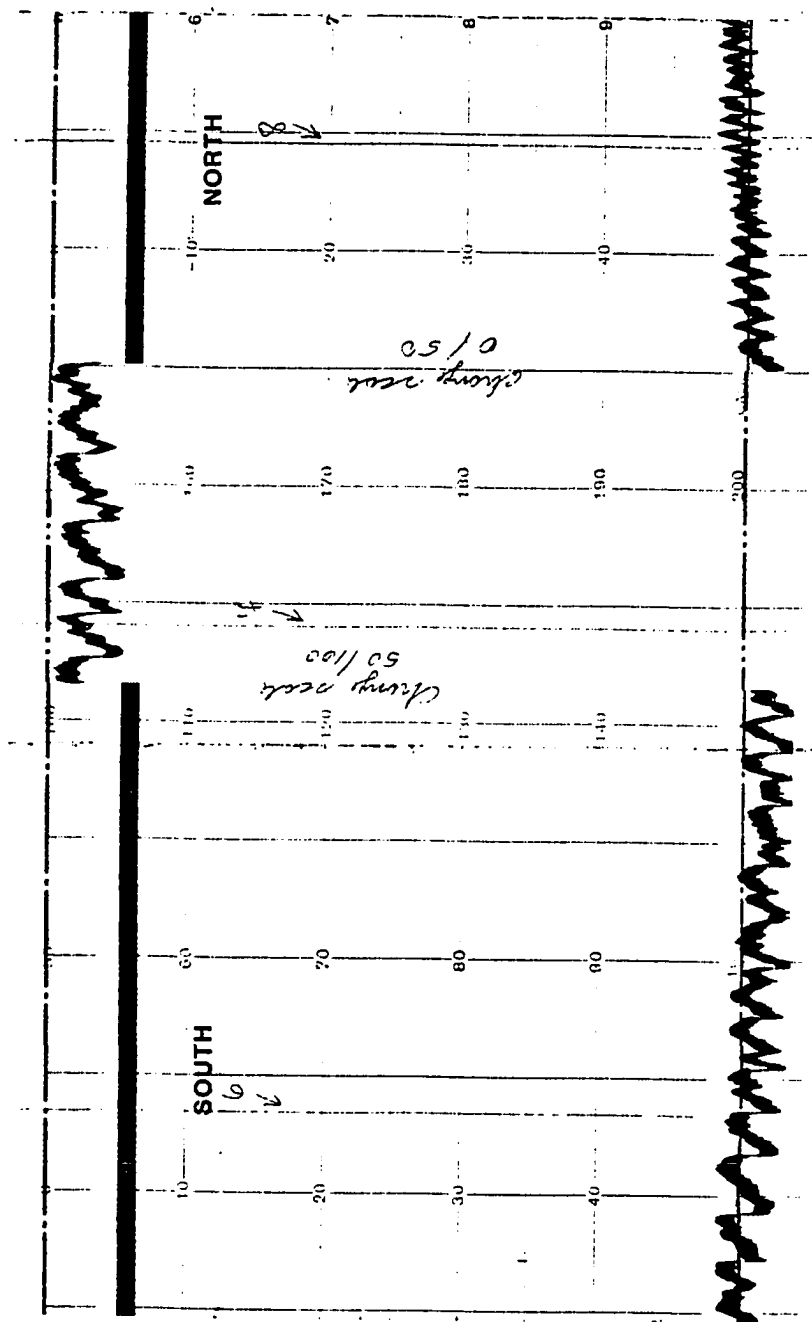
Fig. 3. Echosounding record of the field of ripples in the Chesapeake Channel. The distribution of the field is indicated in Fig. 2. Distance between fix marks is approximately 500 m. The vertical scale is in feet (1 foot = 0.3048 m).

Fig. 4. Bathymetric chart of the sand wave area. The
         sand wave studied in the present research is
         delimited by the isobath of 9 m at the center
         of the chart.

SAND WAVE BATHYMETRY
LOWER CHESAPEAKE BAY
JUNE 12, 1980
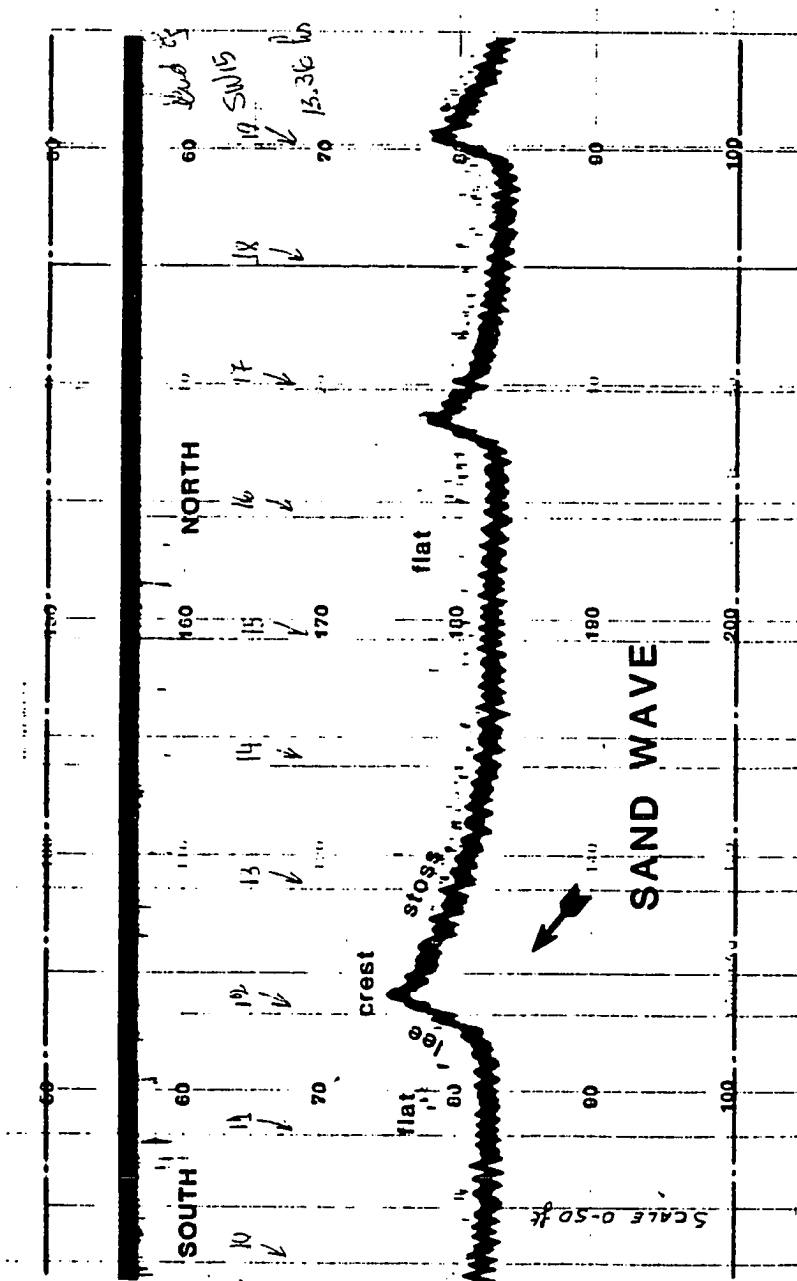
Fig. 5. Echosounding record of the sand wave. Distance between fix marks is approximately 49 m. The vertical scale is in feet (1 foot = 0.3048 m). The smaller features on the bottom record were produced by the rolling of the vessel due to surface waves.
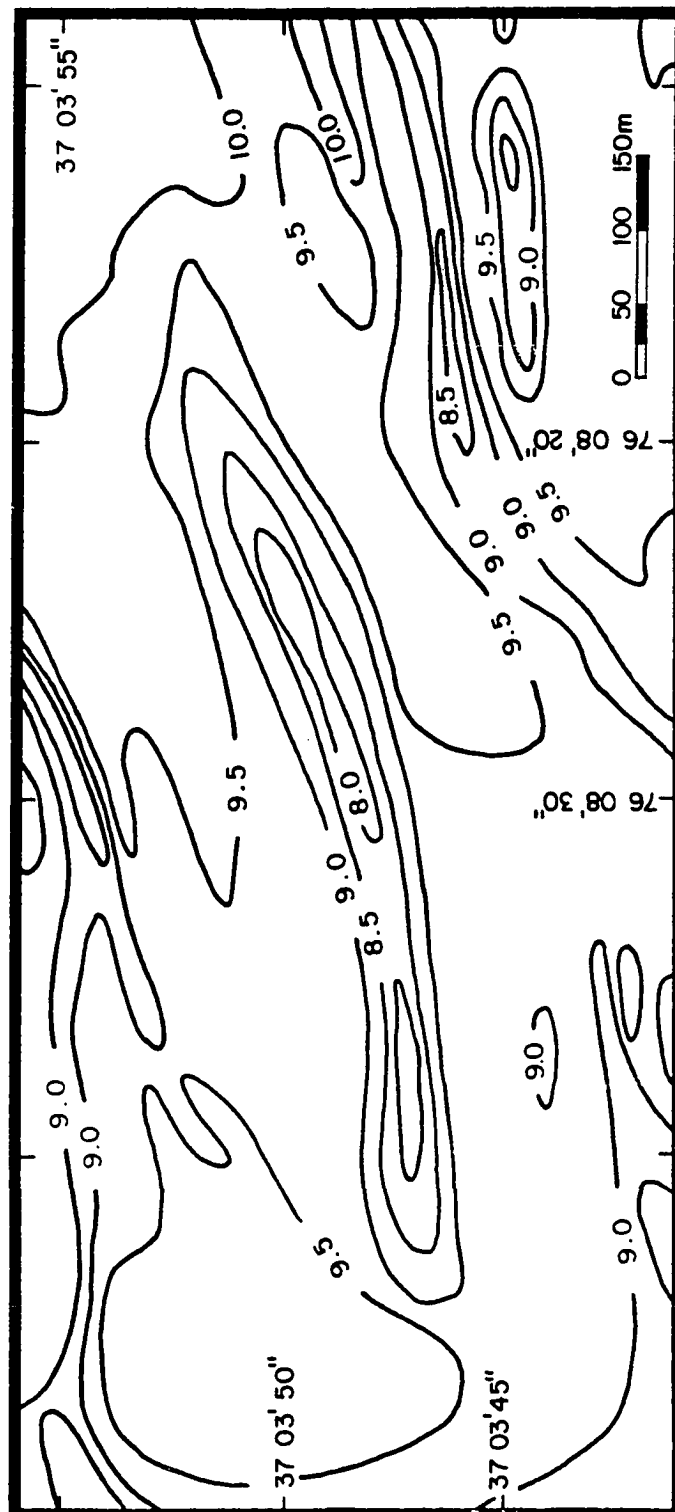
Fig. 6. Enlargement of the central portion of Fig. 4. The elongated feature at the center of the diagram is the sand wave sampled intensively.
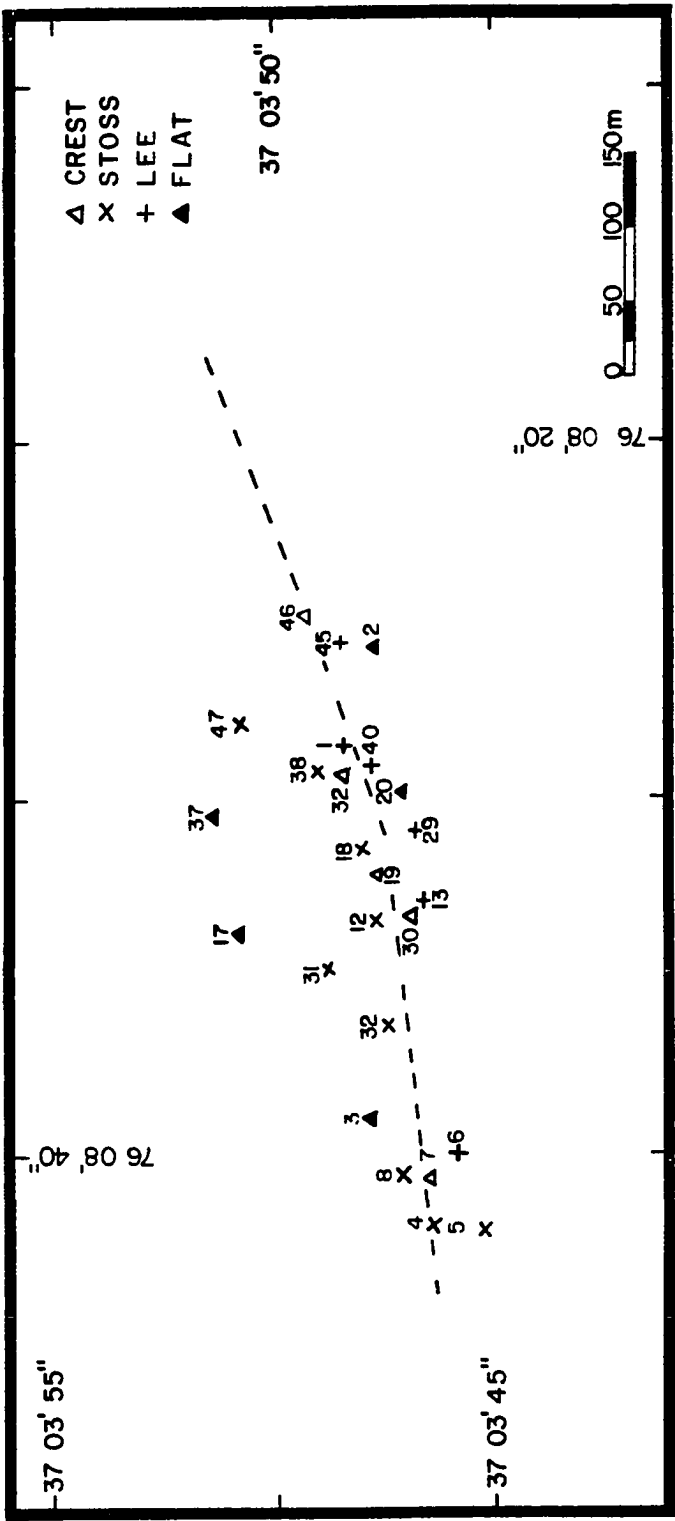
Fig. 7. Map of the location of Shipek samples. The position of the box cores 4, 5, 6, and 7 coincide with samples 31, 12, 19, and 29, respectively.
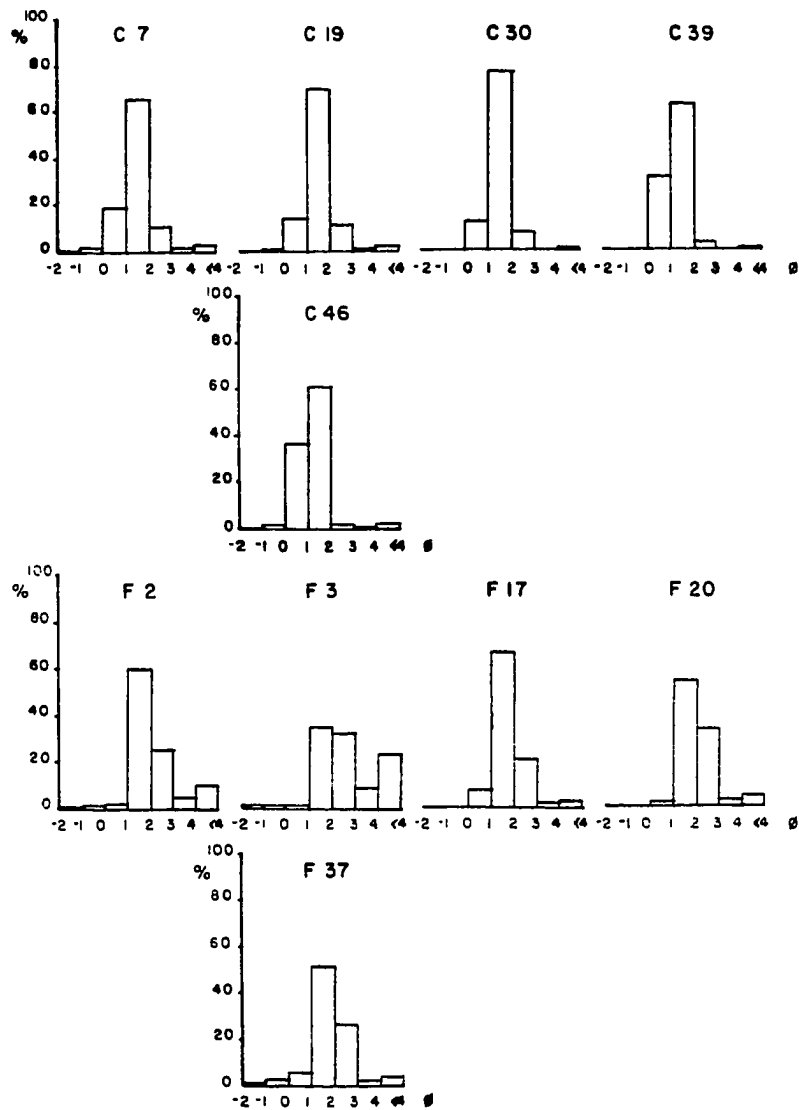
Fig. 8. Histogram representation of crest
(C) and flat (F) samples.
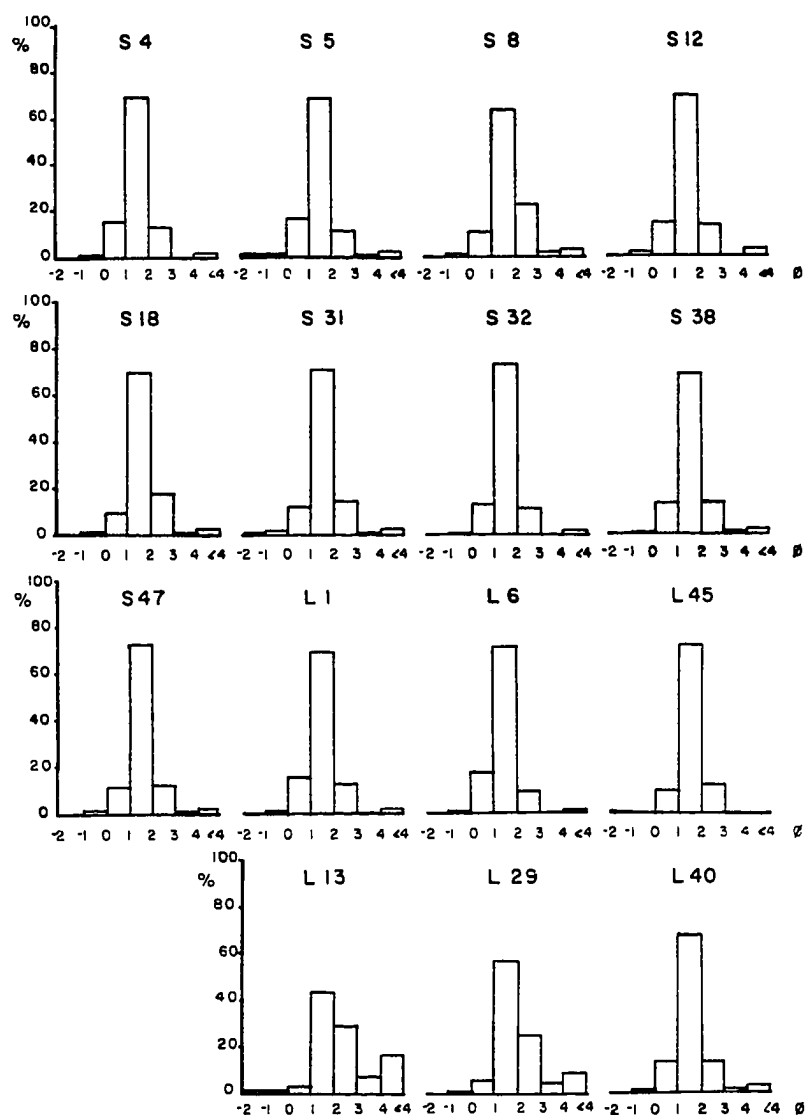
Fig. 9. Histogram representation of stoss
(S) and lee (L) samples.
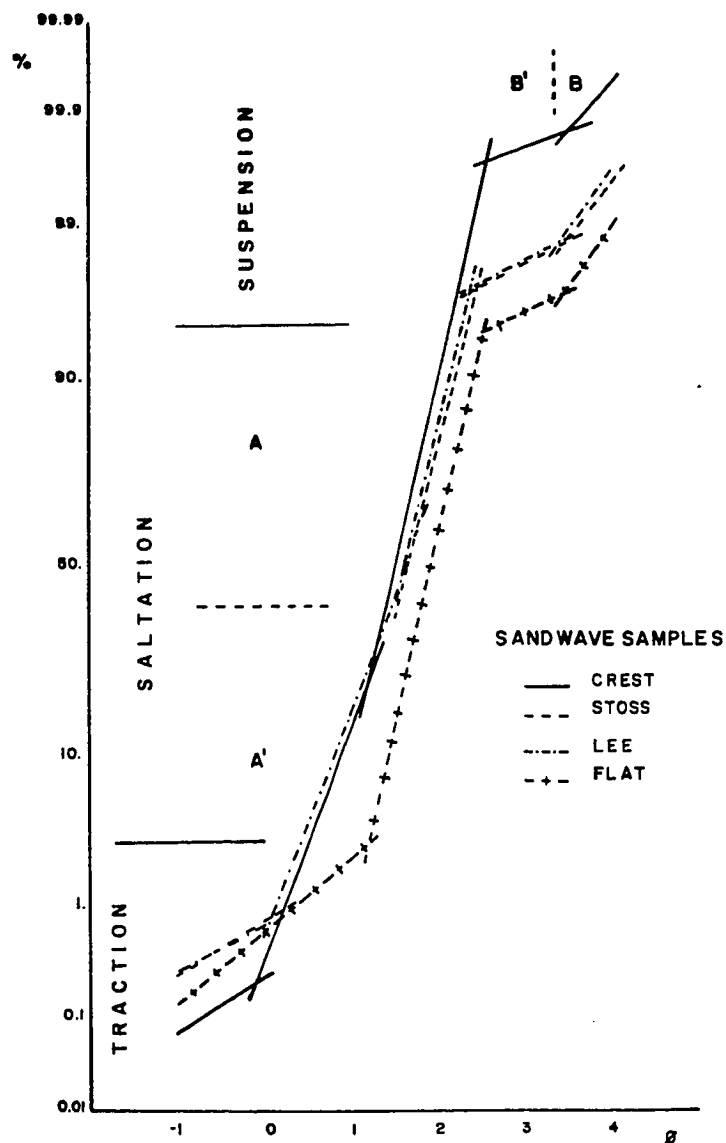
Fig. 10. Cumulative curves of four typical
samples representing each of the
segments in which the sand wave
was divided.
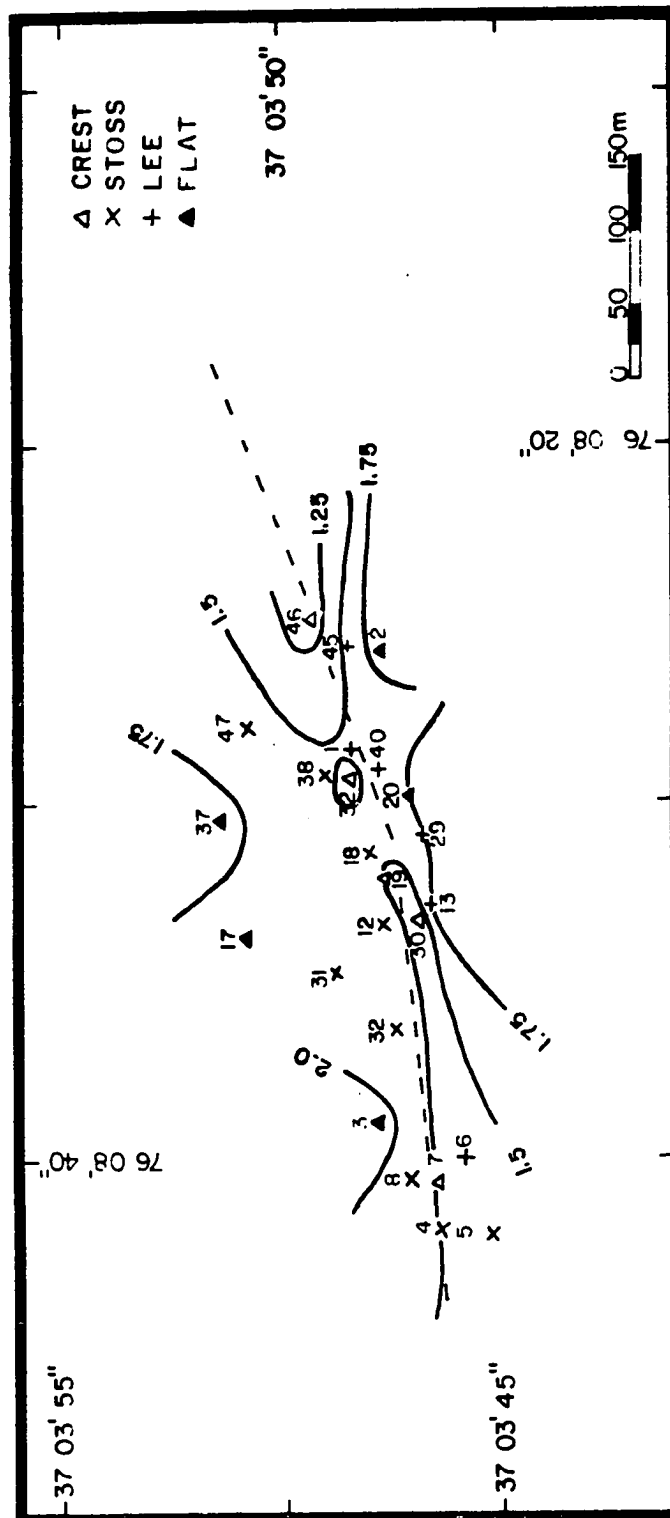
Fig. 11. Plan view distribution of textural parameters: Mean.
Equidistance = 0.25 ϕ.
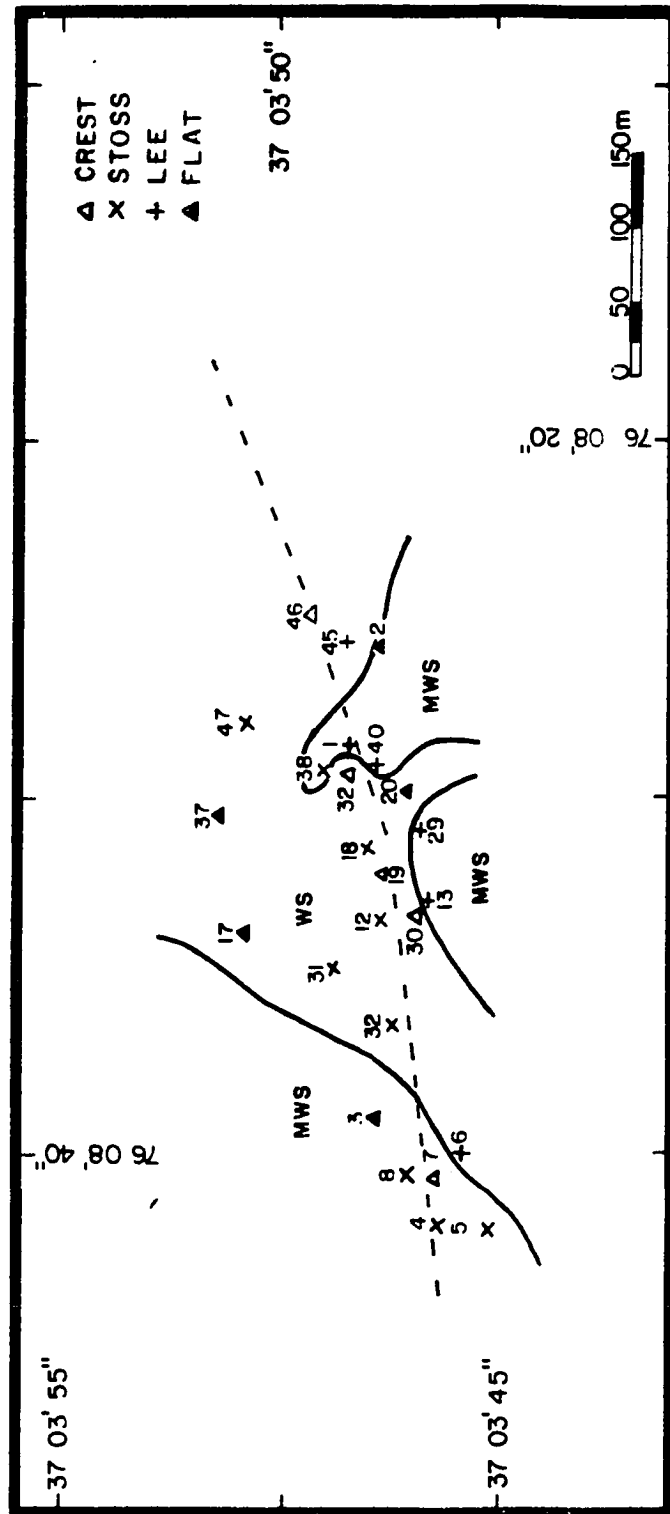
Fig. 12. Plan view distribution of textural parameters: Standard Deviation. WS = well sorted, MWS = moderately well sorted. Line represents $\sigma = 0.5 \emptyset$.
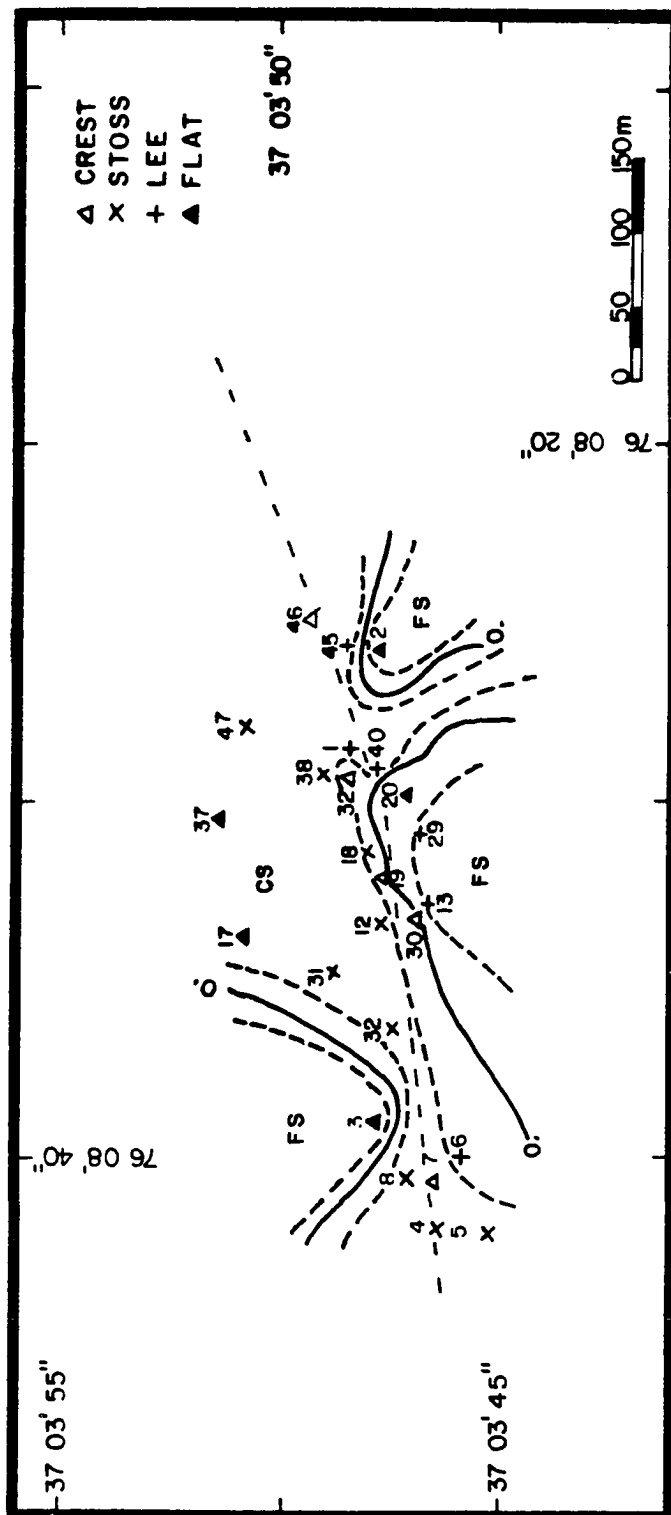
Fig. 13. Plan view distribution of textural parameters: Skewness. CS = coarse skewed, FS = fine skewed. Area between dashed line indicates nearly symmetric samples.

124
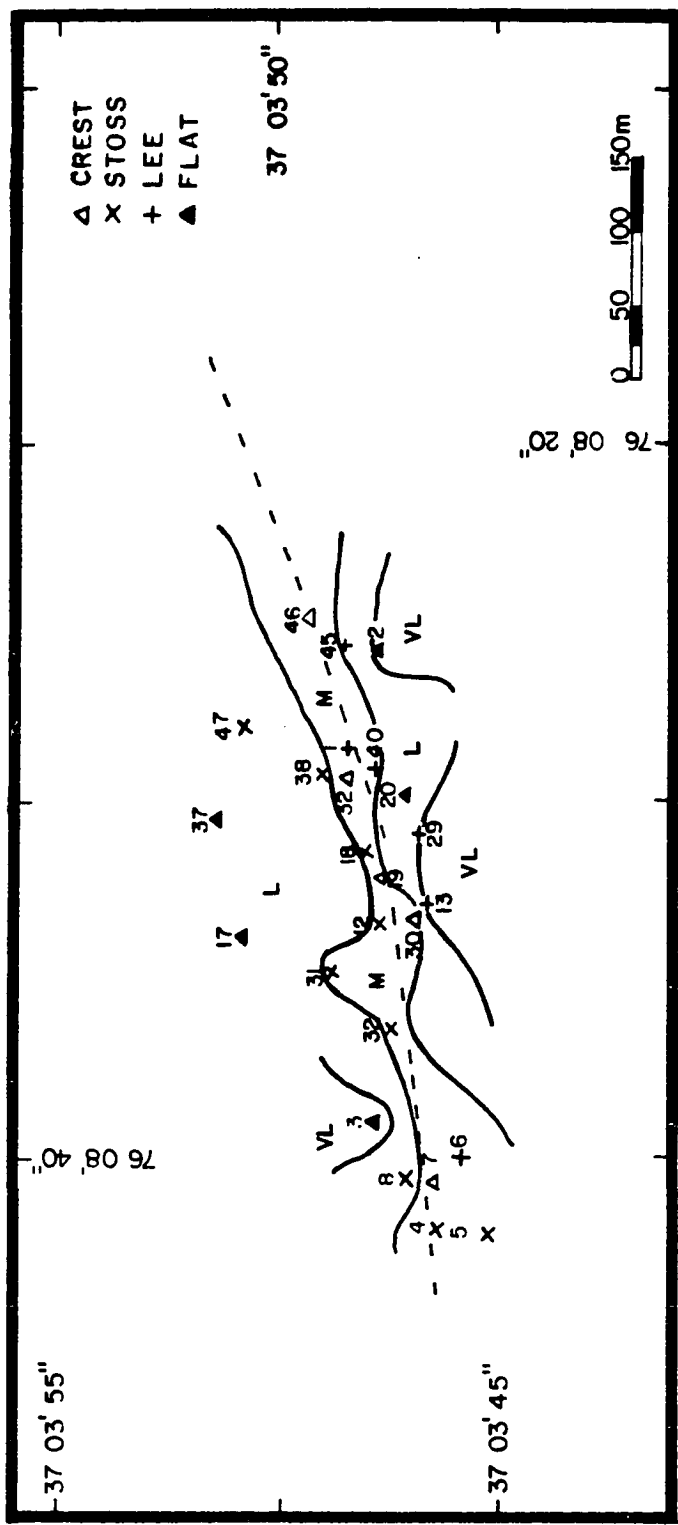
Fig. 14. Plan view distribution of textural parameters: Kurtosis.
M = mesokurtic, L = leptokurtic, VL = very leptokurtic.
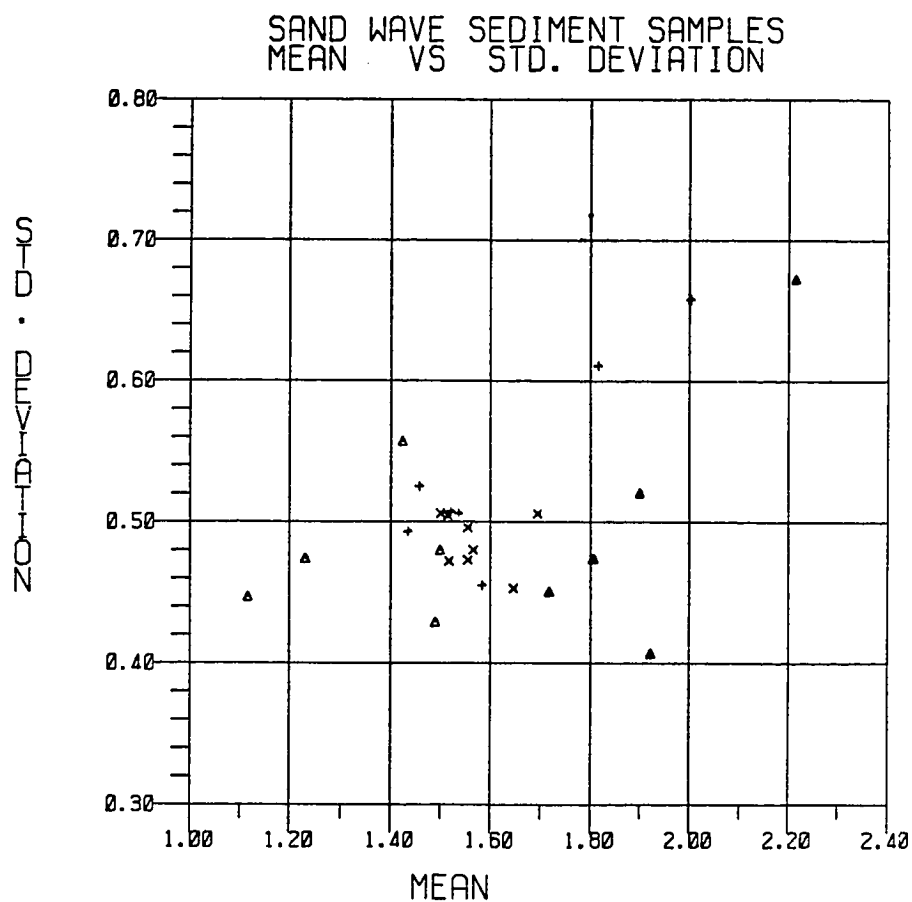
Fig. 15. Correlation between textural parameters:
Mean versus Standard Deviation.
Δ = crest, + = lee, x = stoss, ▲ = flat.
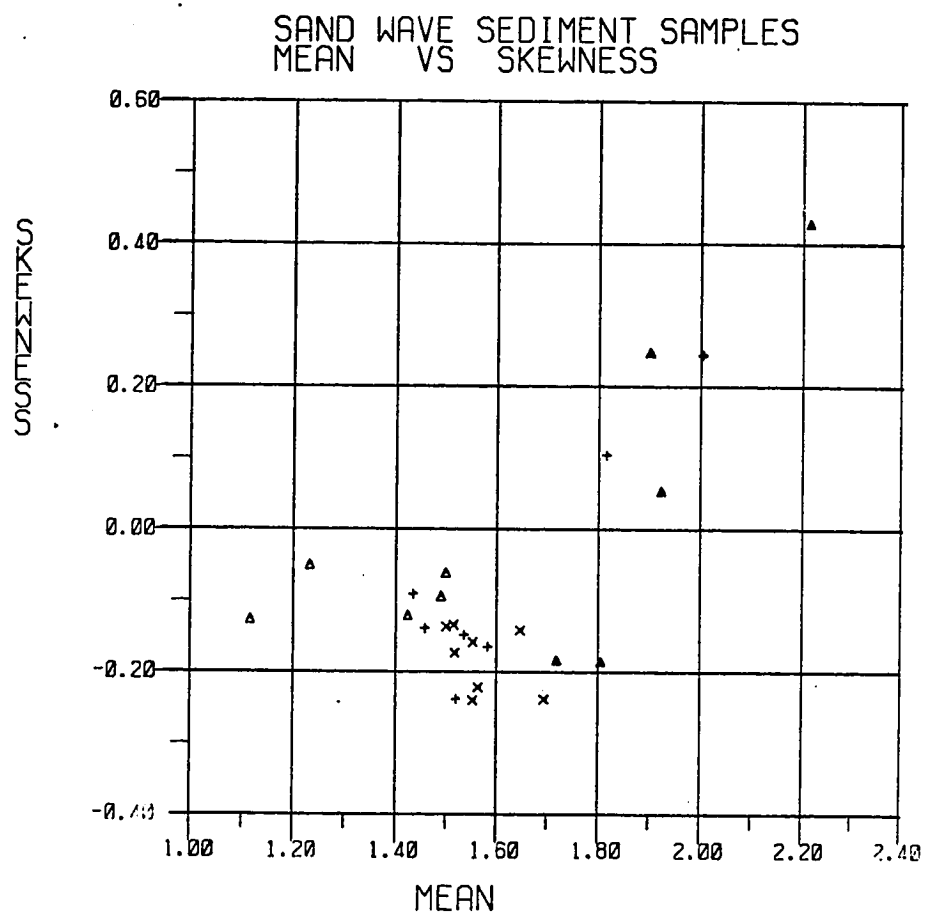
Fig. 16. Correlation between textural parameters:
Mean versus Skewness. Δ = crest,
+ = lee, x = stoss, ▲ = flat.
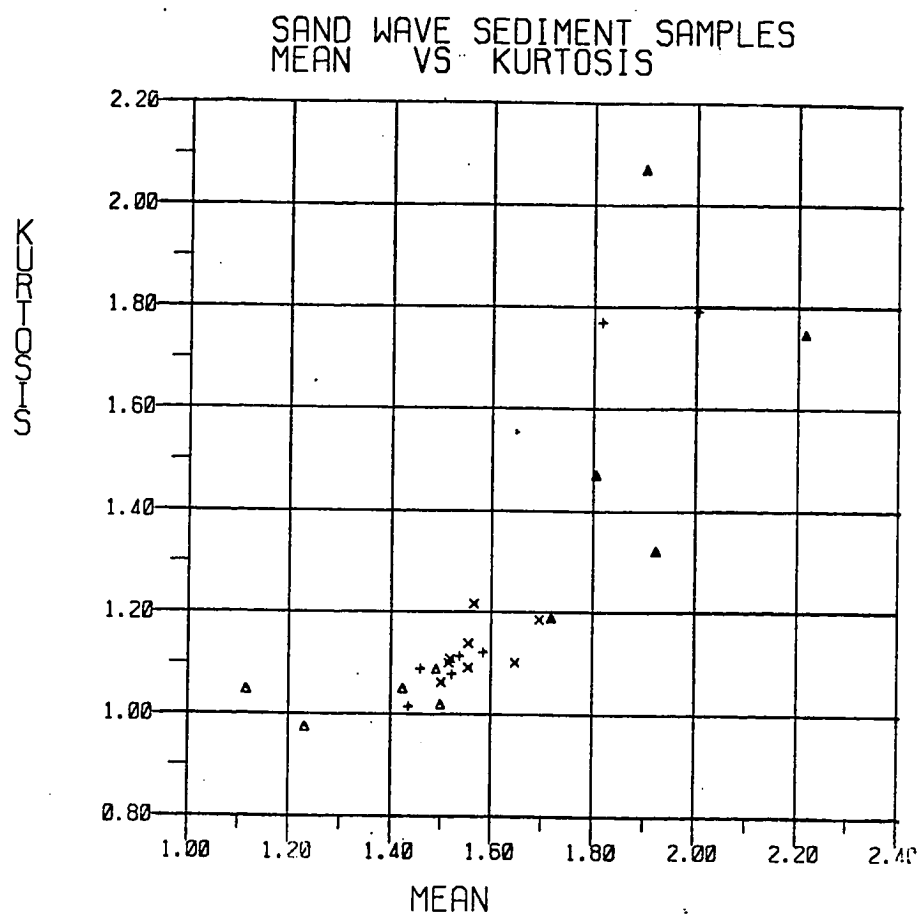
Fig. 17. Correlation between textural parameters: Mean versus Kurtosis. Δ = crest, + = lee, x = stoss, ▲ = flat.
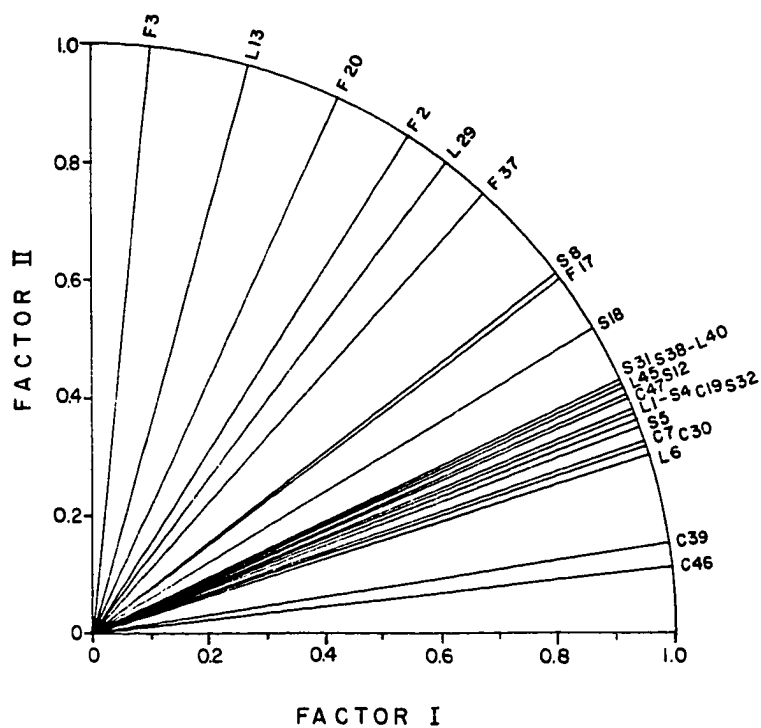
Fig. 18. Plot of rotated loadings for
factors I and II from Q-mode
factor analysis of the 25
samples.
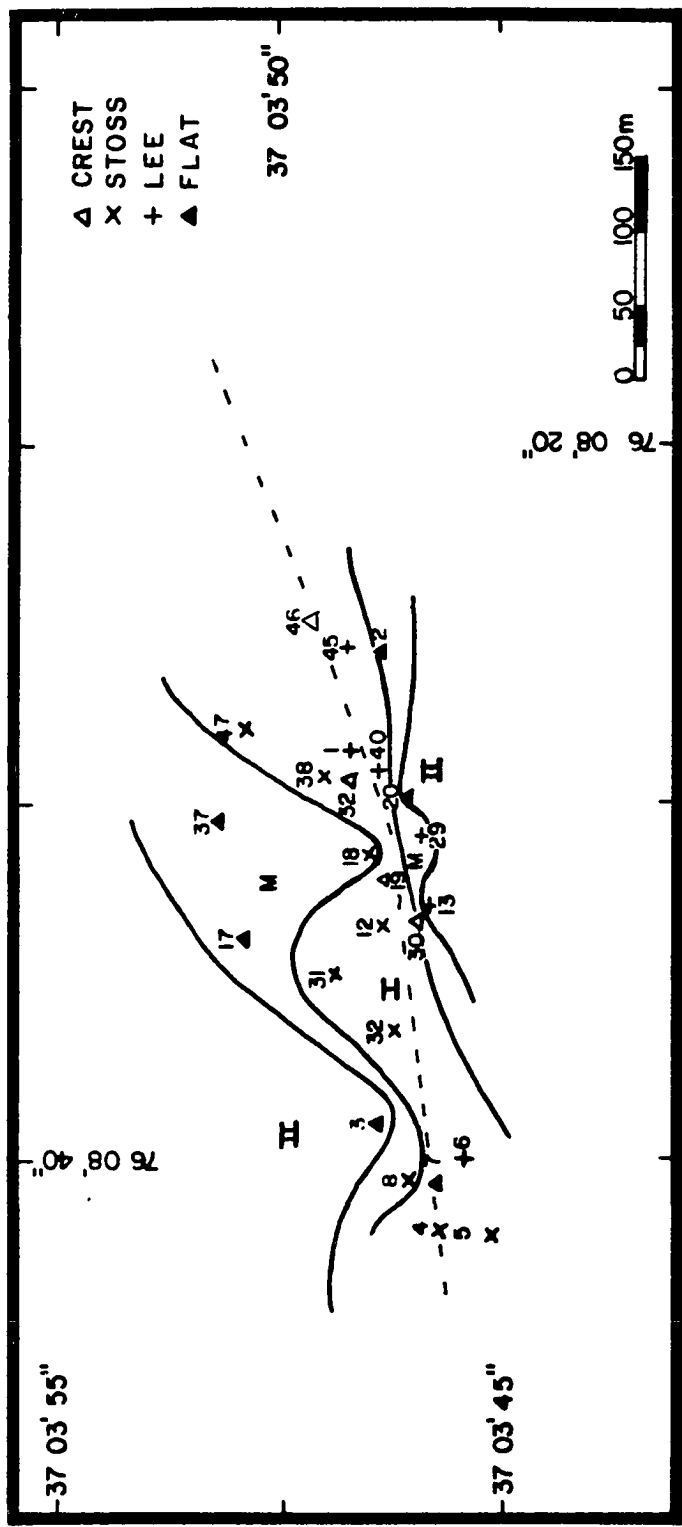
Fig. 19. Distribution of rotated factor loadings. I = 61% of factor I.
II = 61% of factor II. M = both factors between 41 and 60%.

SIZE ANALYSIS

Millimeters
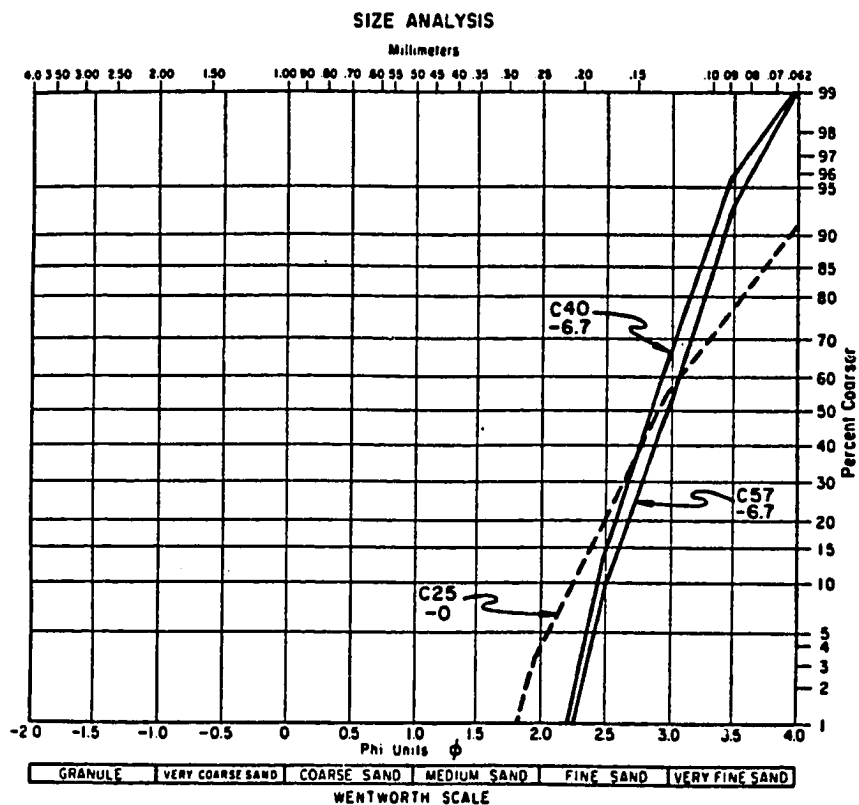
Fig. 20. Cumulative curves of typical samples
from the fine gray sand unit (after
Meisburger, 1972).
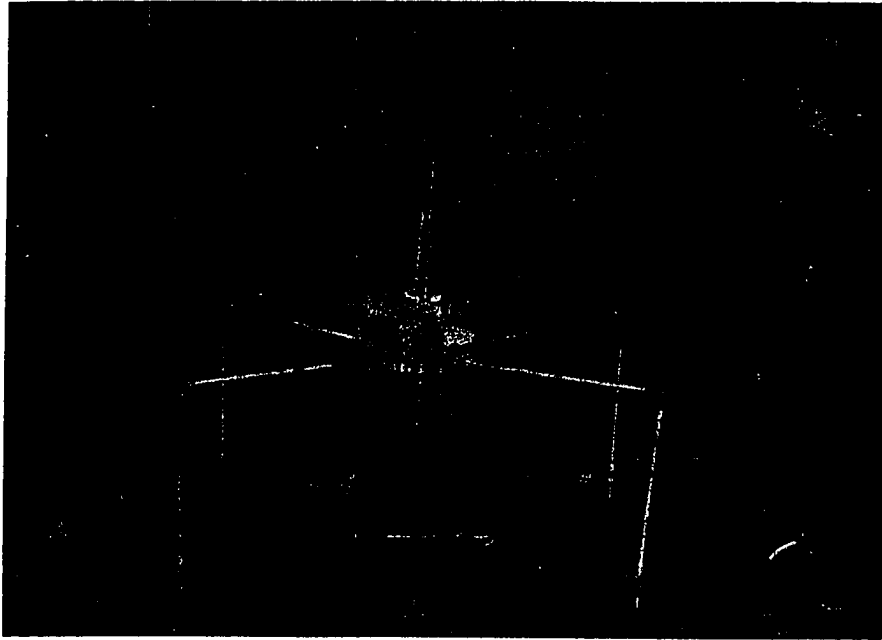
Fig. 21. Photography of the tetrapod in the present study.
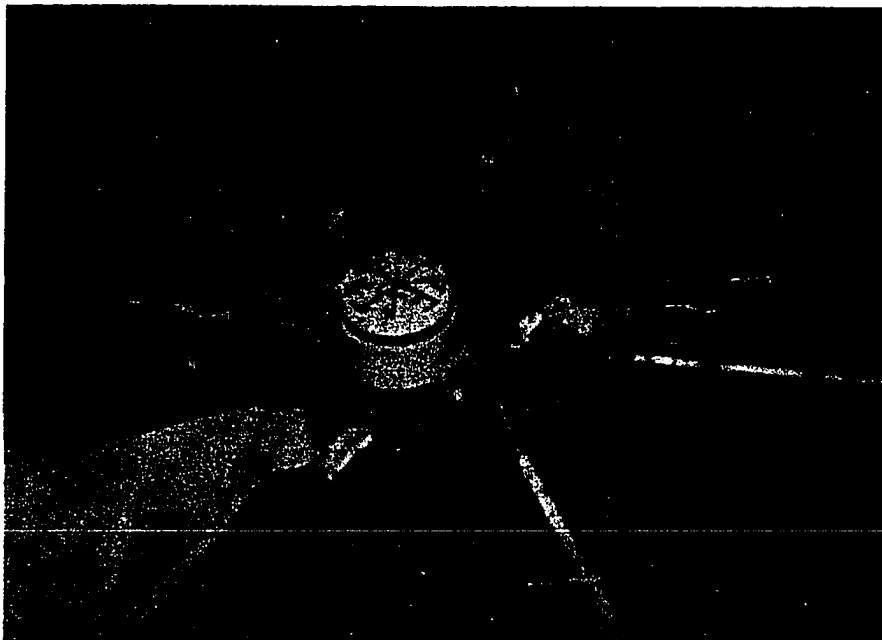
Fig. 22. Photography of the central platform of the tetrapod.
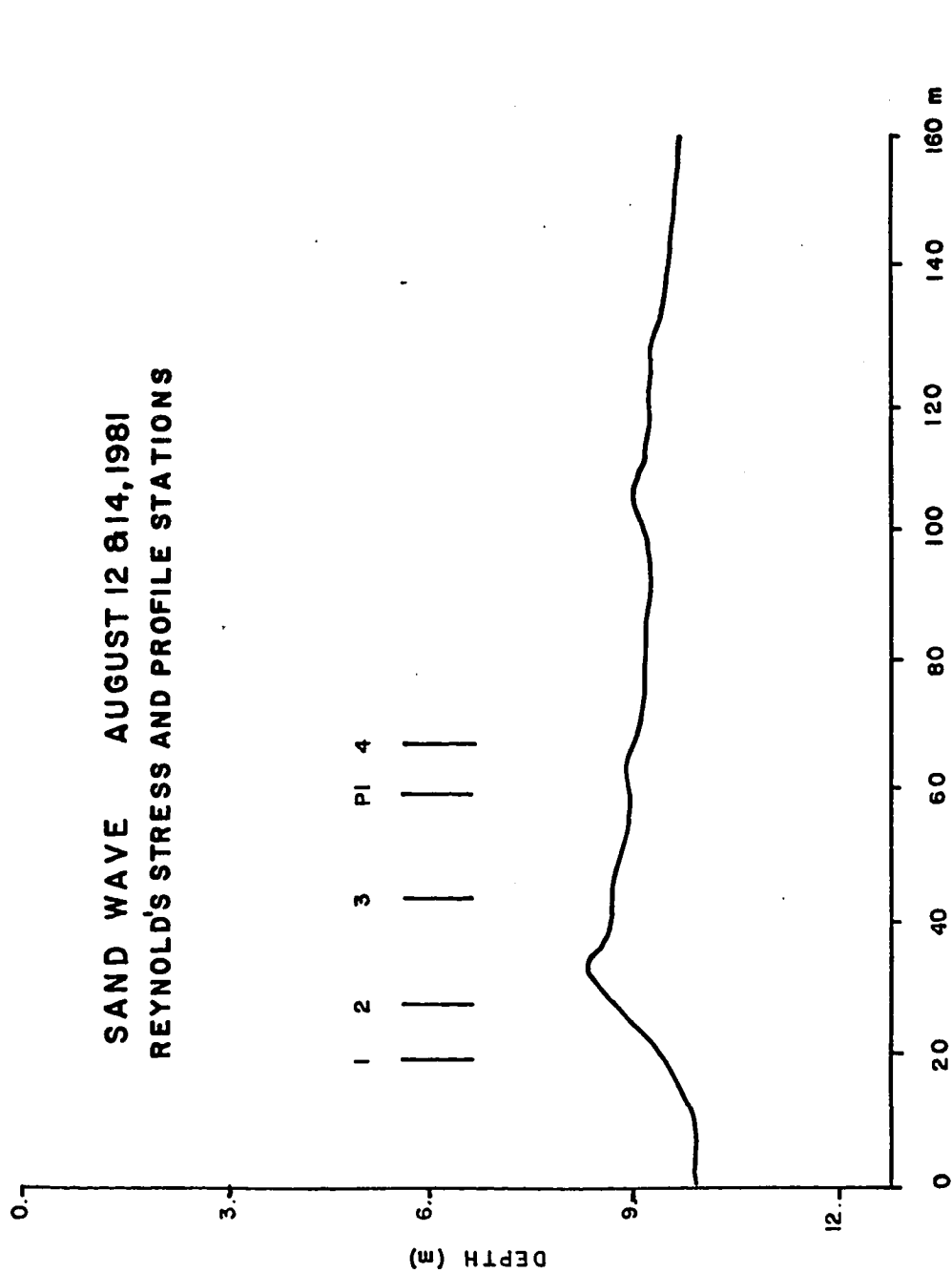
Fig. 23. Distribution of the stations along the profile of the sand wave. Station P1 was occupied twice on August 12, 1981. Five iterations were made on stations 1, 2, 3 and 4 on August 14, 1981.
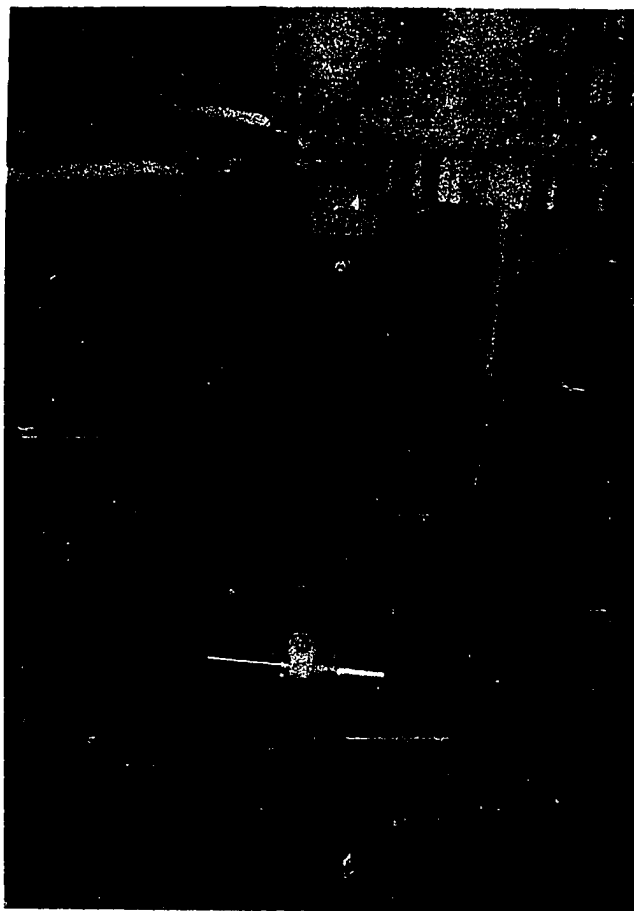
Fig. 24. Photography of the probe in the horizontal position.

Fig. 25. Photography of the data acquisition system: current meter and digital recorder.
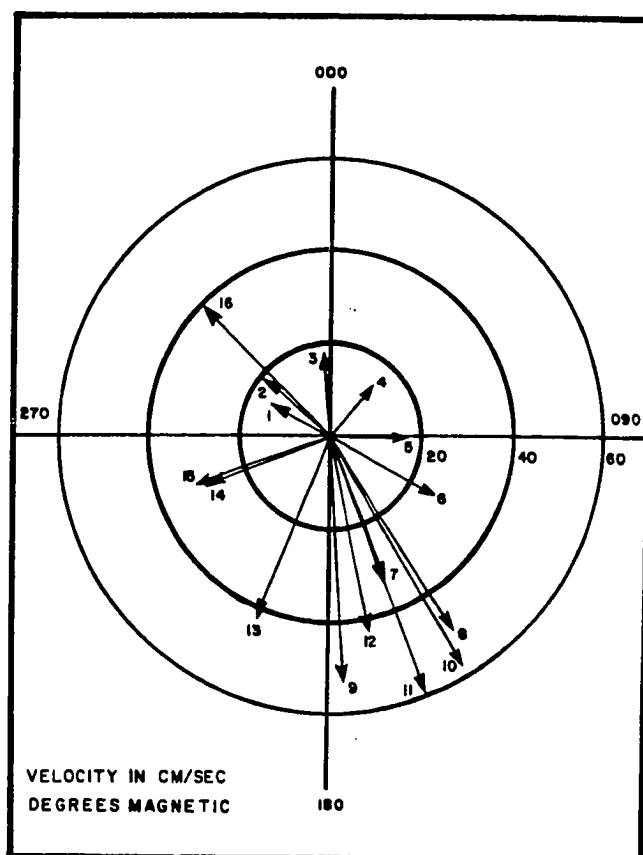
Fig. 26. Near surface current vectors. Data obtained on August 14, 1981. The numbers on the vectors correspond to the records in Table VIII and numbered marks in Fig. 27.
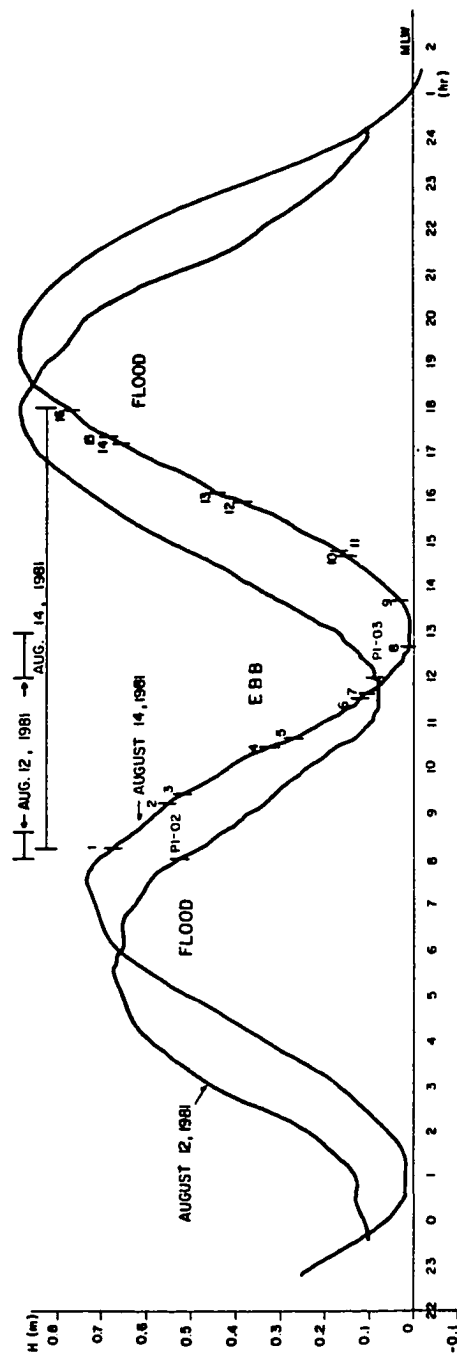
Fig. 27. Tidal height curves for August 12 and 14, 1981. The numbers on the second curve correspond to the vectors in Fig. 26 and Table VIII. The starting time for the bottom measurements (probe horizontal) was 5 to 10 minutes after the marked vectors.

Fig. 28. Vertical profiles of σ_t obtained on August 12
          and 14, 1981. Numbers indicated the time of
          the first measurement at the bottom level.
          The approximate tidal conditions during the
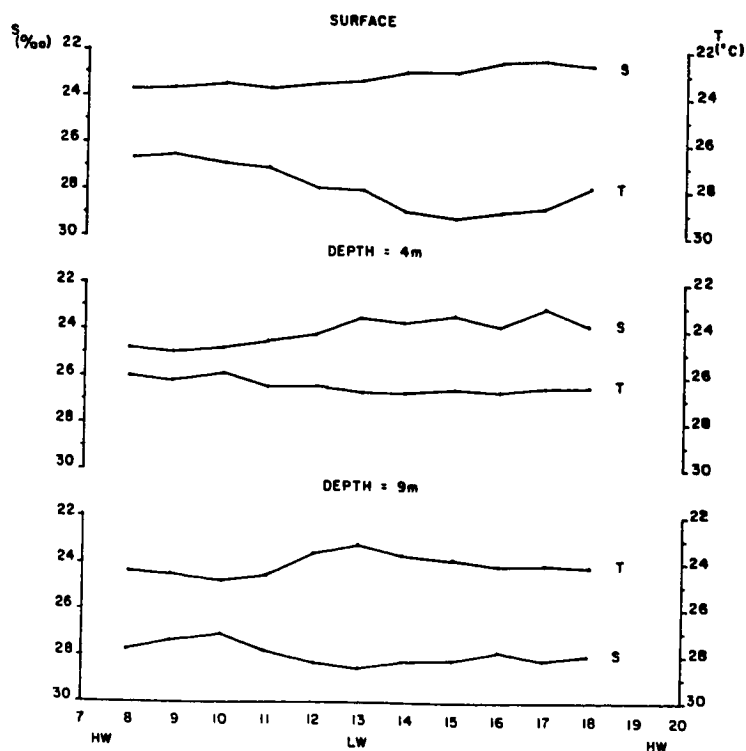   measurement are indicated.
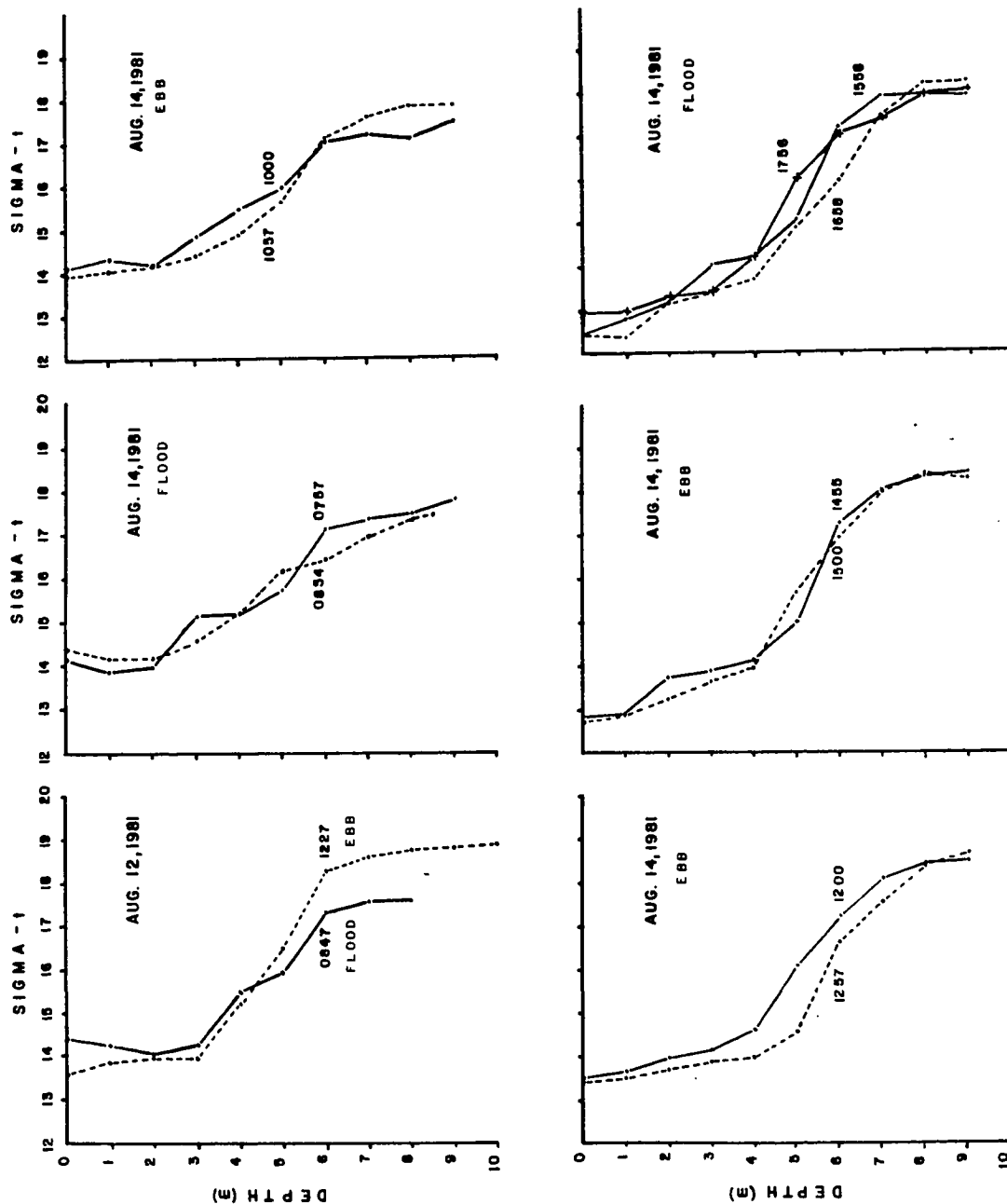
Fig. 29. Hourly distribution of salinity
(S) and temperature (T) at the
surface, 4 and 9 m for data
obtained on August 14. 1981.
Note the coherent inverse
behavior of S and T at the
surface and 9 m levels. The
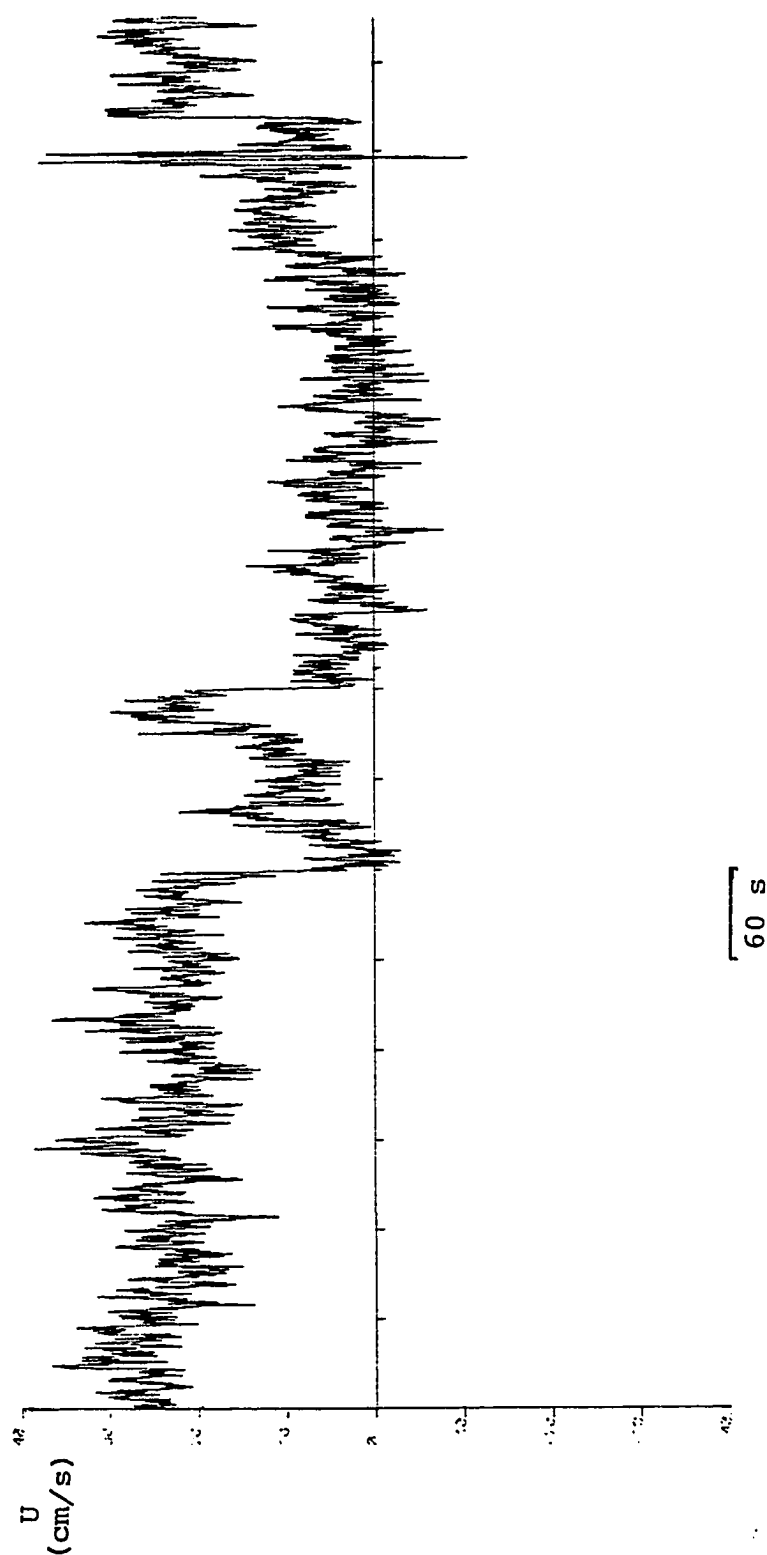pycnocline developed at about the
4 m level.

139

Fig. 30. Plot of U(t) as function of time for record P1-03. Data obtained at maximum ebb on August 12, 1981. Surface velocity = 282.17 cm/s. Note the large variation in the mean velocity at the center of the figure.
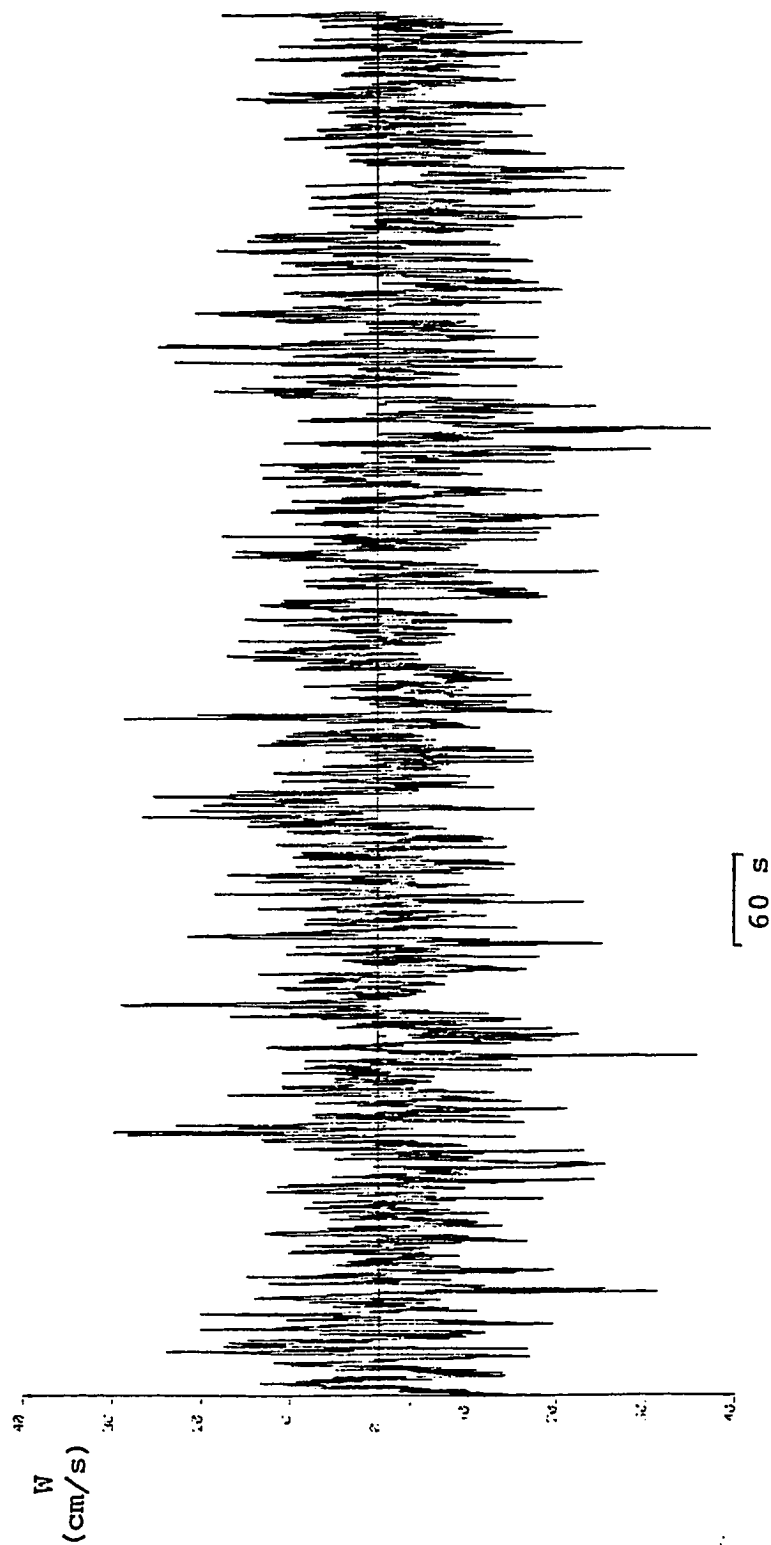
Fig. 31. Plot of W(t) as function of time for record Pl-03. Data obtained at maximum ebb on August 12, 1981. Surface velocity = 282.17 cm/s. Note the highly turbulent behavior of the vertical component of the flow in comparison to the plot of U(t) (Fig. 30).
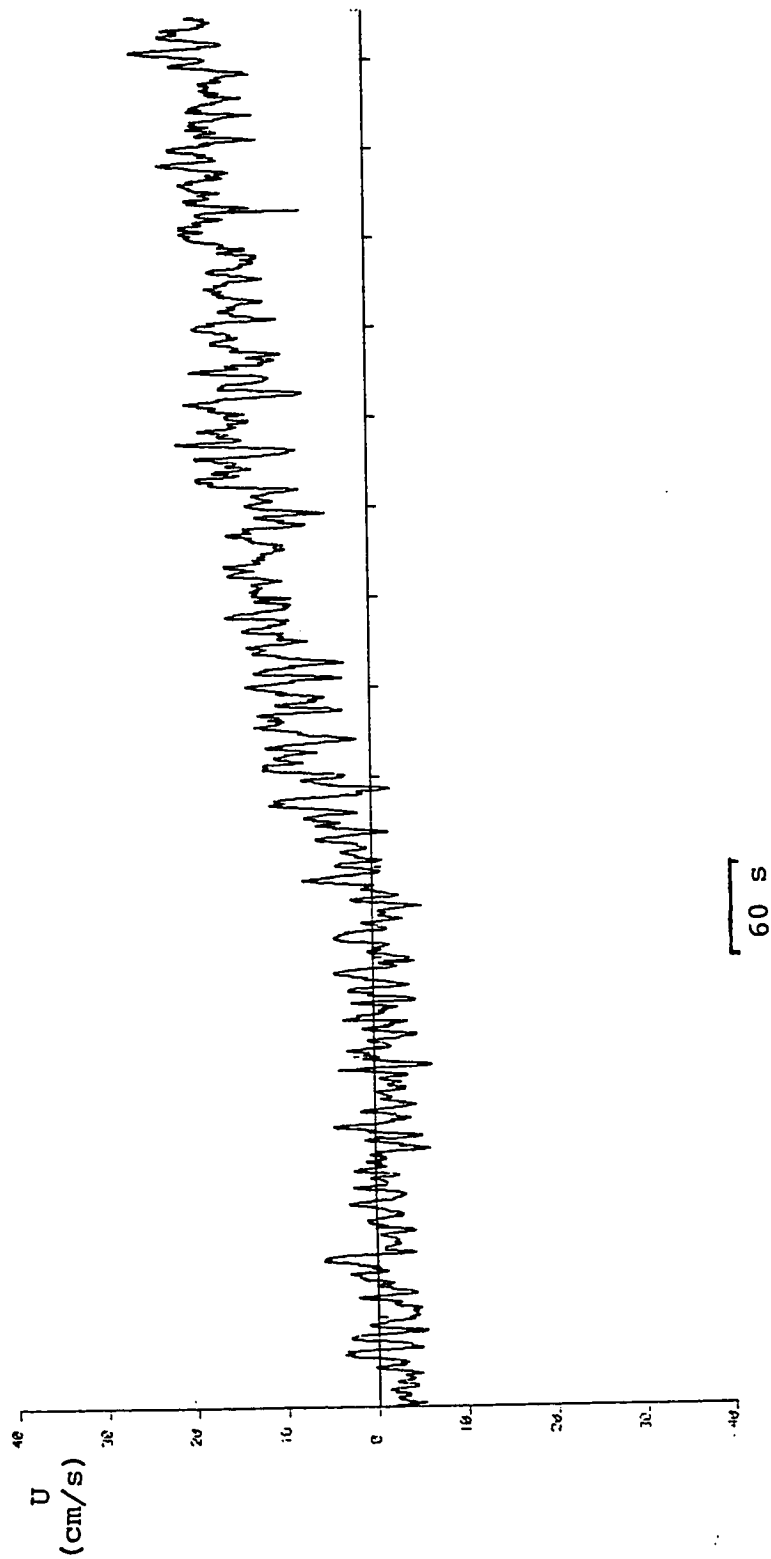
141

Fig. 32. Plot of U(t) as function of time for record 2-05. Surface velocity equals to 16.32 cm/s. Data corresponds to mark 5 in Fig. 27, on the curve for August 14, 1981. Note the long period trend and the wave period phenomena.
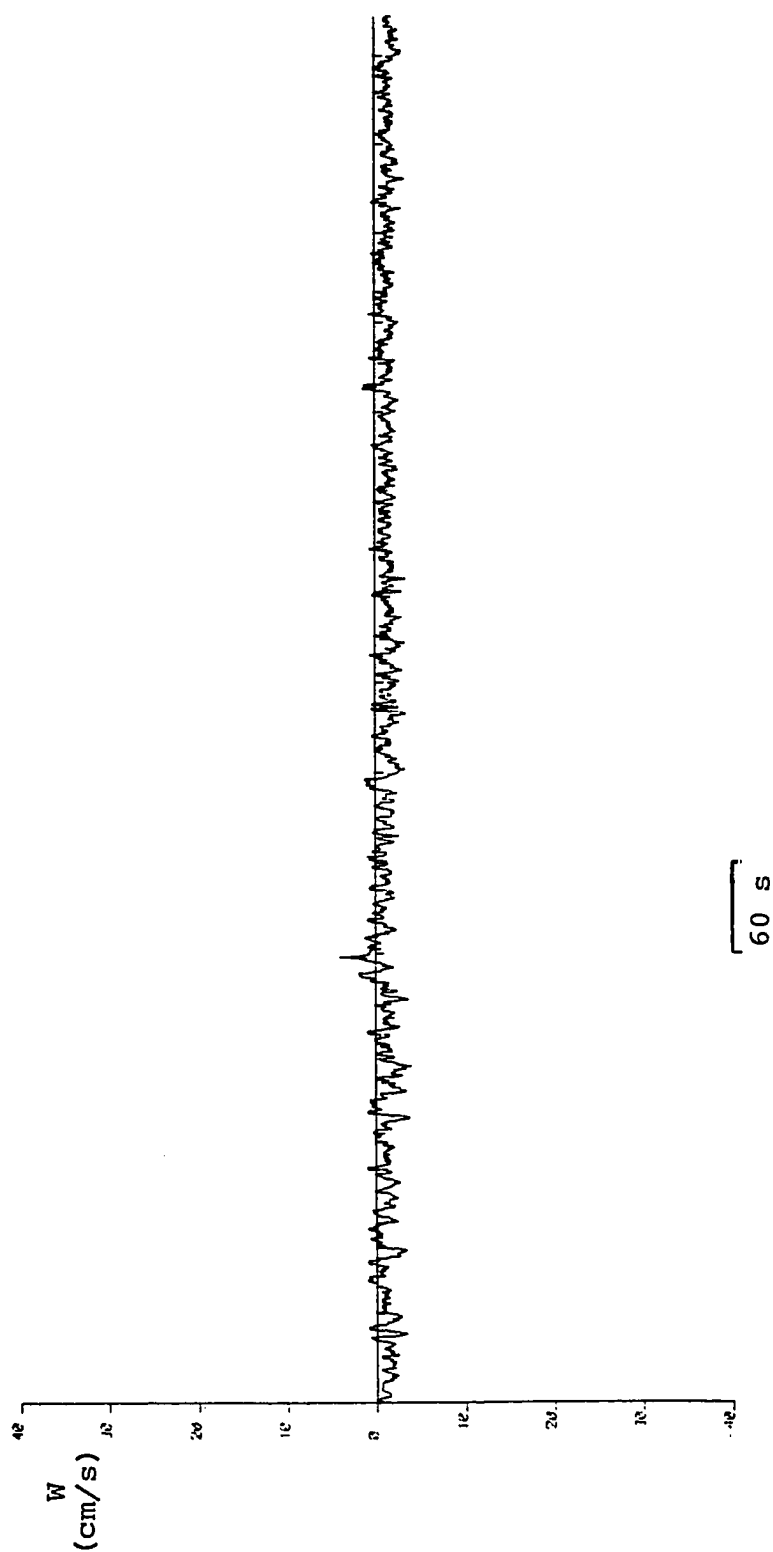
W
(cm/s)

60 s

Fig. 33. Plot of W(t) as function of time for record 2-05. Surface velocity
equals to 16.32 cm/s. Data corresponds to mark 5 in Fig. 27, on the
curve for August 14, 1981.

143

Fig. 34. Plot of U(t) as function of time for record 4-07. Surface velocity = 41.83 cm/s. Data corresponds to mark 13 in Fig. 27, on the curve for August 14, 1981. Note the long period trends (T = 3 minutes) as it falls off at the end of the record.
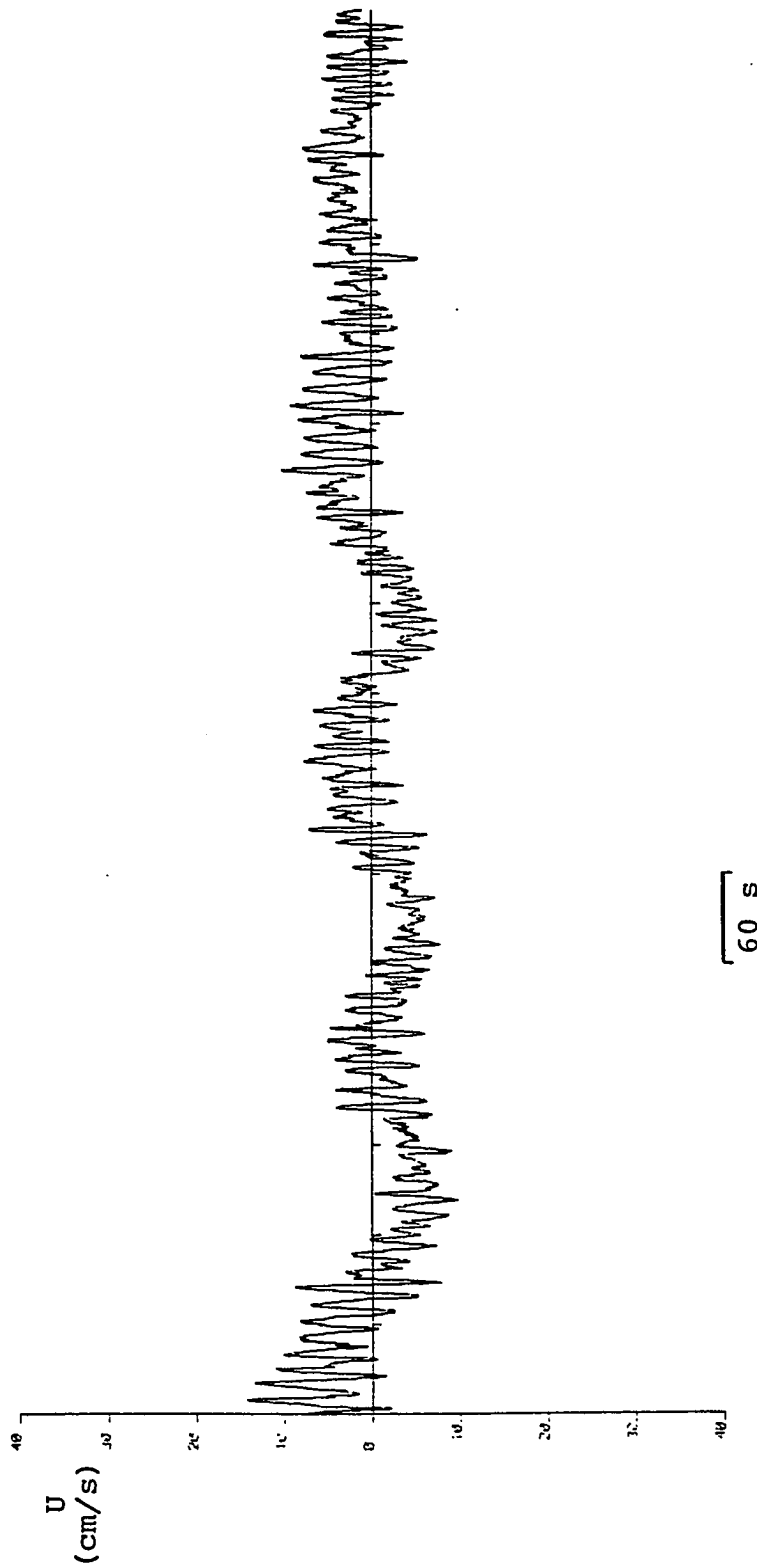
60 s

U
(cm/s)
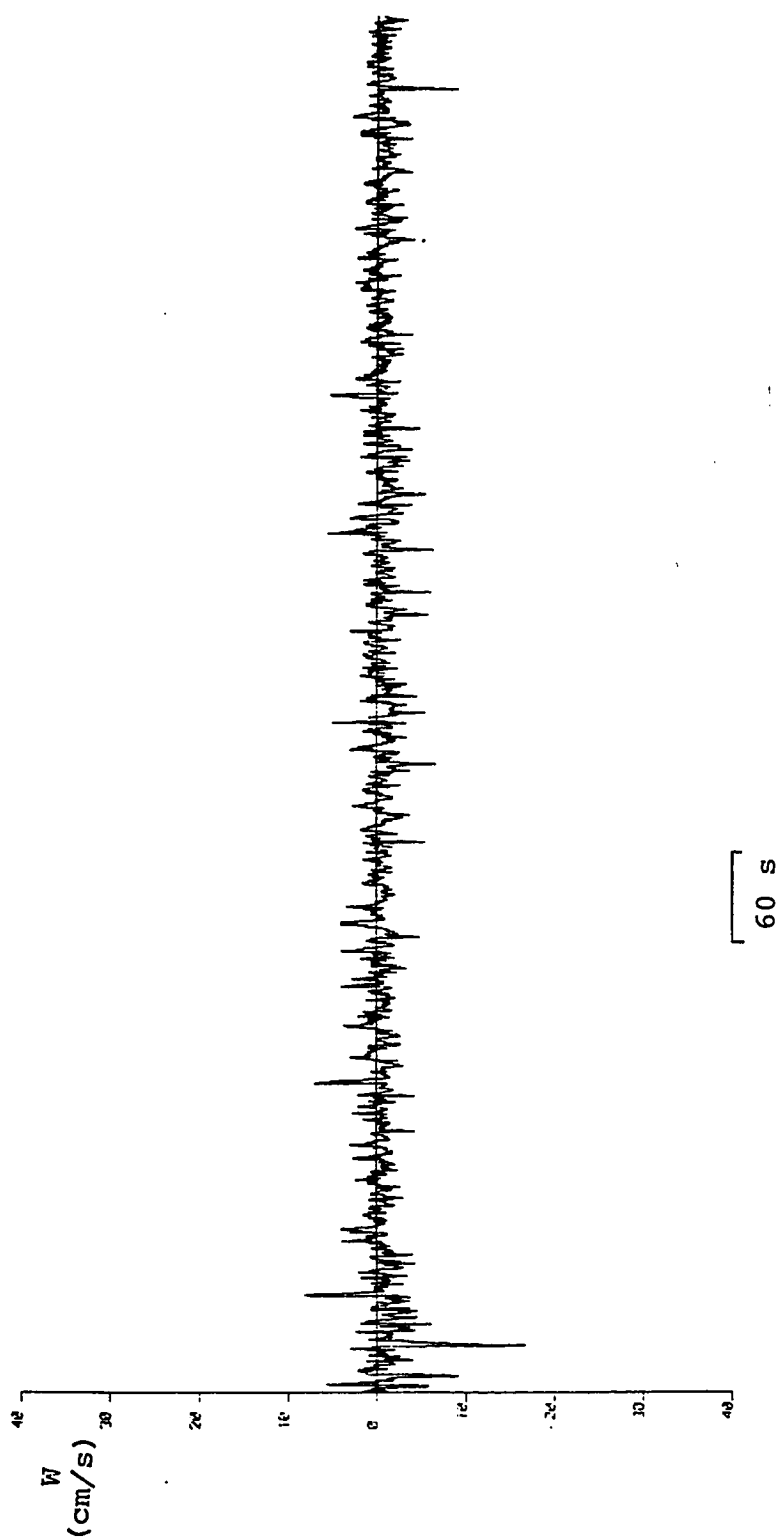
Fig. 35. Plot of W(t) as function of time for record 4-07. Surface velocity = 41.83 cm/s. Data correspond to mark 13 in Fig. 27, on the curve for August 14, 1981.

Fig. 36. Plot of U(t) as function of time for record 1-04. Surface velocity = 14.34 cm/s. Data correspond to mark 4 in Fig. 27, on the curve for August 14, 1981. Note the negative steady current (-9.0 cm/s)

146
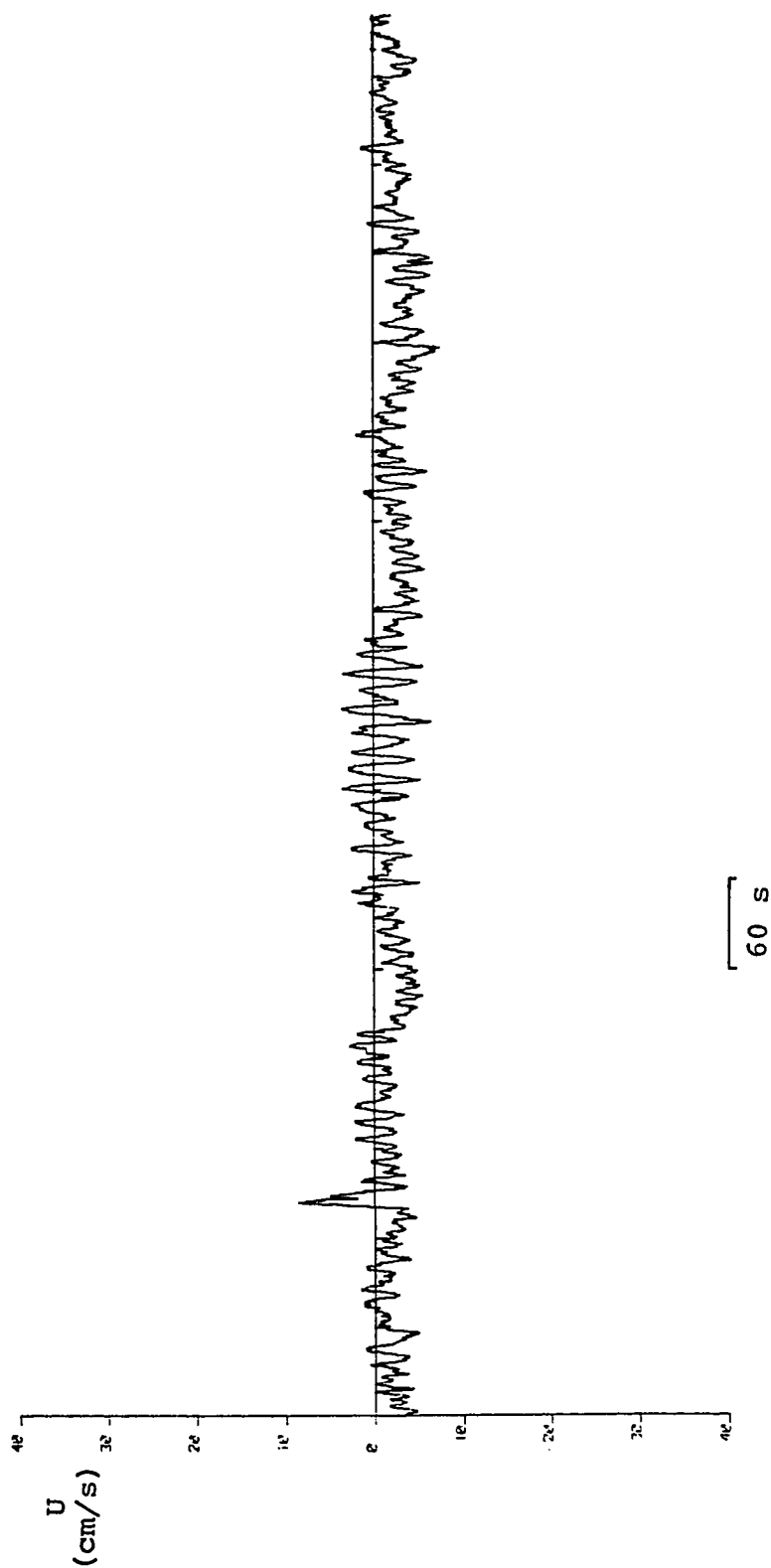

Fig. 37. Plot of W(t) as function of time for record 1-04. Surface velocity = 14.34 cm/s. Data correspond to mark 4 in Fig. 27, on the curve for August 14, 1981.

W
(cm/s)

60 s

147
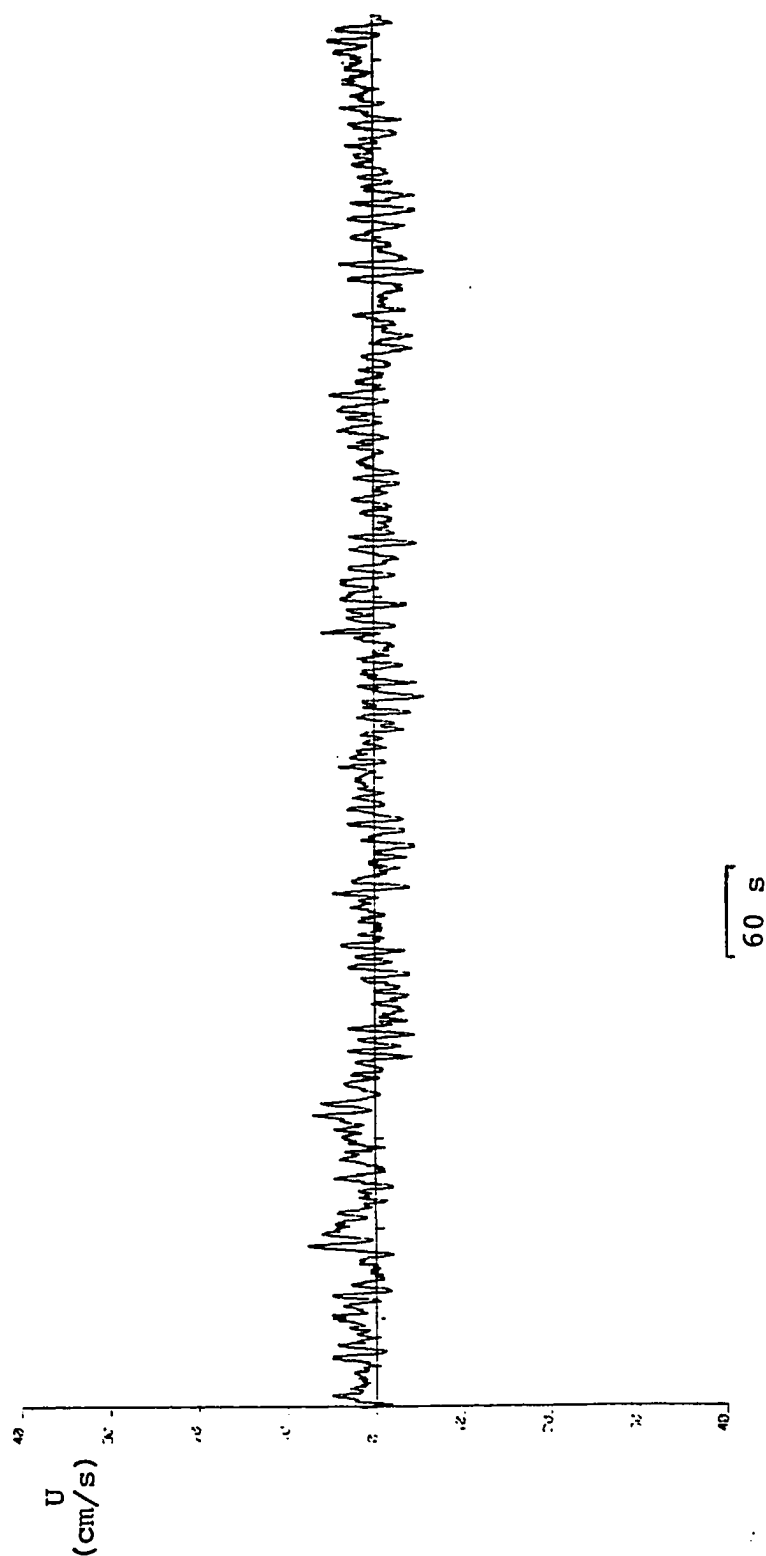
Fig. 38. Plot of U(t) as function of time for record 2-07. Surface velocity = 58.94 cm/s. Data correspond to mark 11 in Fig. 27, on the curve for August 14, 1981. Note long period trends (T = 3 minutes) starting at about 3.5 minutes from the origin.
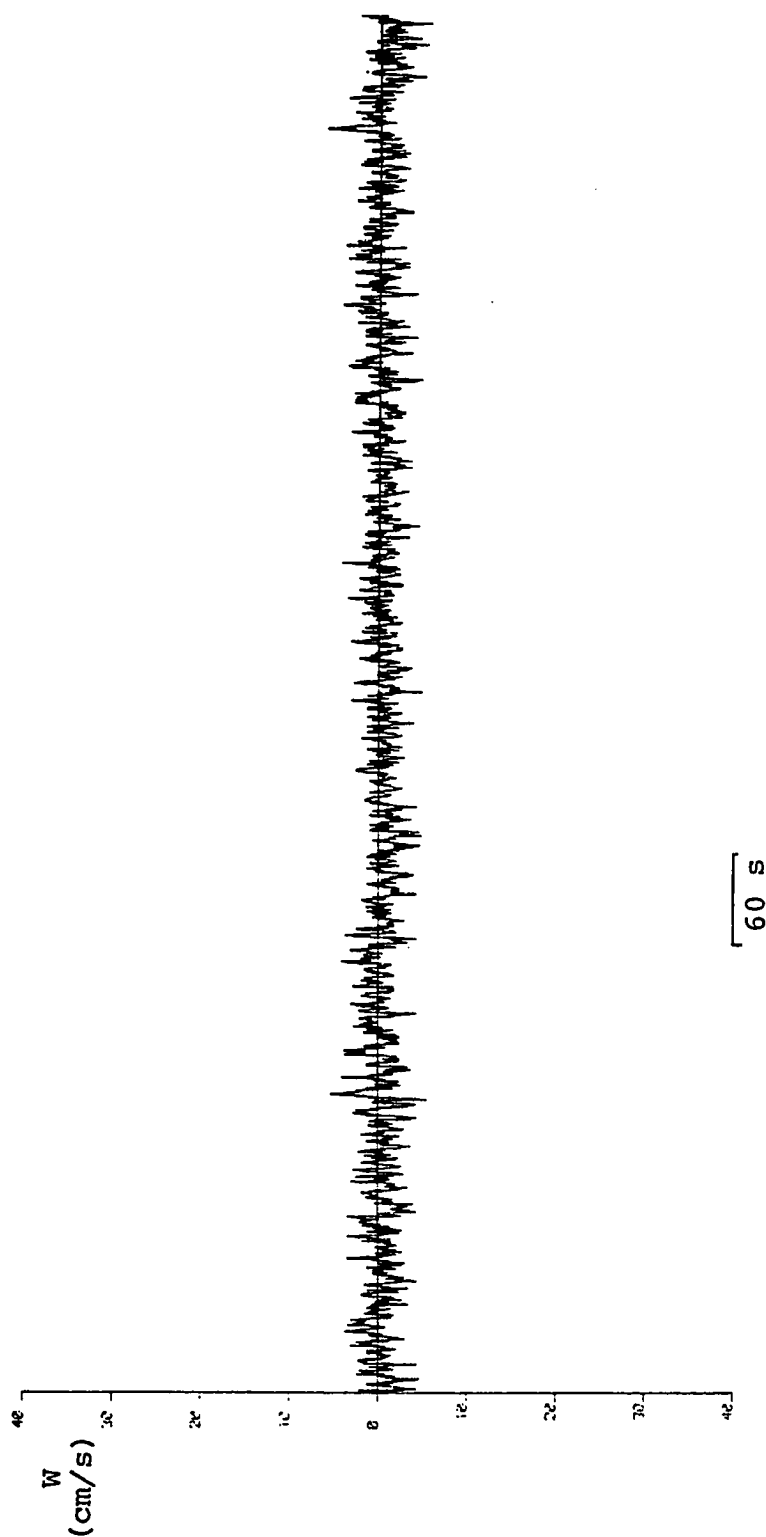
Fig. 39. Plot of W(t) as function of time for record 2-07. Surface velocity = 58.94 cm/s. Data correspond to mark 11 in Fig. 27, on the curve for August 14, 1981. Note the long period trends at the origin and end of the plot.
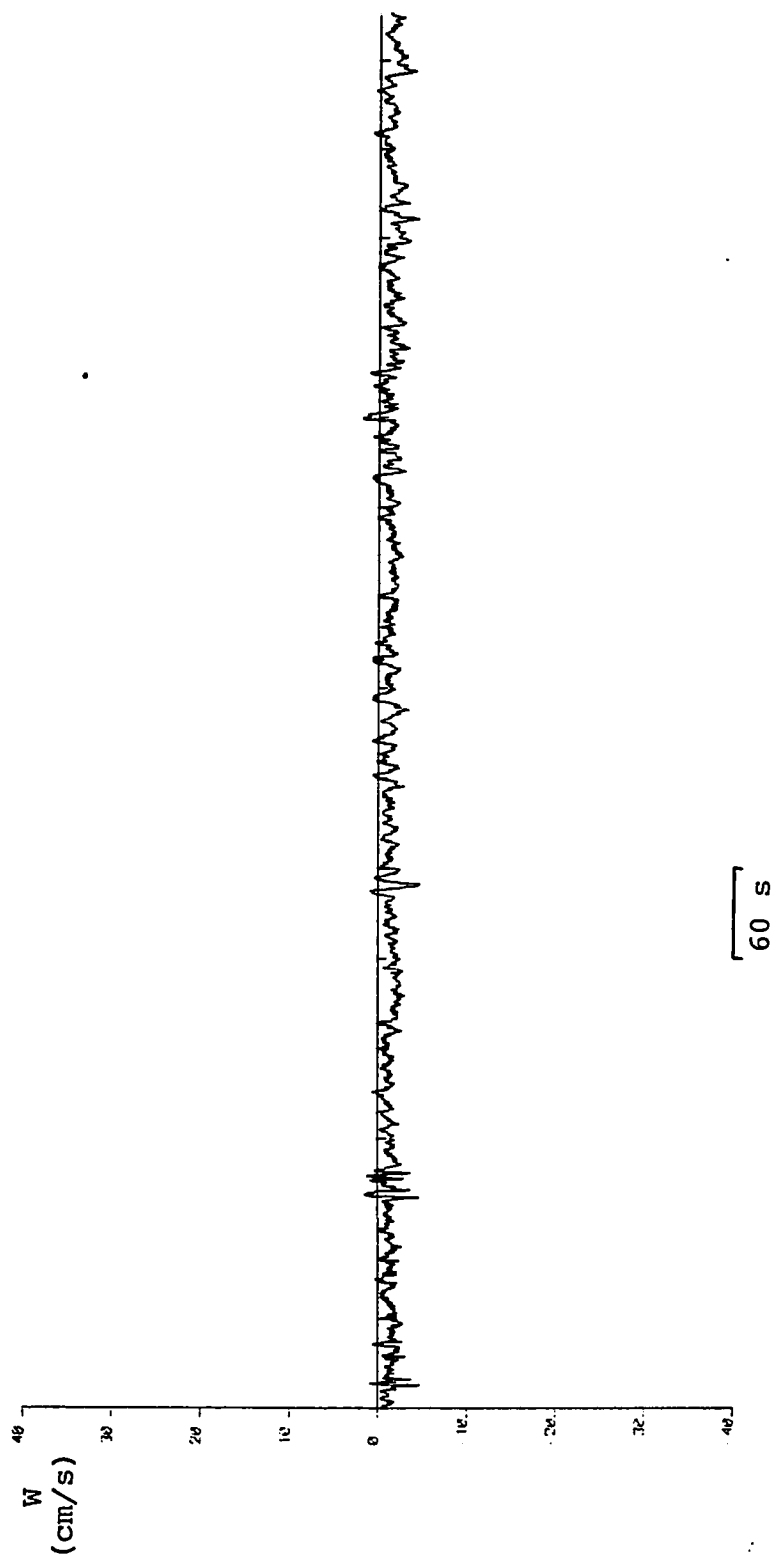
149
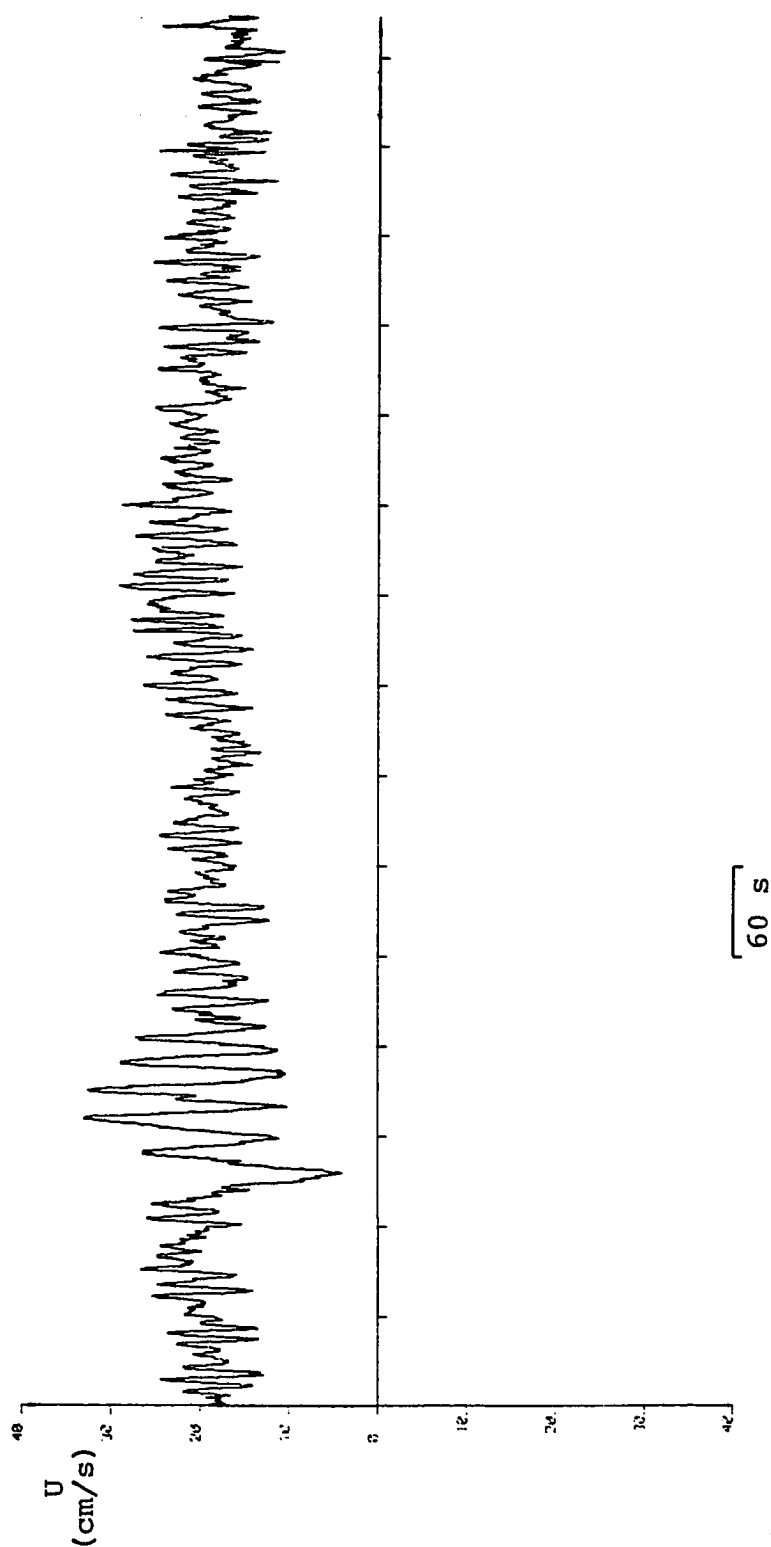
Fig. 40. Plot of U(t) as function of time for record 3-07. Surface velocity = 42.78 cm/s. Data correspond to mark 12 in Fig. 27, on the curve for August 14, 1981. Note the steady velocity (about 20 cm/s) and the waves (T = 11 seconds).

W
(cm/s)

60 s
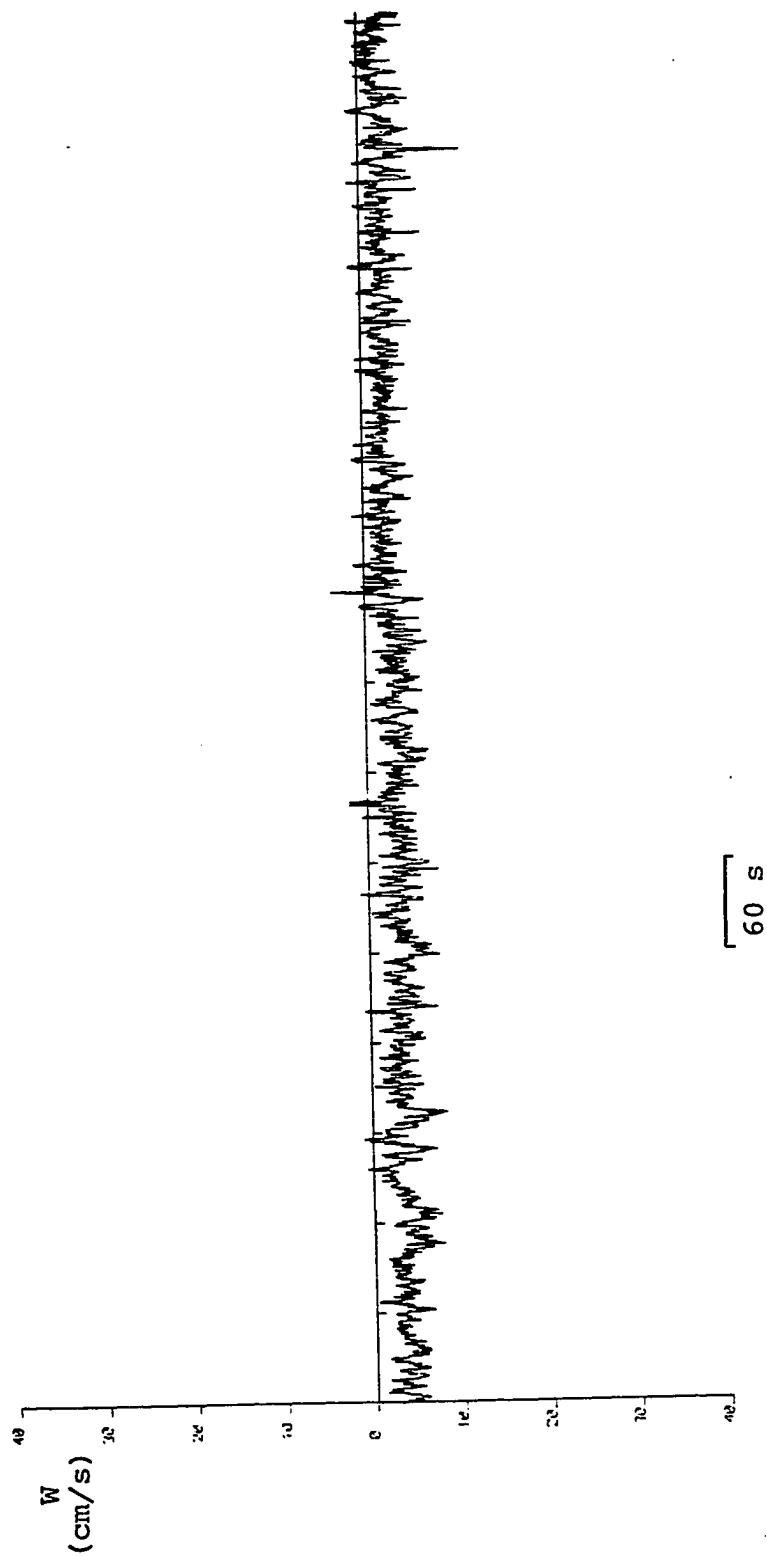
Fig. 41. Plot of W(t) as function of time for record 3-07. Surface velocity = 42.78 cm/s. Data correspond to mark 12 in Fig. 27, on the curve for August 14. 1981.
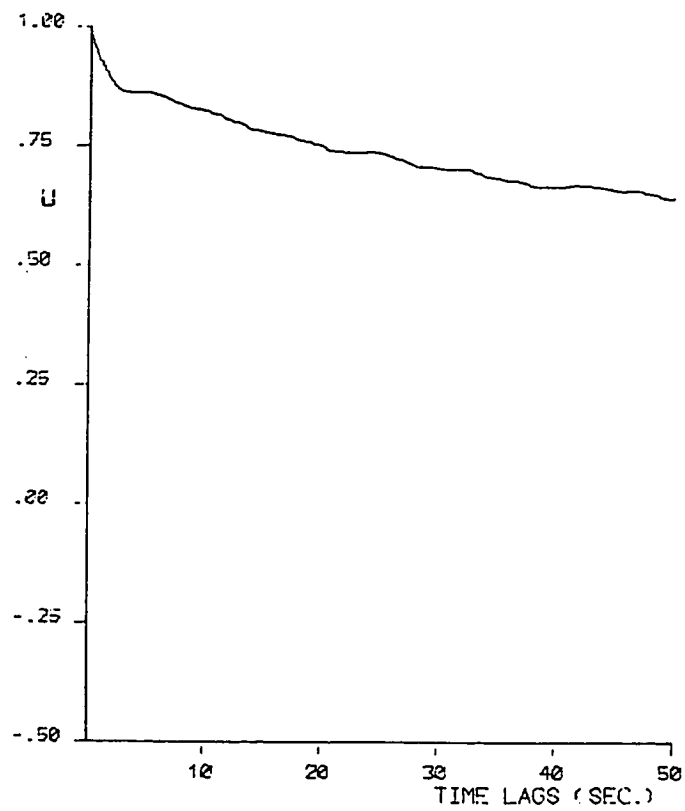
Fig. 42. Autocorrelation of U, record P1-03, unfiltered data.
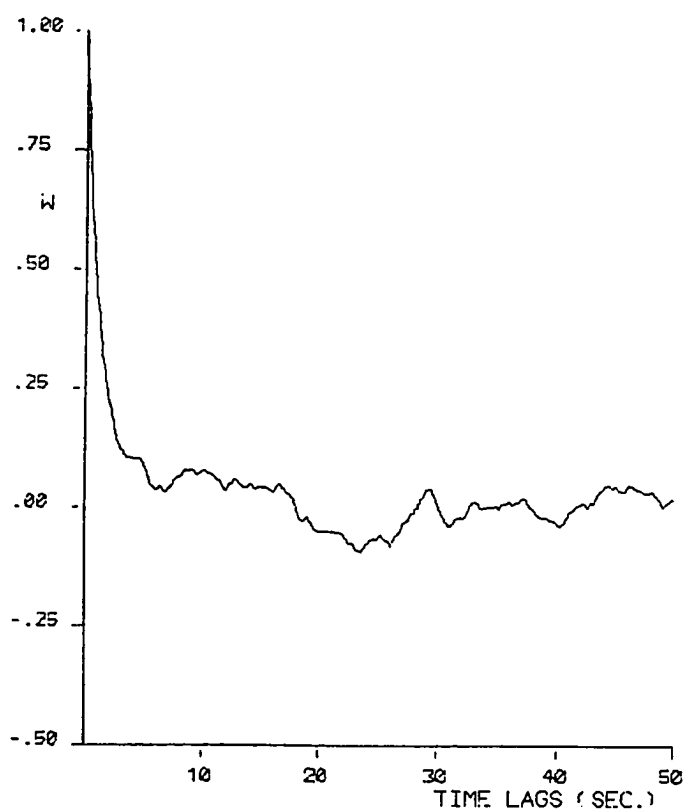
Fig. 43. Autocorrelation of W, record P1-O3, unfiltered data.
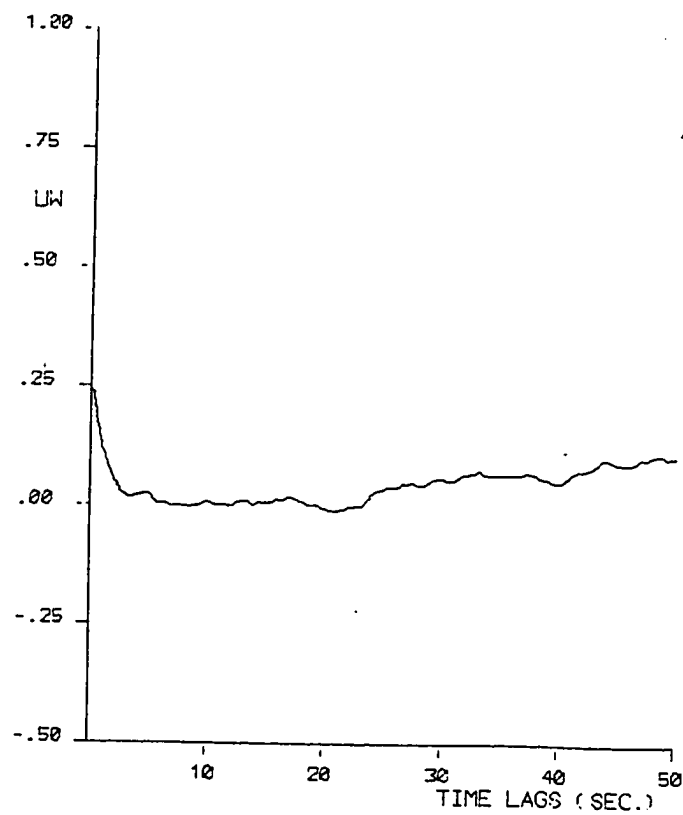
Fig. 44. Crosscorrelation of UW, record
P1-03, unfiltered data.
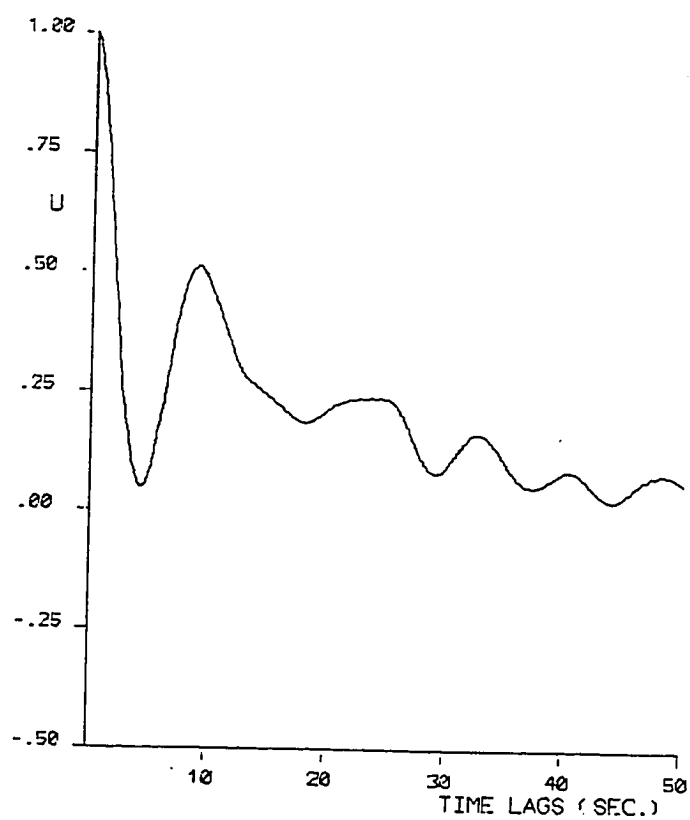
Fig. 45. Autocorrelation of U. record
2-07, unfiltered data.
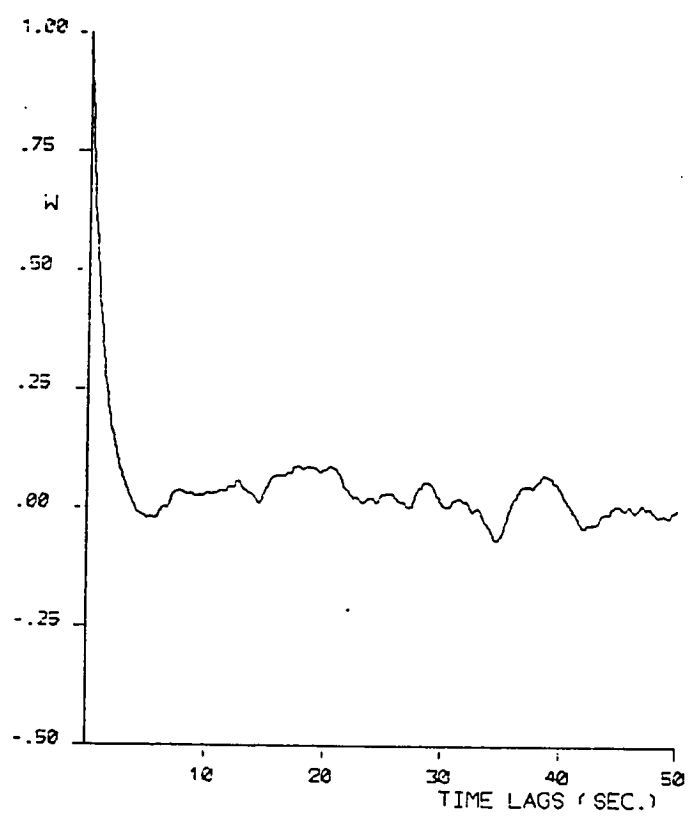
Fig. 46. Autocorrelation of W, record
2-07, unfiltered data.
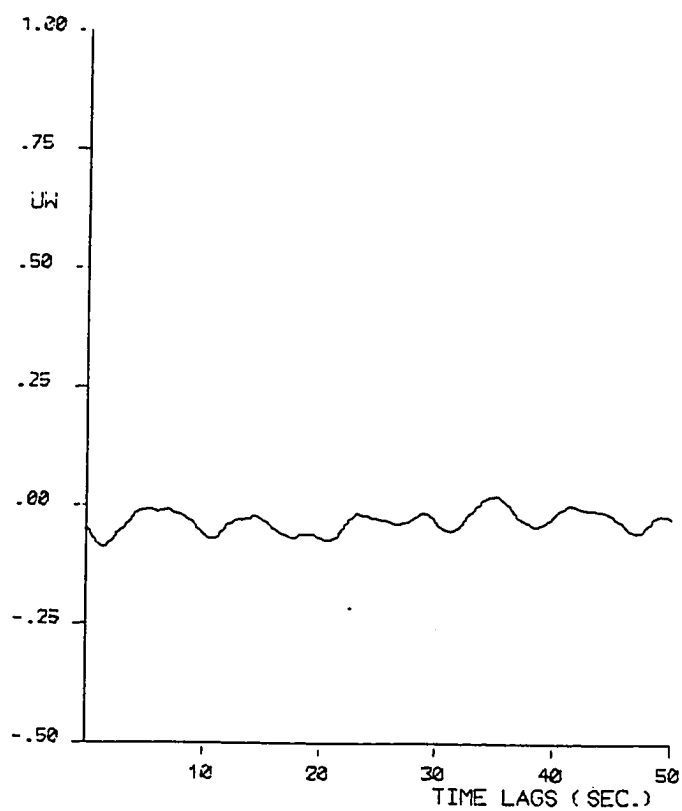
Fig. 47. Crosscorrelation of UW. record
2-07, unfiltered data.
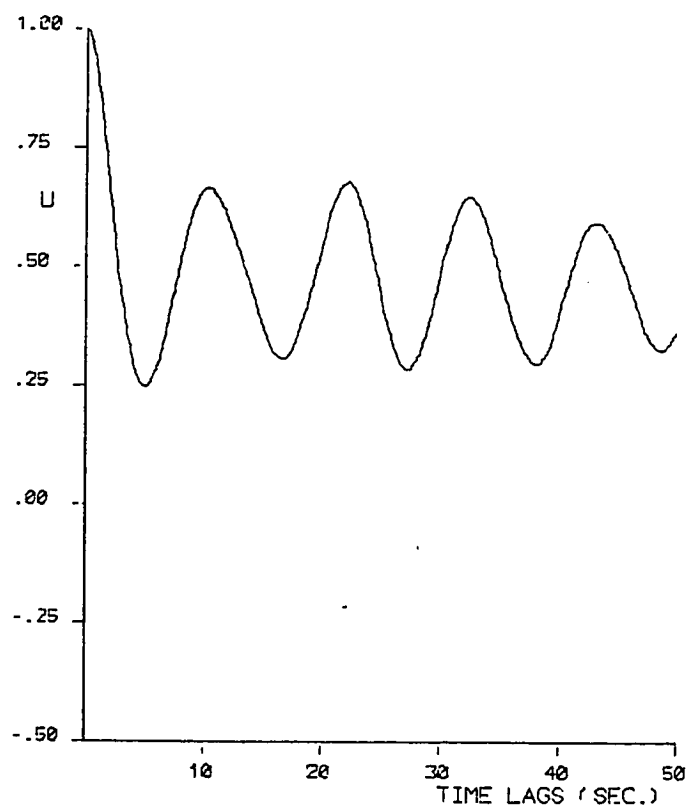
Fig. 48. Autocorrelation of U. record 1-08,
unfiltered data.
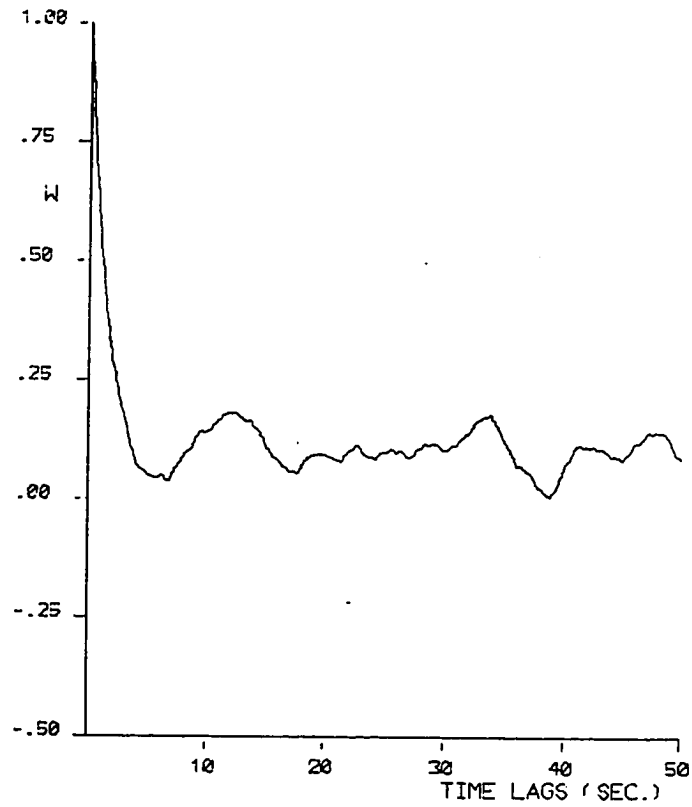
Fig. 49. Autocorrelation of W, record
1-08, unfiltered data.
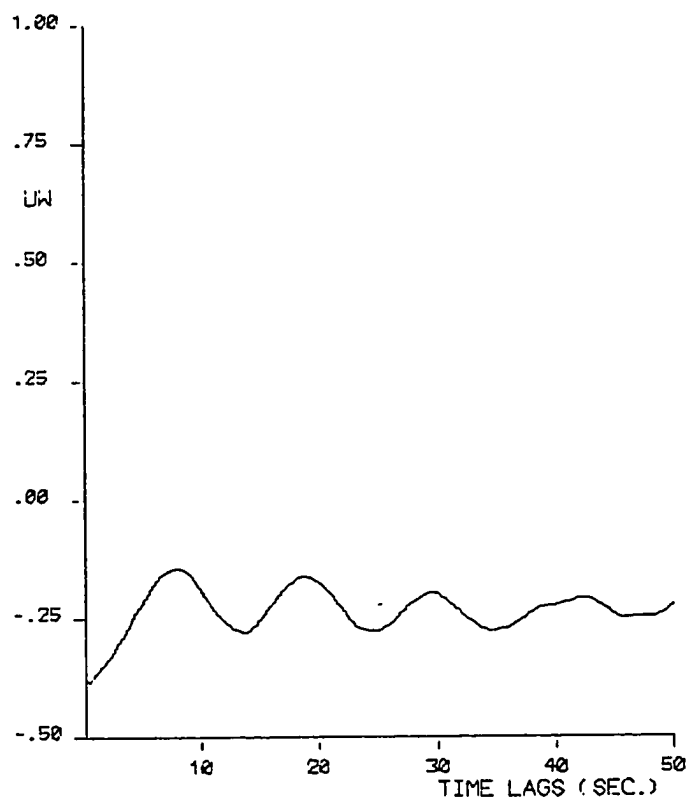
Fig. 50. Crosscorrelation of UW, record 1-08, unfiltered data.
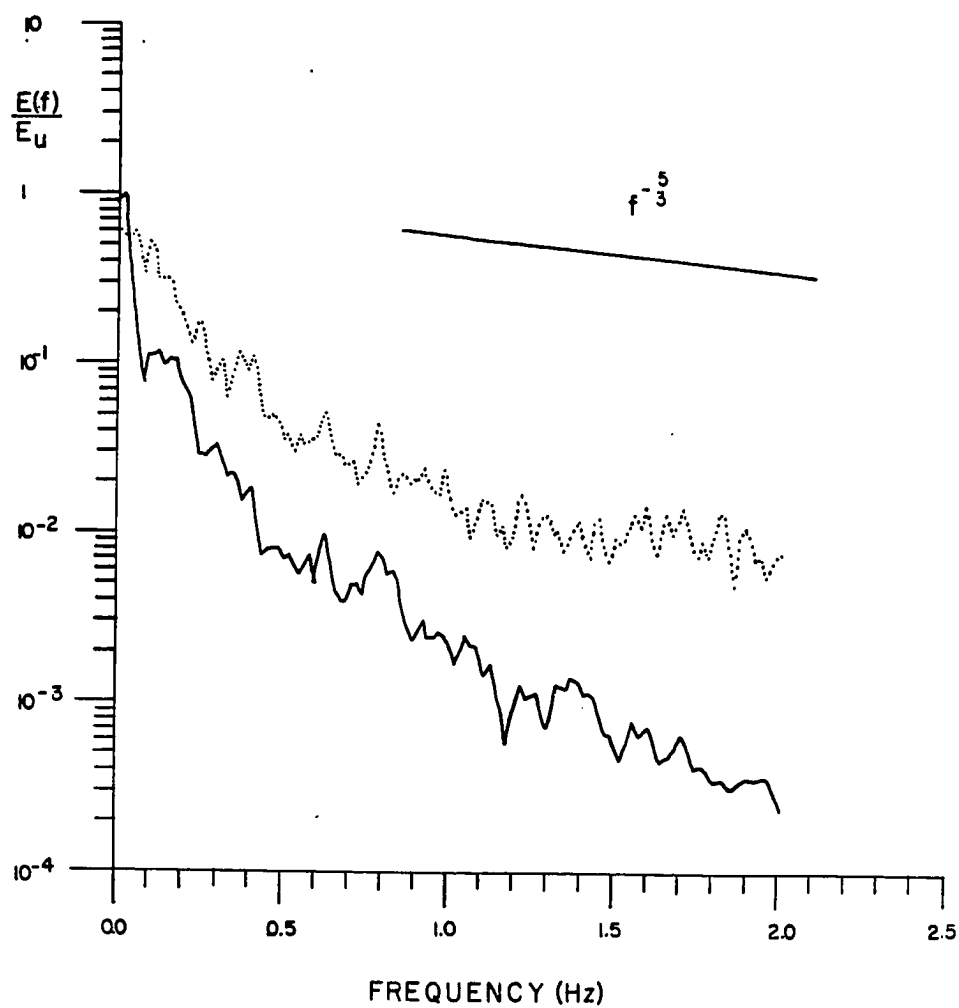
Fig. 51. Spectrum function (E(f)) of U and W, unfiltered data, record P1-03. The energy was normalized by the peak energy of E_u = 815.31 $cm^2/sec^2/Hz$. U = ———, W = ...
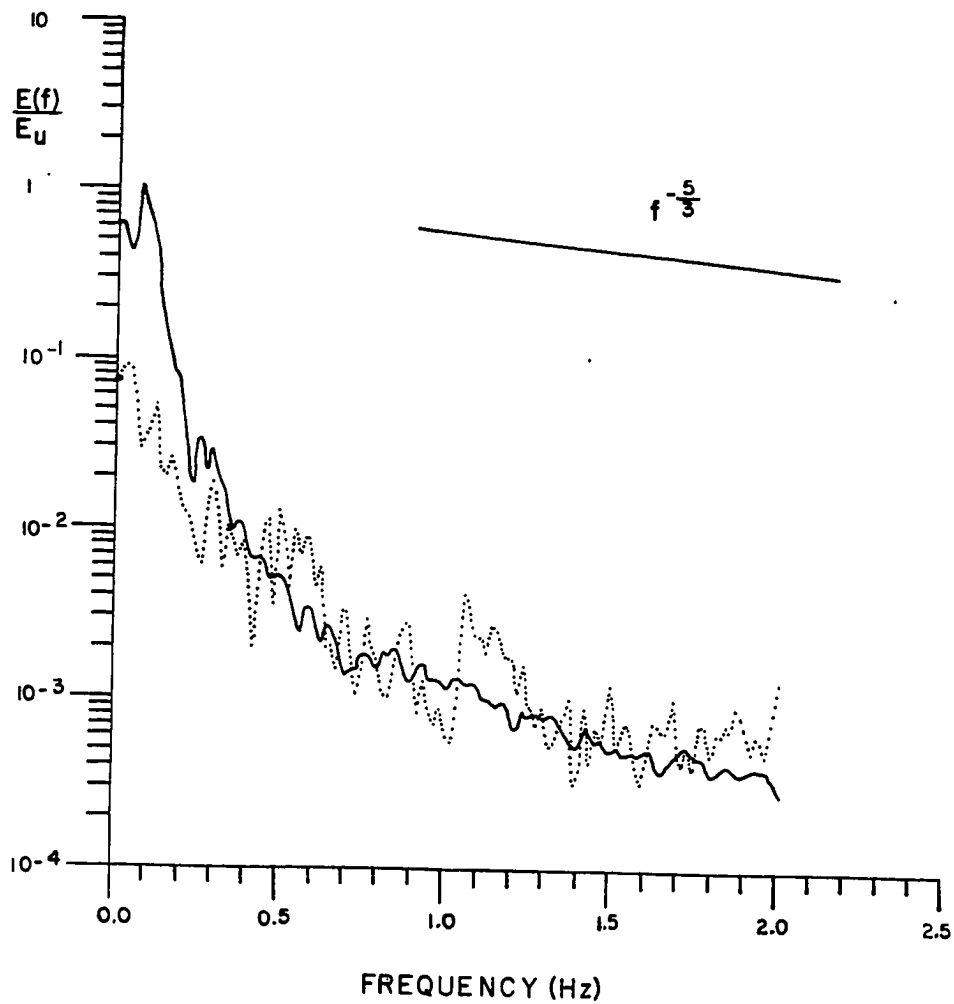
Fig. 52. Spectrum function (E(f)) of U and W, unfiltered data, record 4-04. The energy was normalized by the peak energy of E_u = 54.80 $cm^2/sec^2/Hz$. U = ——, W = ...
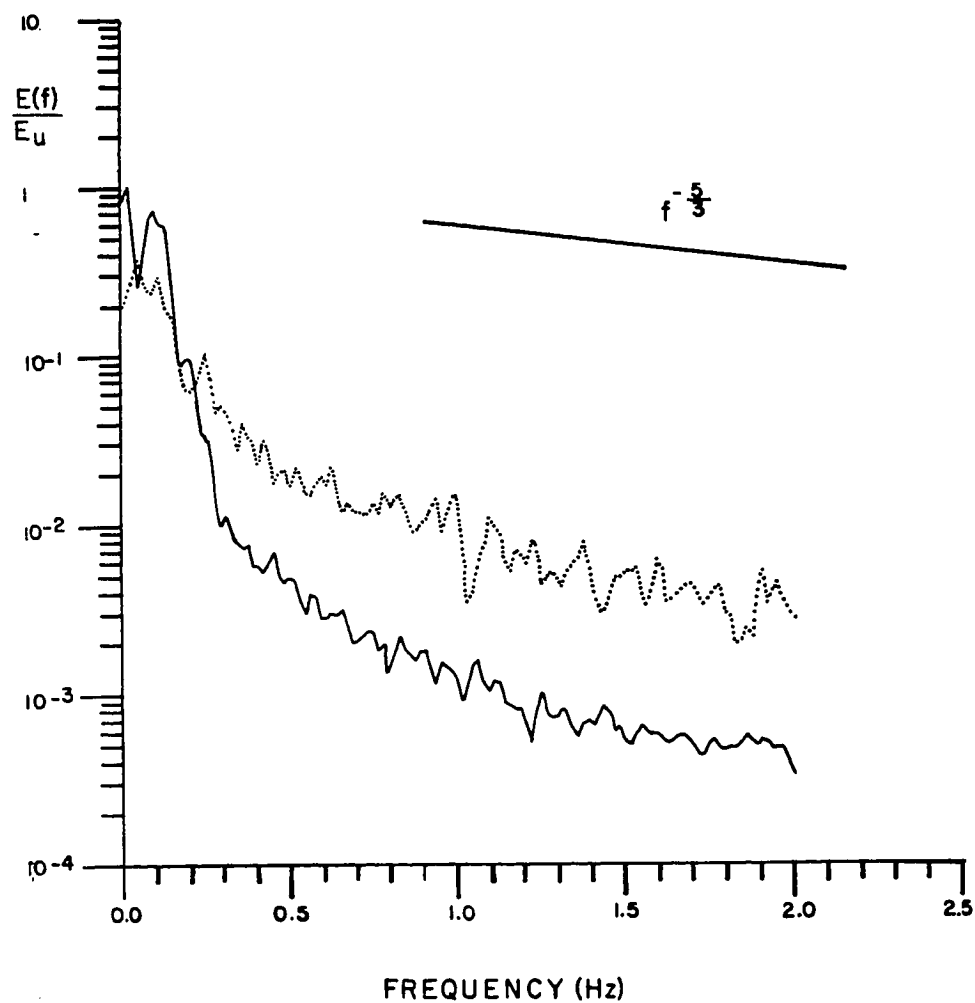
Fig. 53. Spectrum function (E(f)) of U and W, unfiltered data, record 2-07. The energy was normalized by the peak energy of E_u = 52.68 cm^2/sec^2/Hz. U = ———— , W = ...
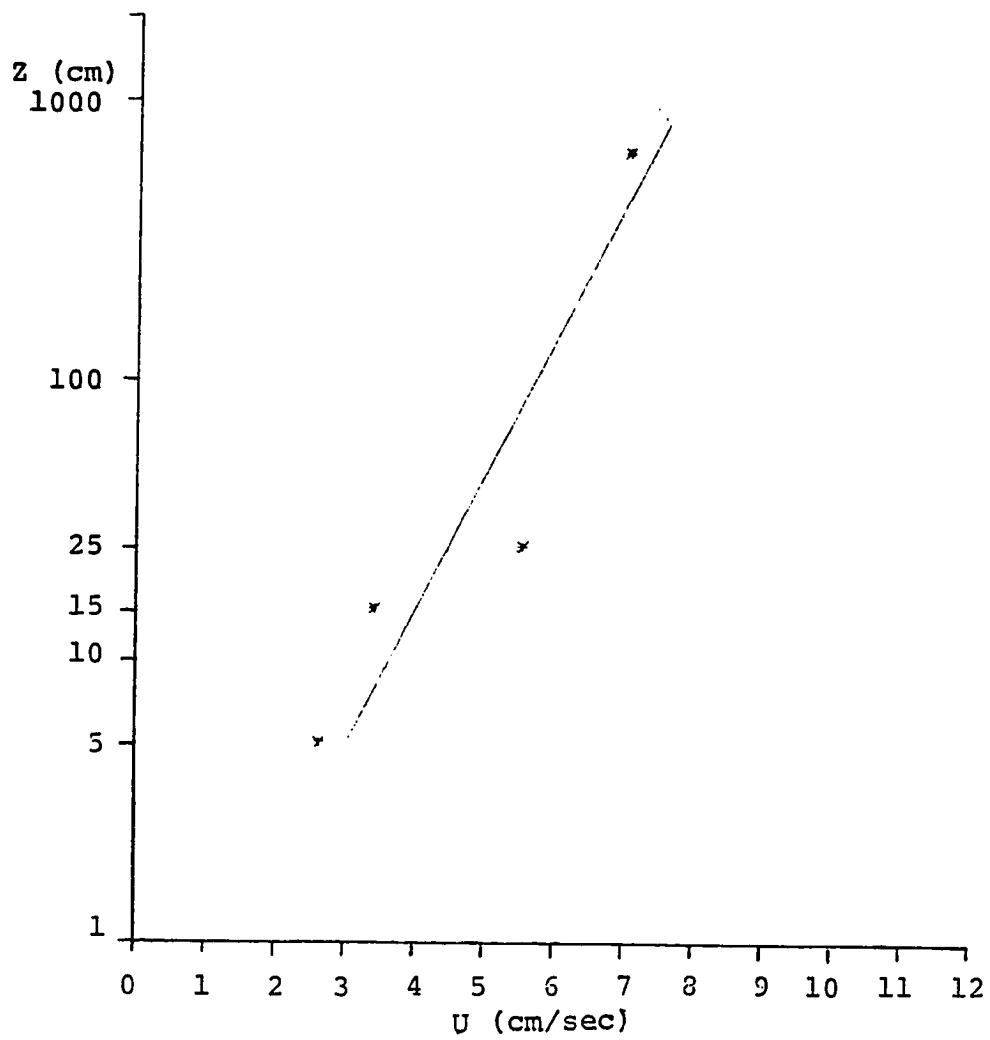
Fig. 54. Velocity profile calculated with equation
(4 2). See Table XI for parameters.
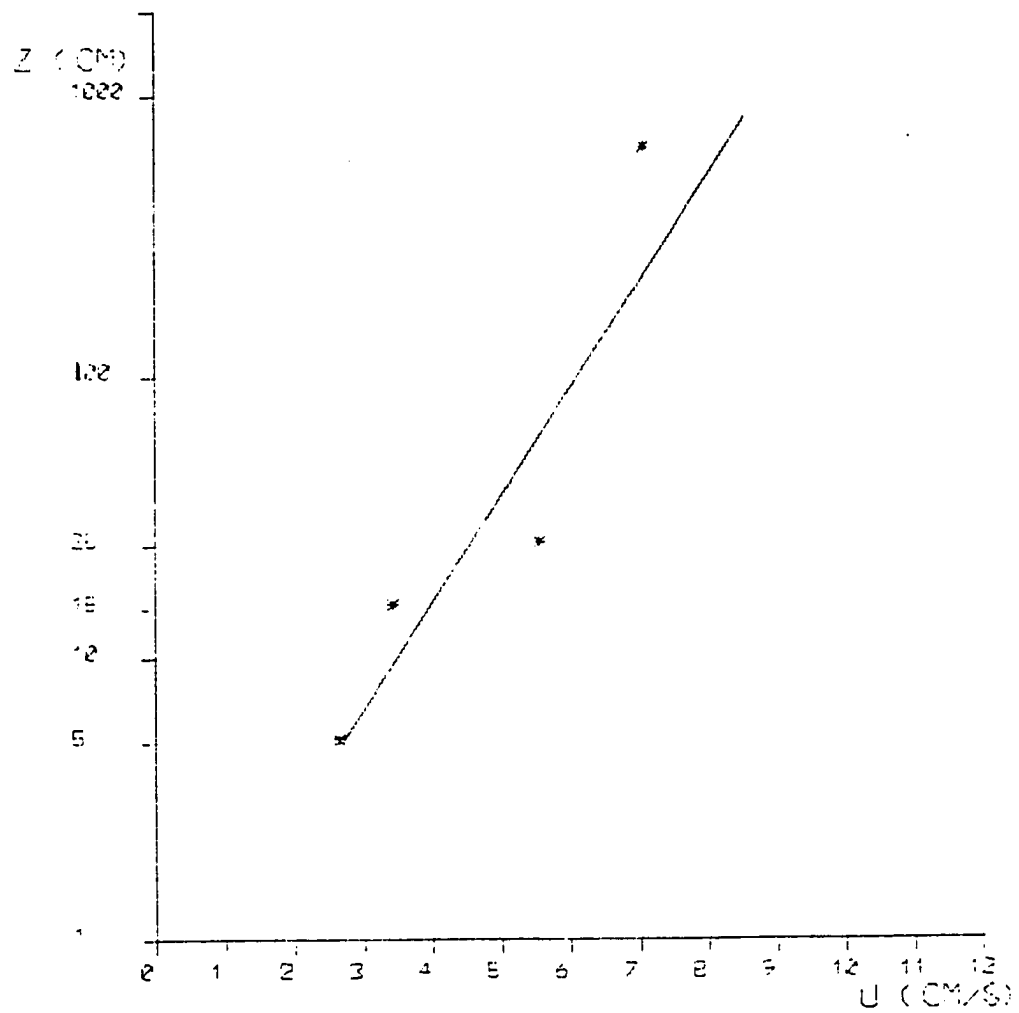
Fig. 55. Velocity profile calculated with equation
(4 3). See Table XI for parameters.
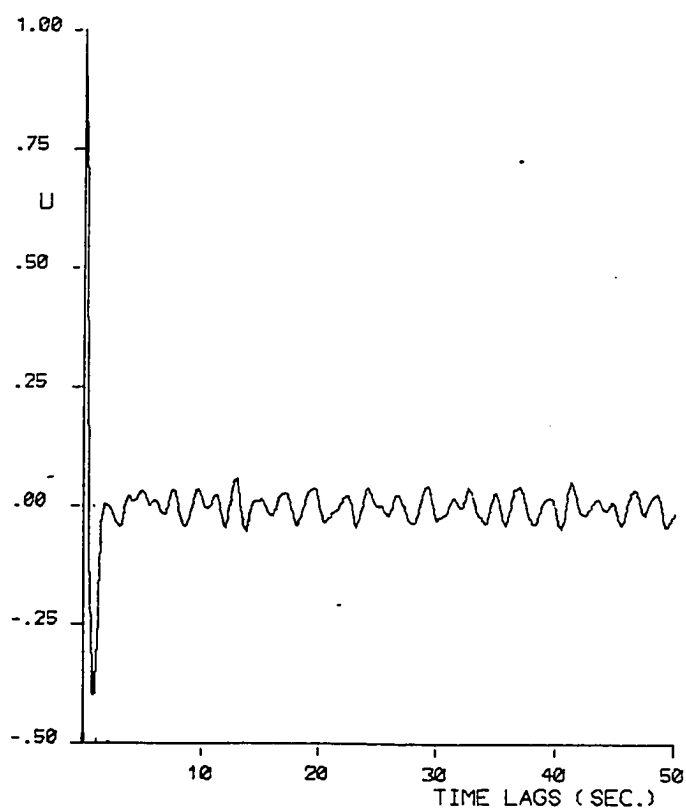
Fig. 56. Autocorrelation of U, record P1-03.
Filtered data at $f_{\frac{1}{2}}$ = 0.2 Hz.
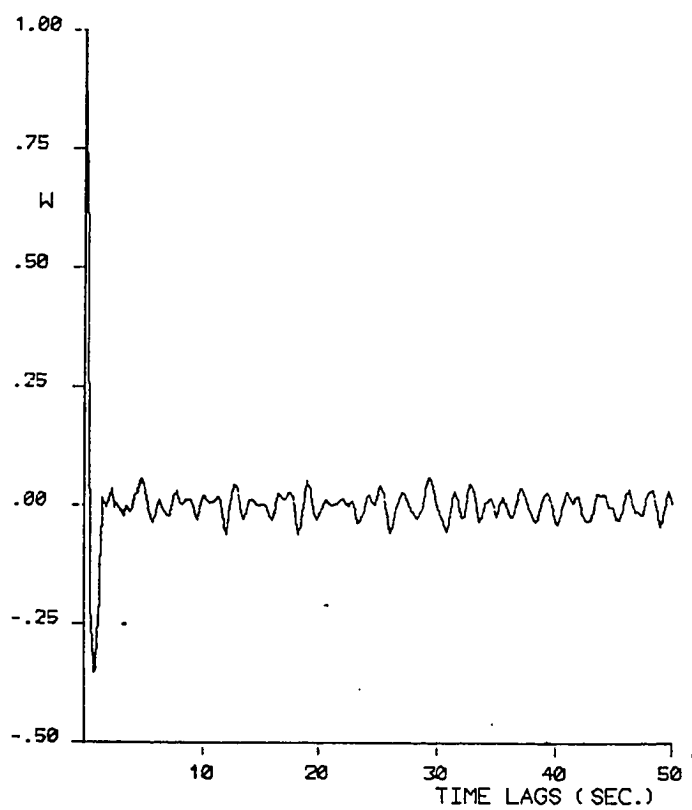
Fig. 57. Autocorrelation of W, record P1-03.
Filtered data at $f_{\frac{1}{2}}=$ 0.2 Hz.
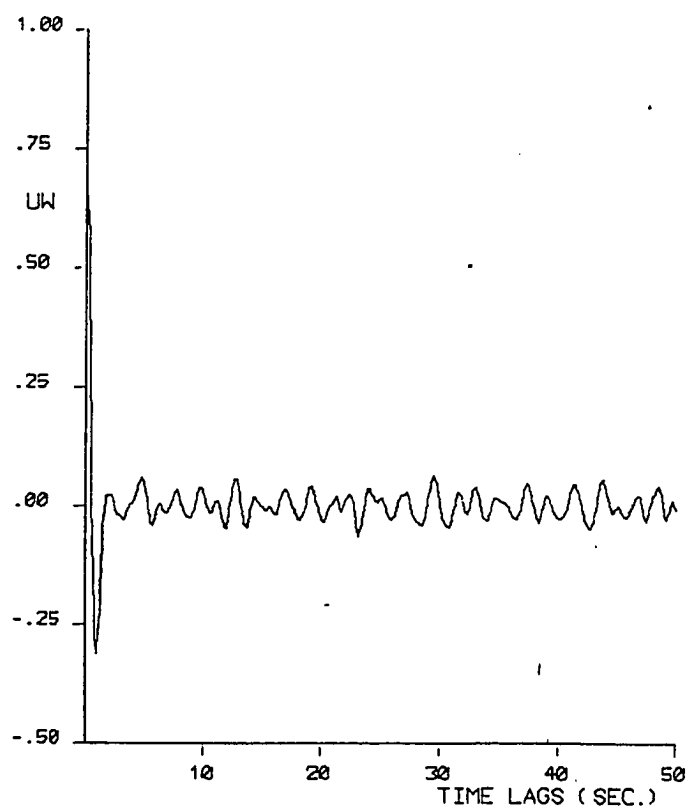
Fig. 58. Crosscorrelation of UW, record
P1-03. Filtered data at $f_{\frac{1}{2}}=0.2$
Hz.
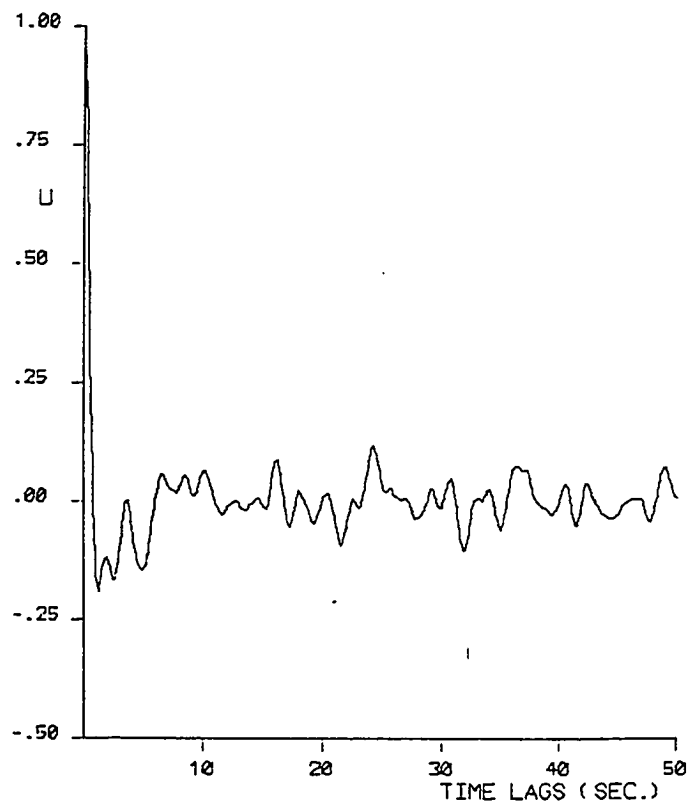
Fig. 59. Autocorrelation of U, record
4-04. Filtered data at $f_{\frac{1}{2}}$ =
0.2 Hz.
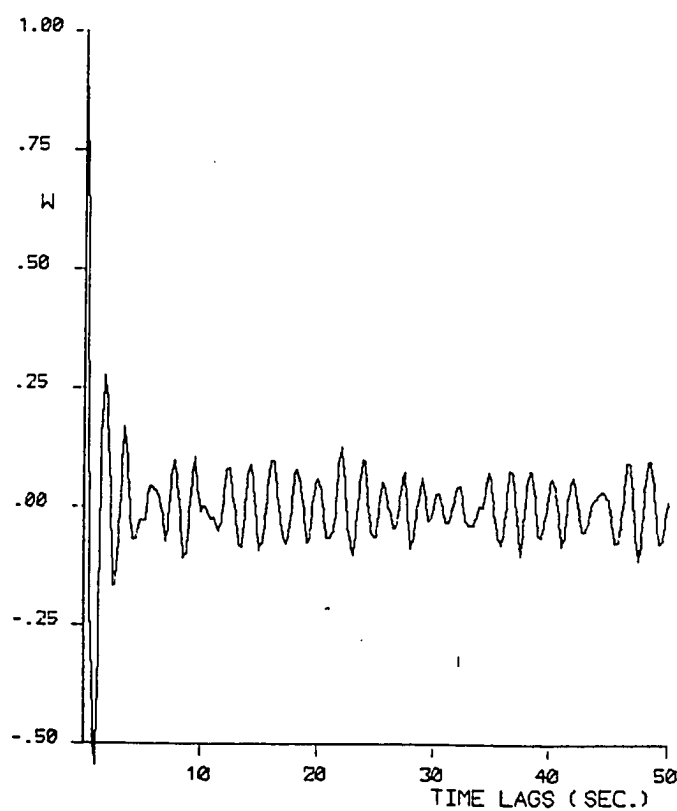
Fig. 60. Autocorrelation of W, record
       4-04. Filtered data at
       $f_{\frac{1}{2}}$ = 0.2 Hz.
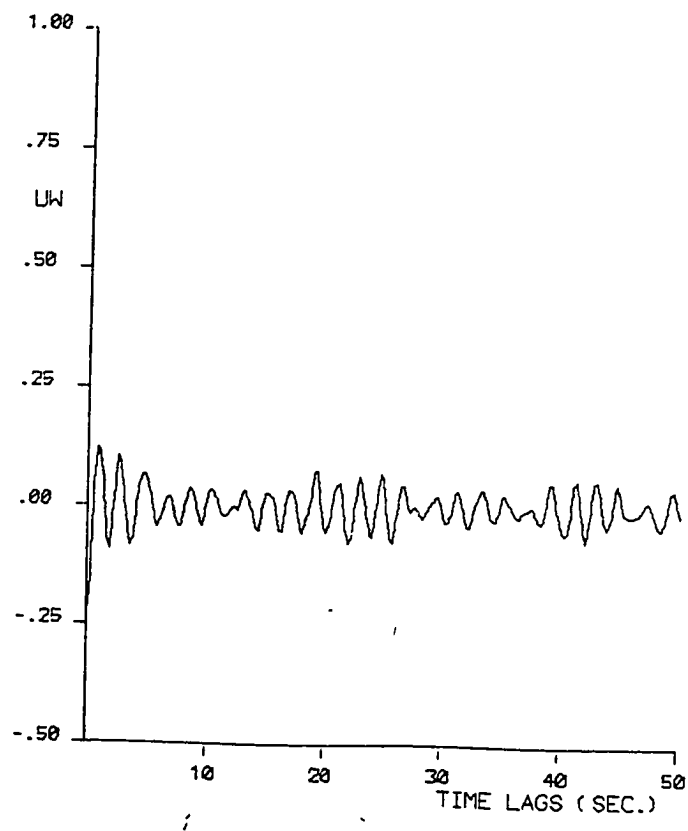
Fig. 61. Crosscorrelation of UW, record 4-04. Filtered data at $f_{\frac{1}{2}} = 0.2$ Hz.
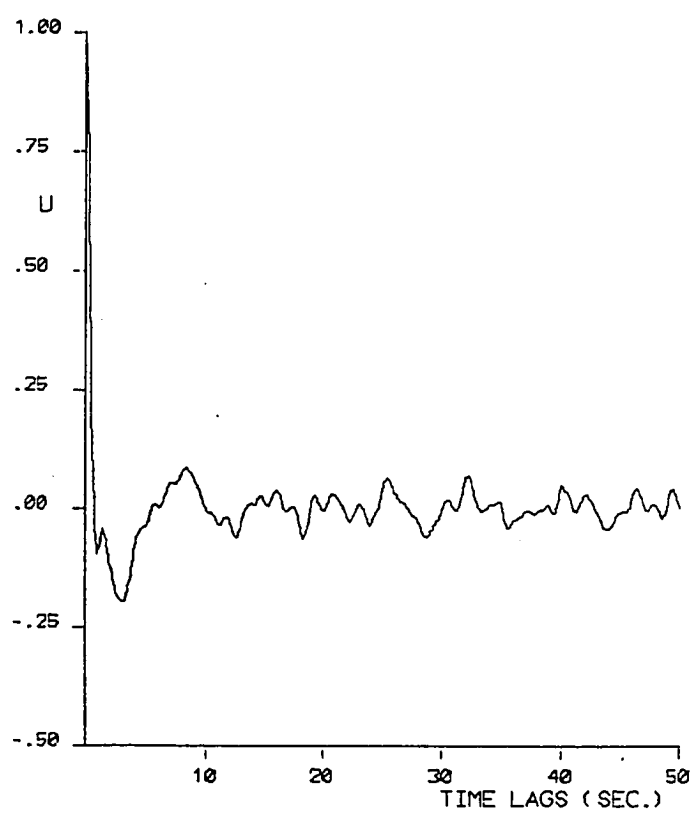
Fig. 62. Autocorrelation of U, record
2-07. Filtered data at $f_{\frac{1}{2}}$ =
0.2 Hz.
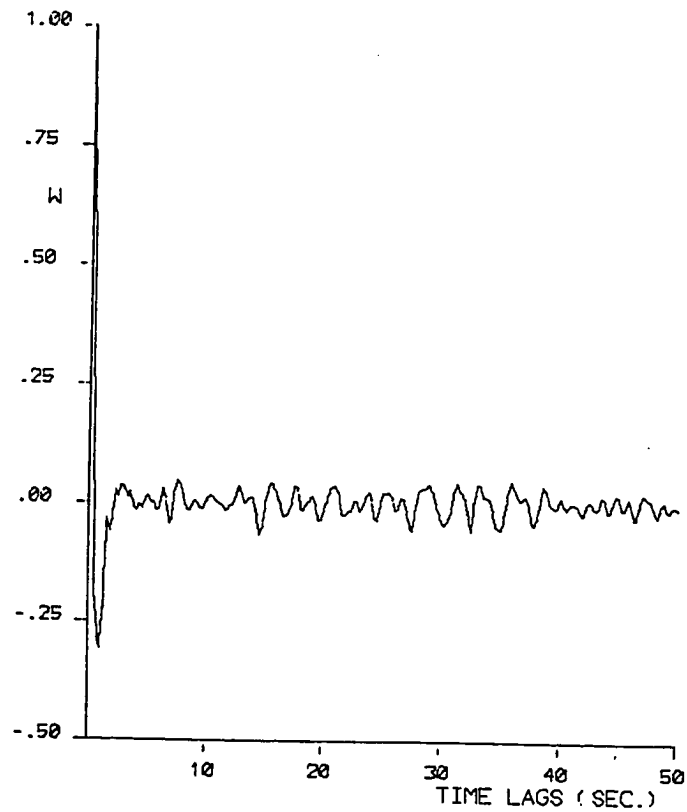
Fig. 63. Autocorrelation of W. record
2-07. Filtered data at $f_{\frac{1}{2}}$ =
0.2 Hz.
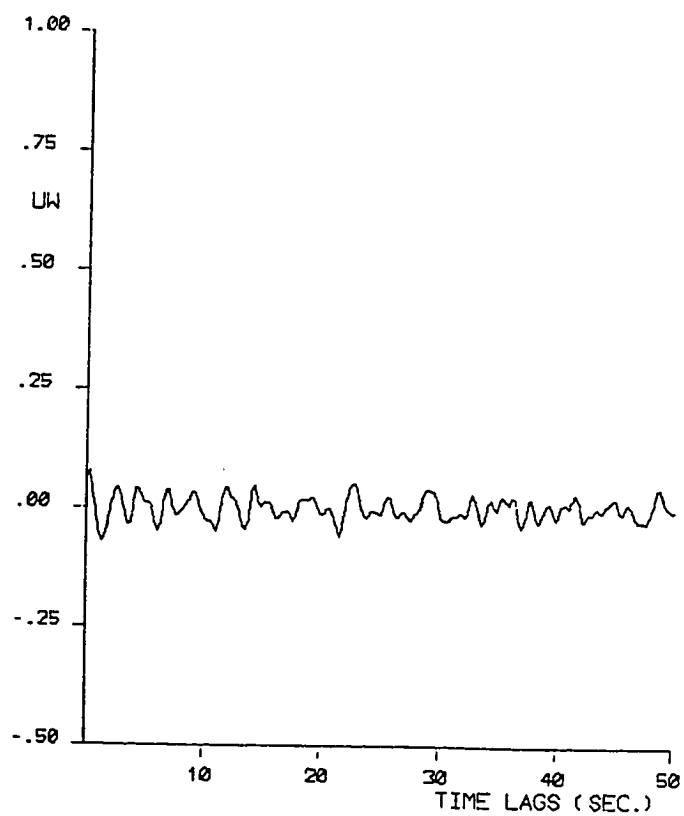
Fig. 64. Crosscorrelation of UW, record
2-07. Filtered data at $f_{\frac{1}{2}} = 0.2$
Hz.
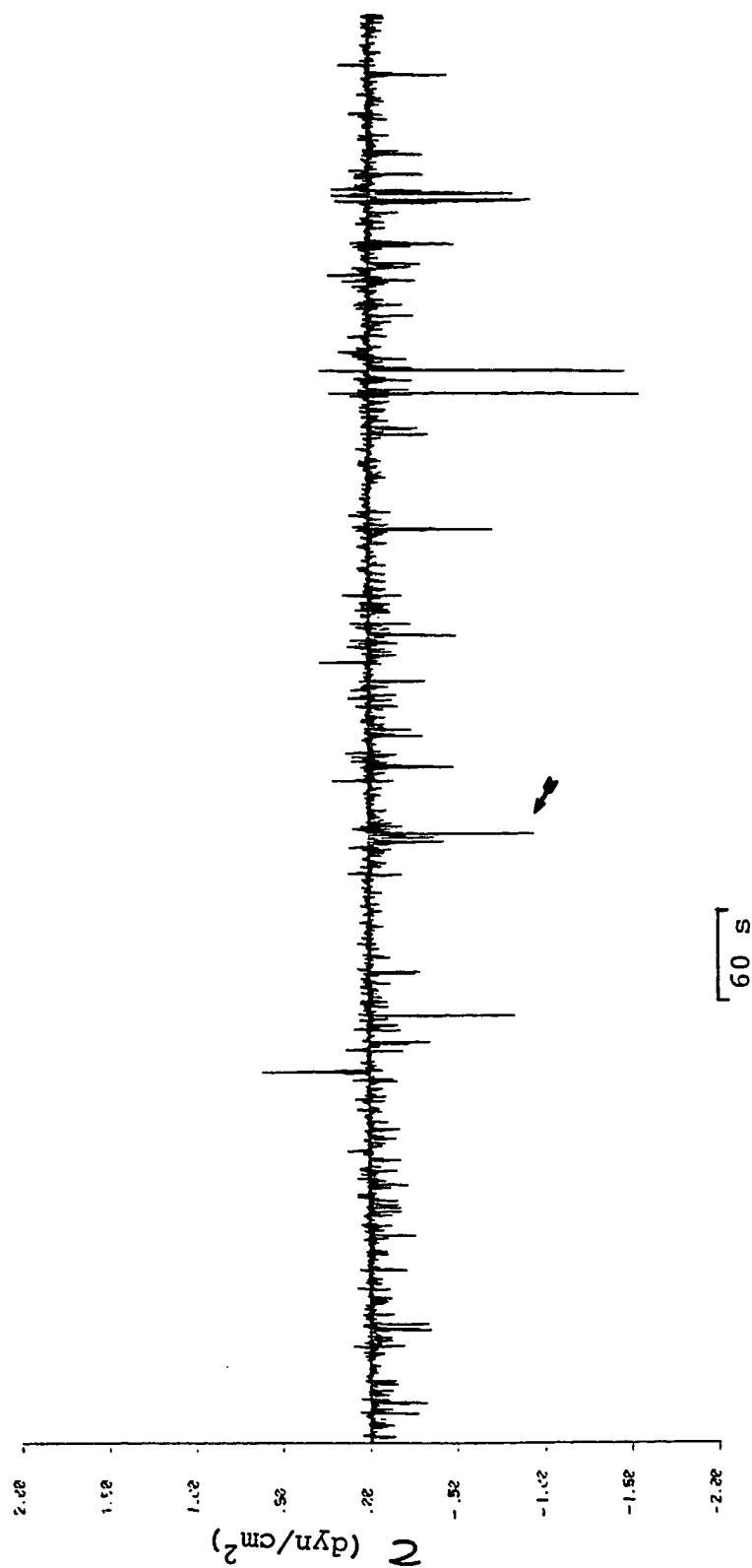
Fig. 65. Plot of instantaneous shear stress as function of time, for record Pl-02. $\bar{\tau} = -0.022$ dyn/cm². Data filtered at $f_{\frac{1}{2}} = 0.2$ Hz. The marked spike is shown enlarged in Fig. 73.
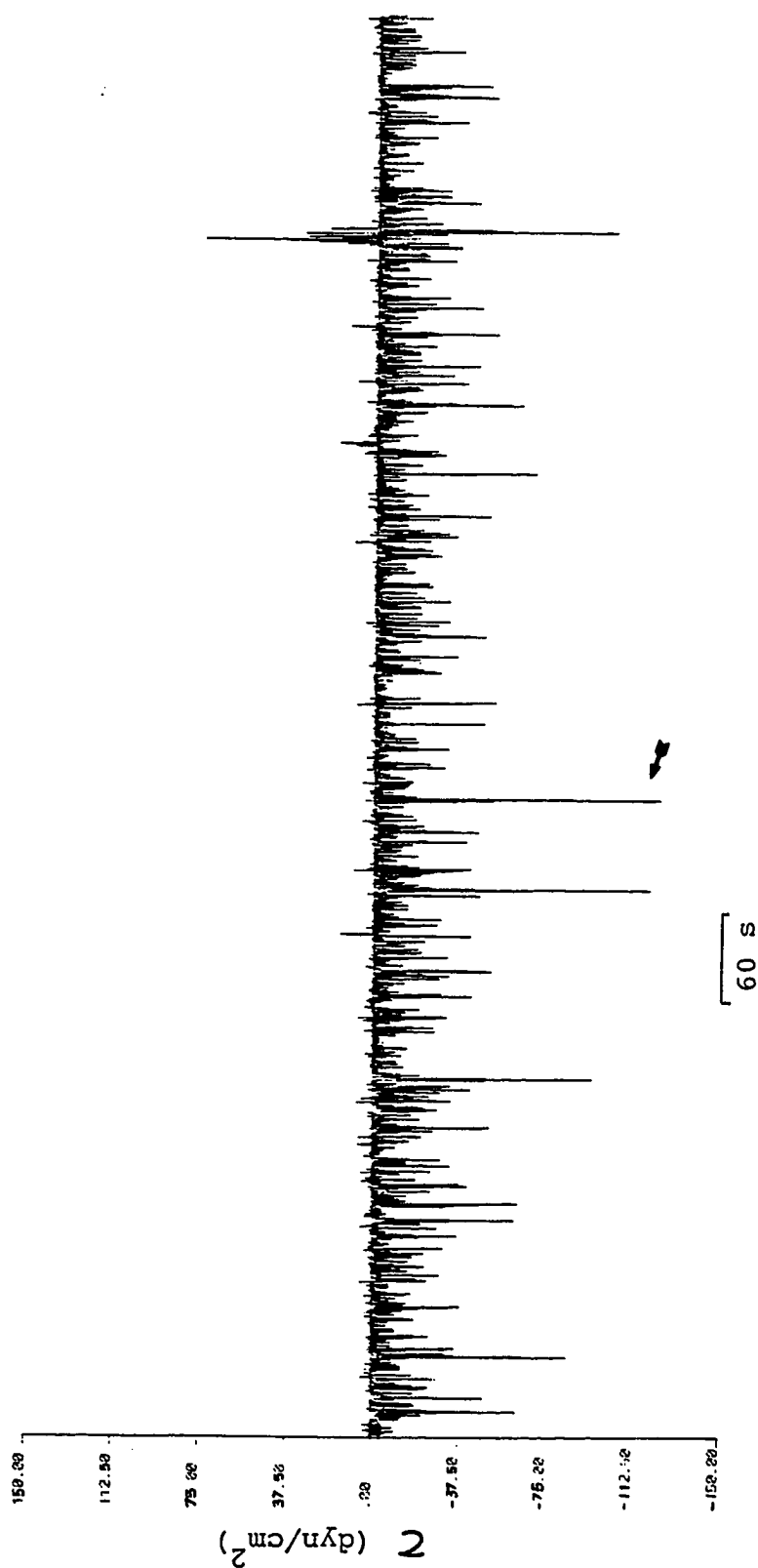
Fig. 66. Plot of instantaneous shear stress as function of time, for record P1-03. $\bar{\tau} = -4.854$ dyn/cm^2. Data filtered at $f_{\frac{1}{2}} = 0.2$ Hz. The marked spike is shown enlarged in Fig. 74.
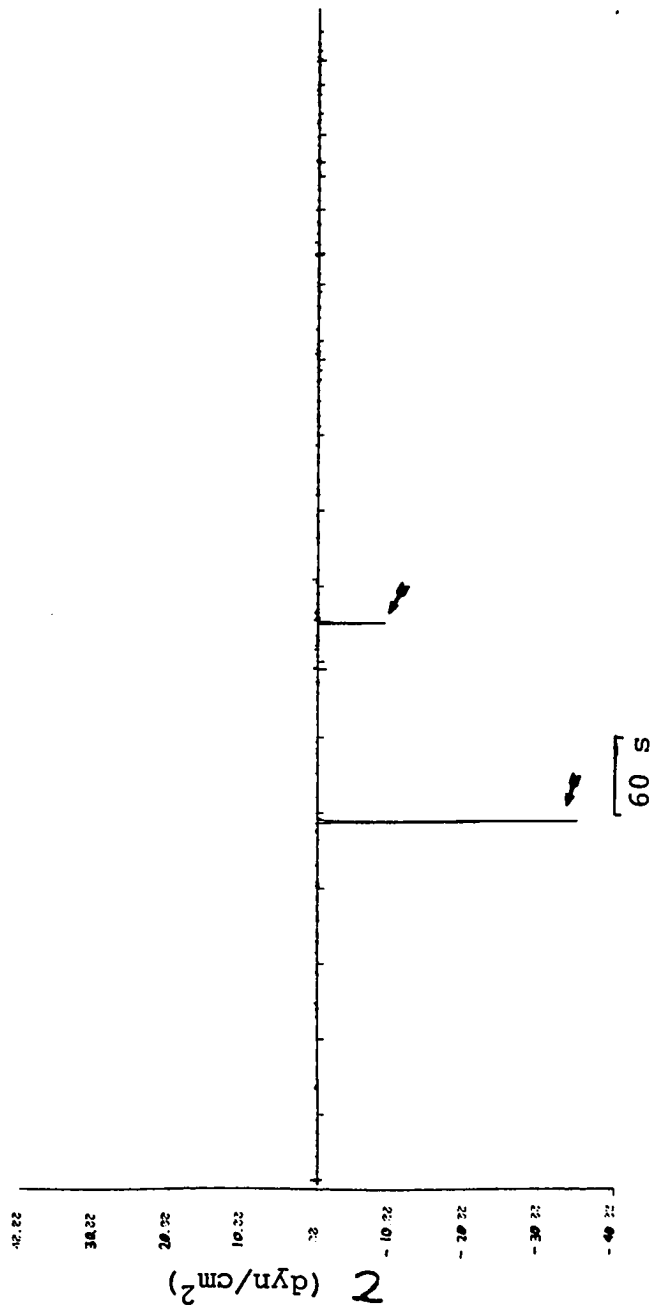
Fig. 67. Plot of instantaneous shear stress as function of time, for record 4-05. $\tau = -0.036$ dyn/cm^2. Data filtered at $f_{\frac{1}{2}} = 0.2$ Hz. Marked spikes are shown enlarged in Figs. 75 and 76.
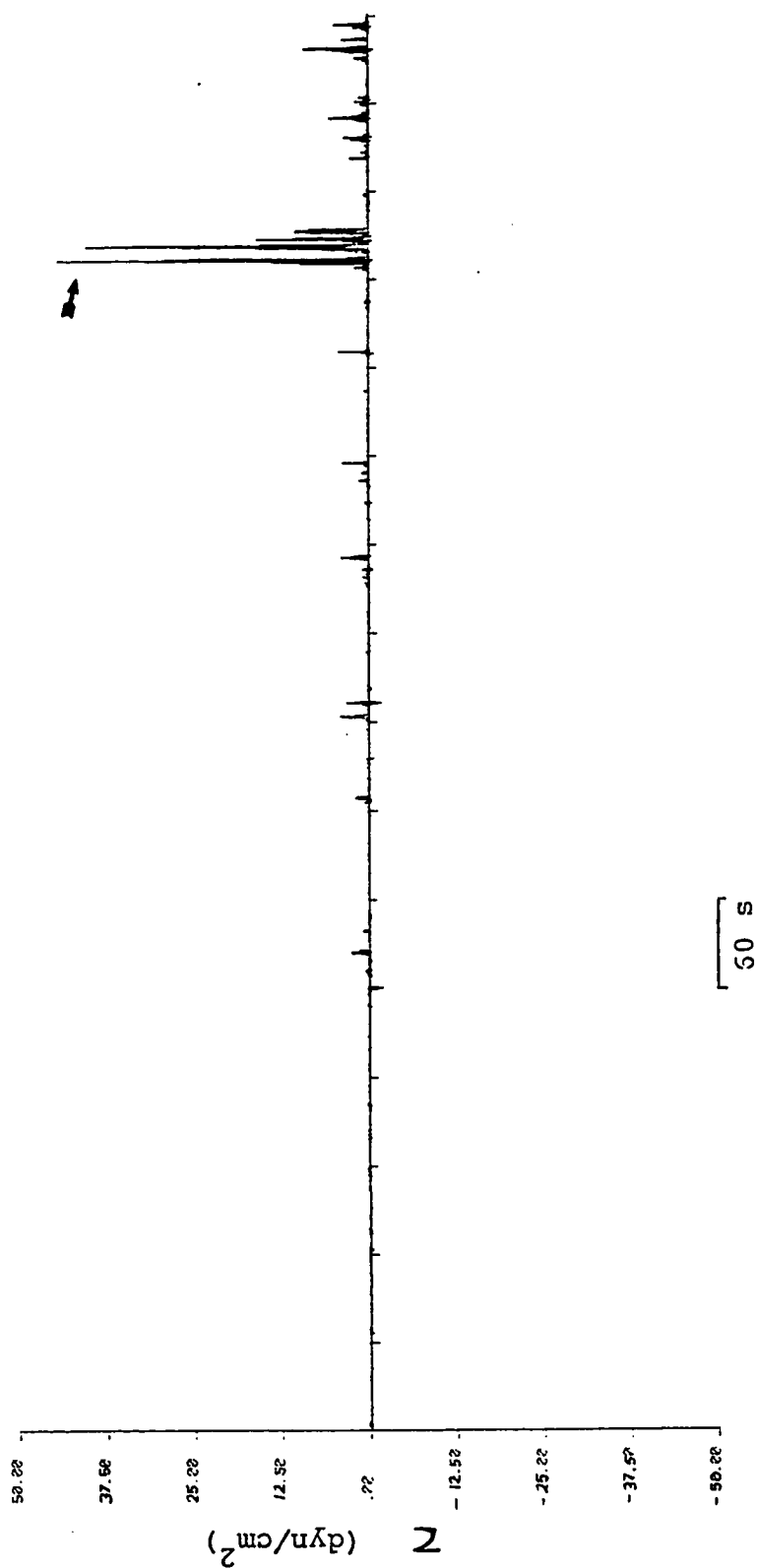
Fig. 68. Plot of instantaneous shear stress as function of time, for record 3-04. τ = 0.192 dyn/cm^2. Data filtered at $f_{1/2}$ = 0.2 Hz. The marked spike is shown enlarged in Fig. 77.
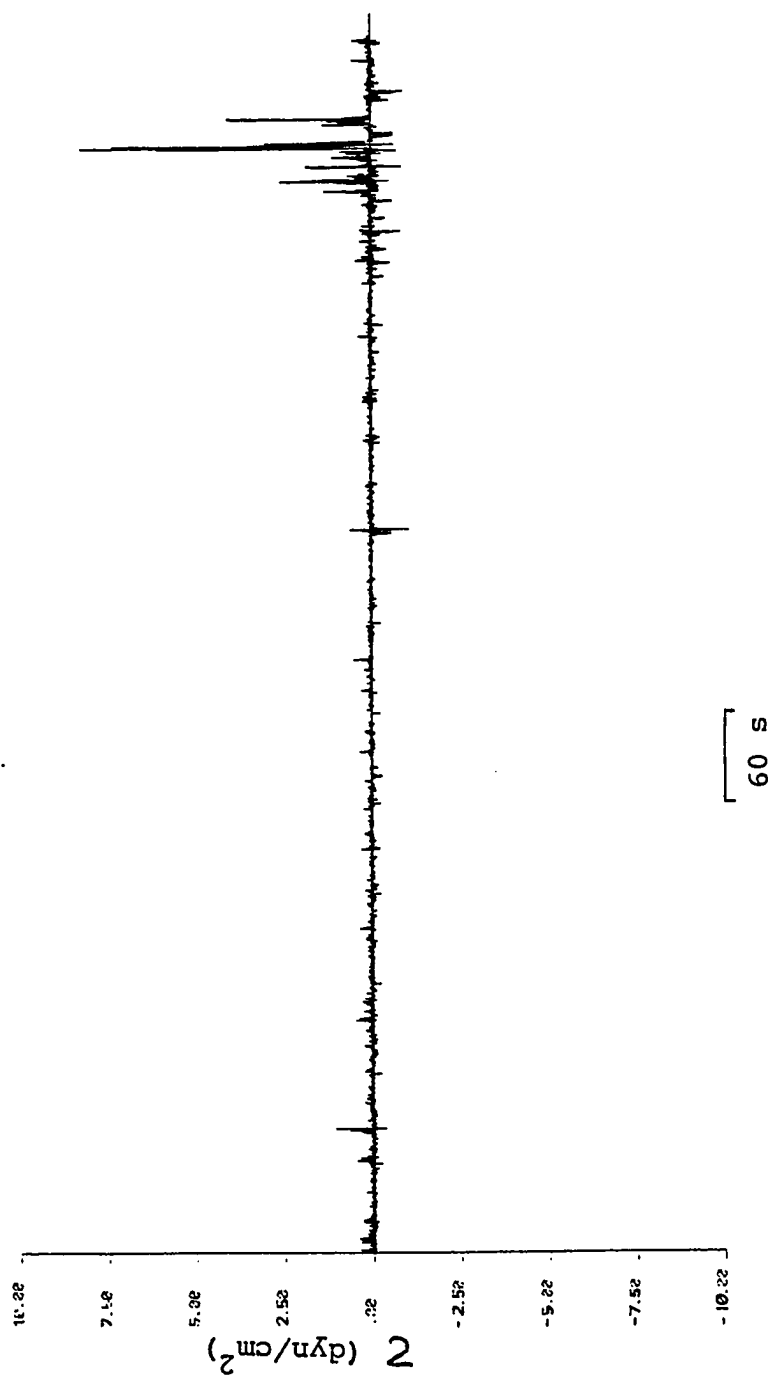
Fig. 69. Plot of instantaneous shear stress as function of time, for record 4-04. $\bar{\tau} = 0.032$ dyn/cm². Data filtered at $f_{\frac{1}{2}} = 0.2$ Hz.

60 s
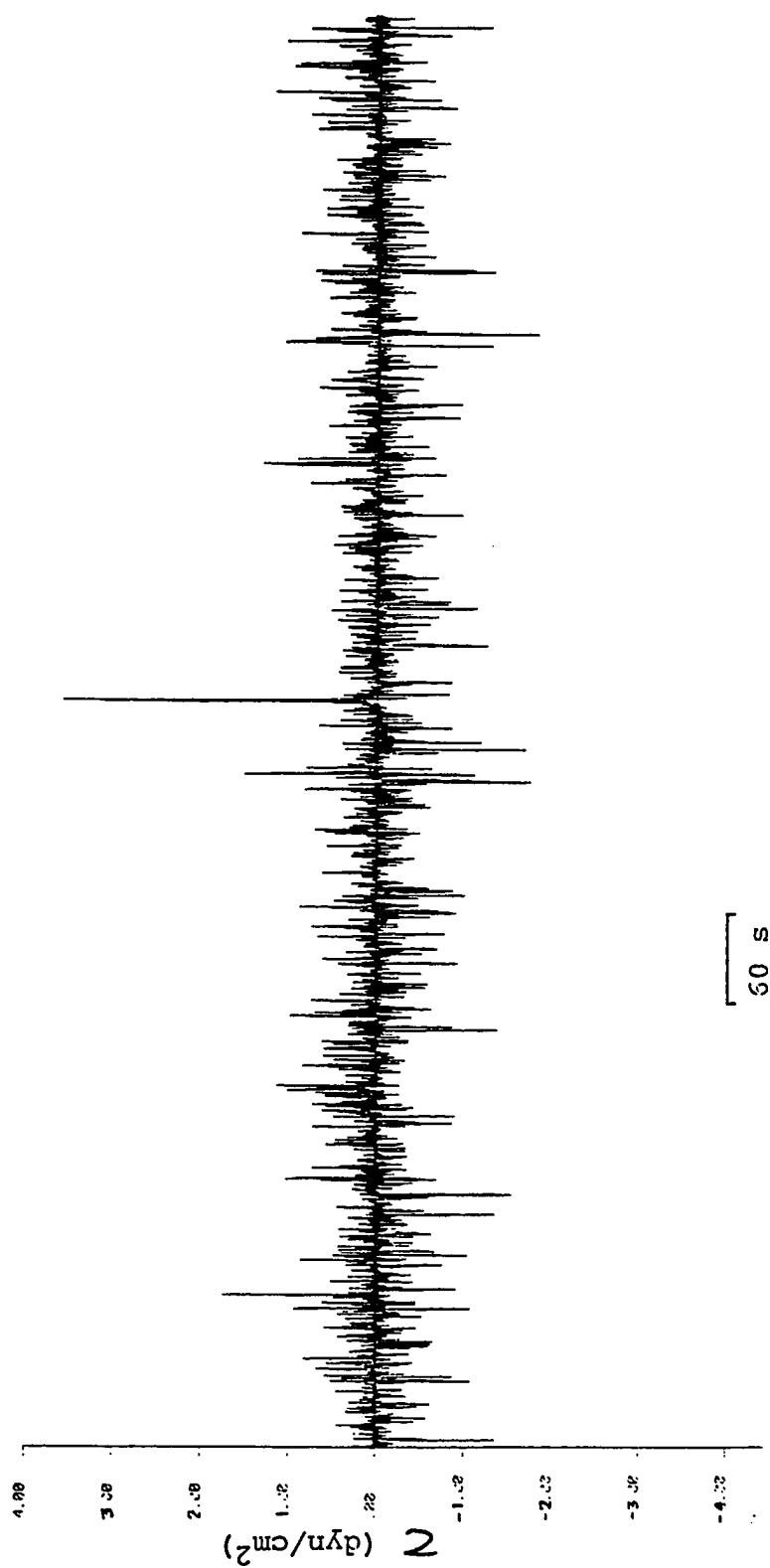
τ (dyn/cm²)

Fig. 70. Plot of instantaneous shear stress as function of time, for record 2-07. $\overline{\tau} = -0.014$ dyn/cm^2. Data filtered at $f_{\frac{1}{2}} = 0.2$
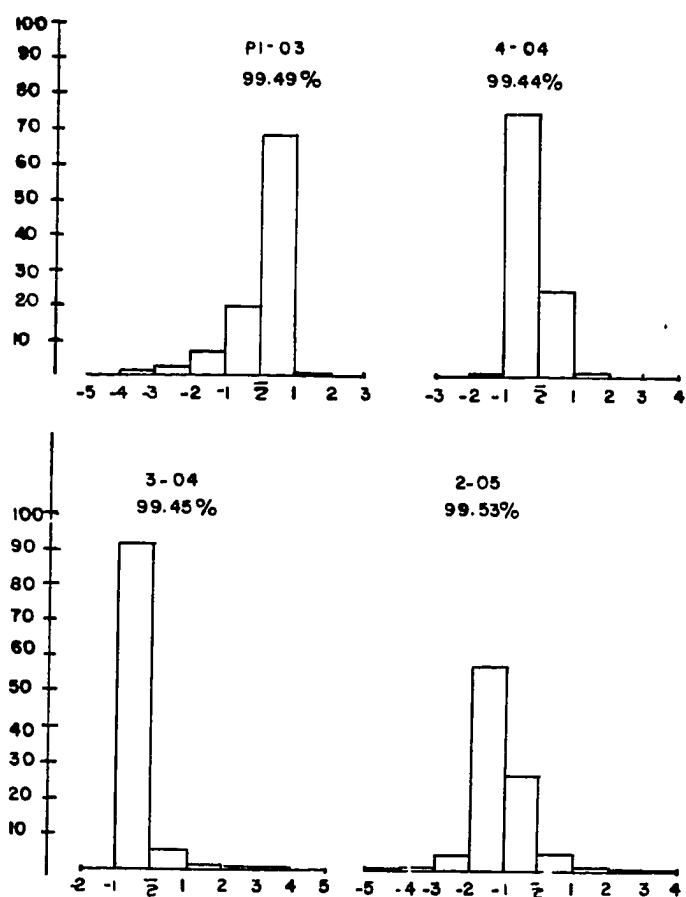
Fig. 71. Frequency percent histogram of shear
stress versus number standard
deviation around the mean. For records
P1-03, 4-04, 3-04 and 2-05. The
percentage of points of each record
represented is indicated.
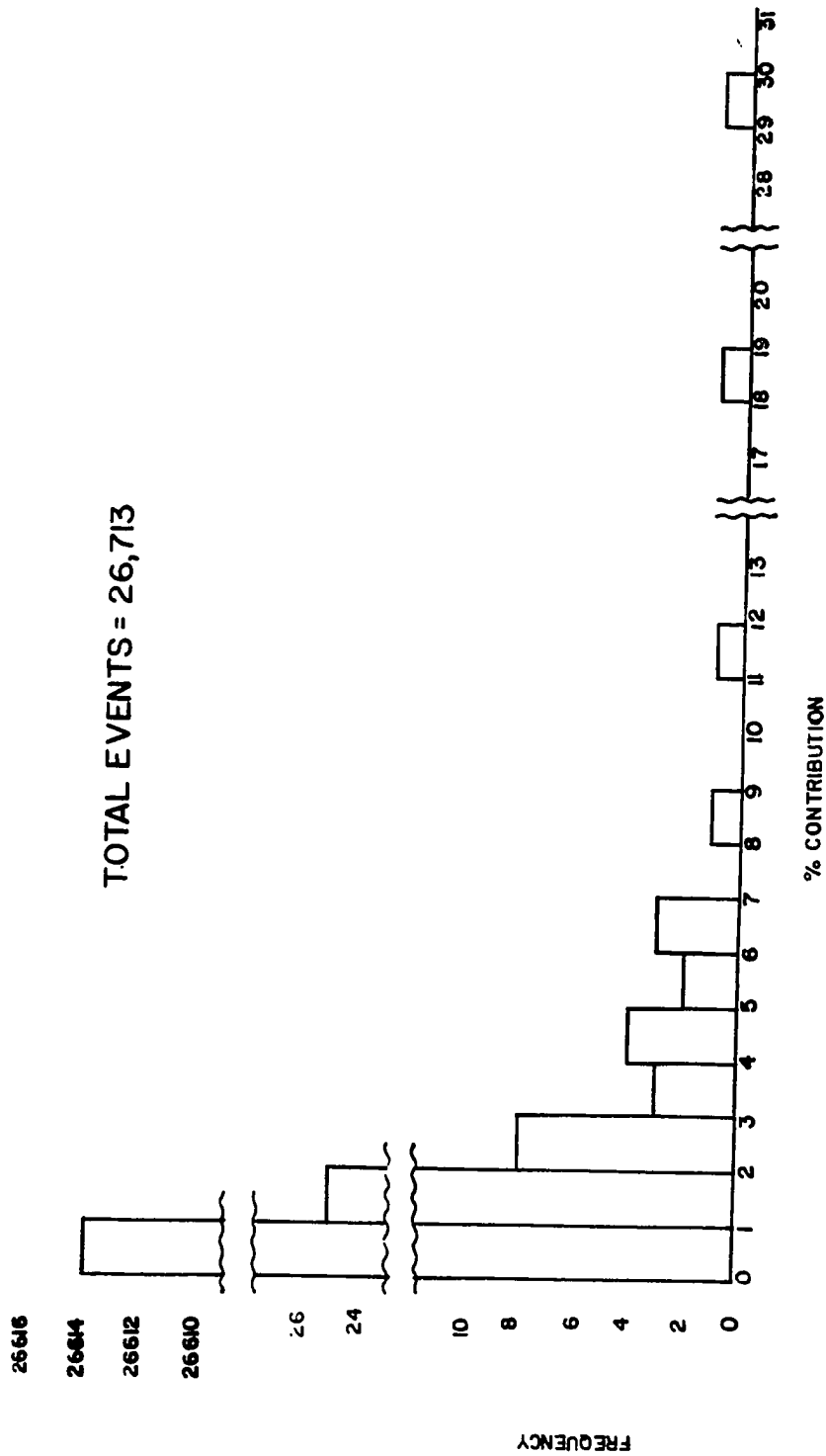
Fig. 72. Frequency histogram for the total number of events calculated from the 18 records as a function of their percentage contribution to the individual shear stresses.
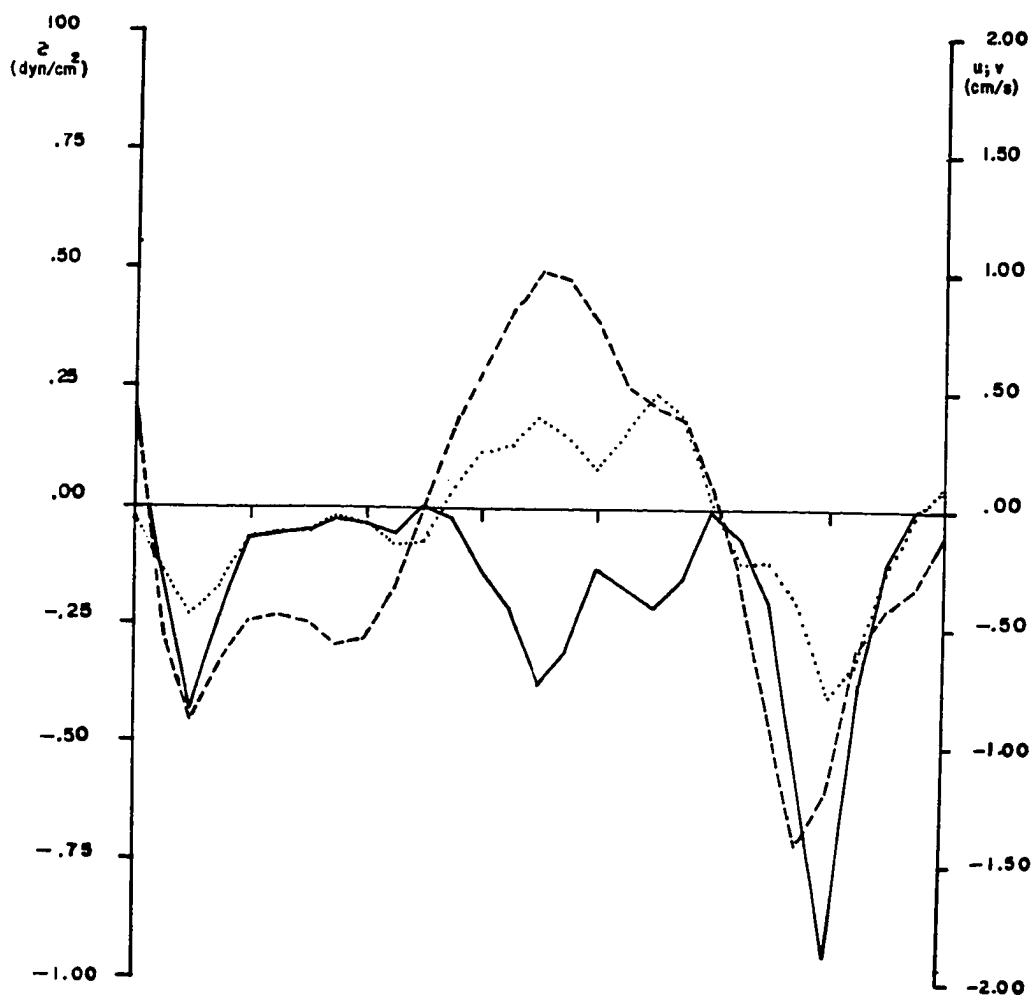
Fig. 73. Expanded spike for record P1-02 (Fig. 65). Time length between zero crossings = 7.0 seconds. Sum of the instantaneous shear stresses between zero crossings = -5.15 dyn/cm². Percent contribution to the value of $\mathcal{T}$ = 3.49%. $\mathcal{T}$ = —— , u = ----. w = ...
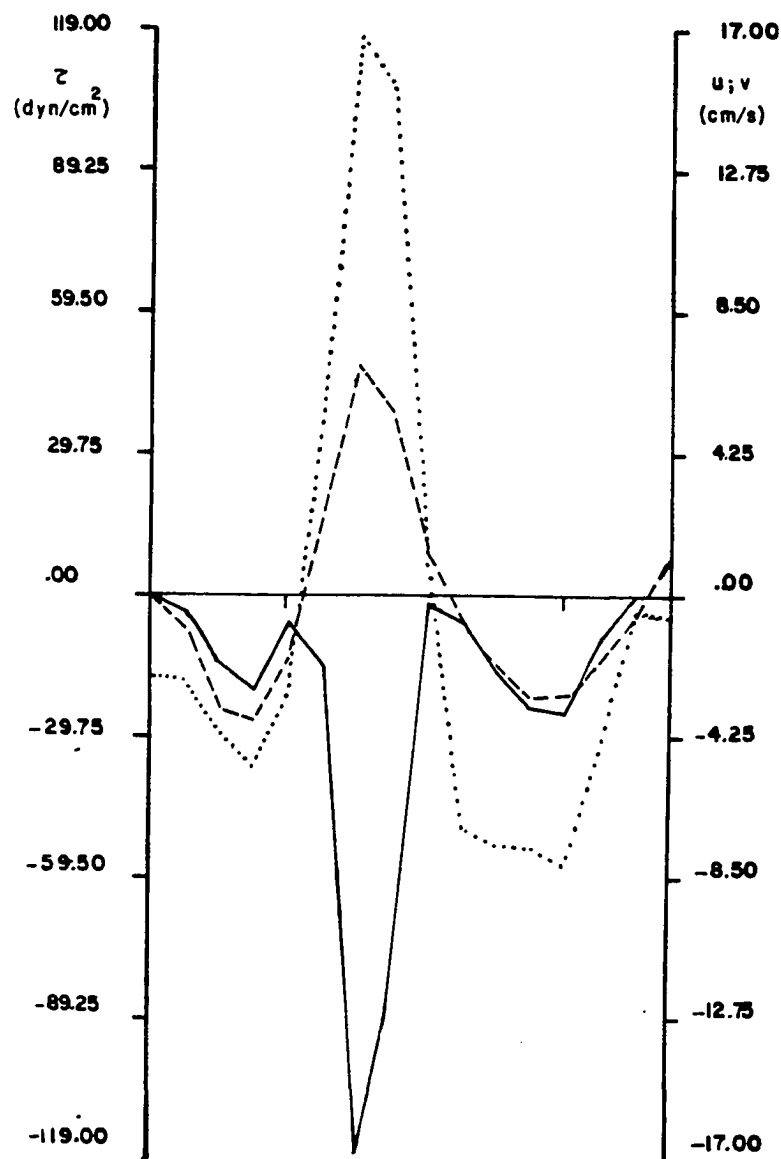
Fig. 74. Expanded spike for record Pl-03 (Fig. 66).
Time length between zero crossings = 3.75
seconds. Sum of the instantaneous shear
stresses between zero crossings = -341.69
dyn/cm². Percent contribution to the value
of τ = 1.54%. τ =——— , u = ————, w = ...
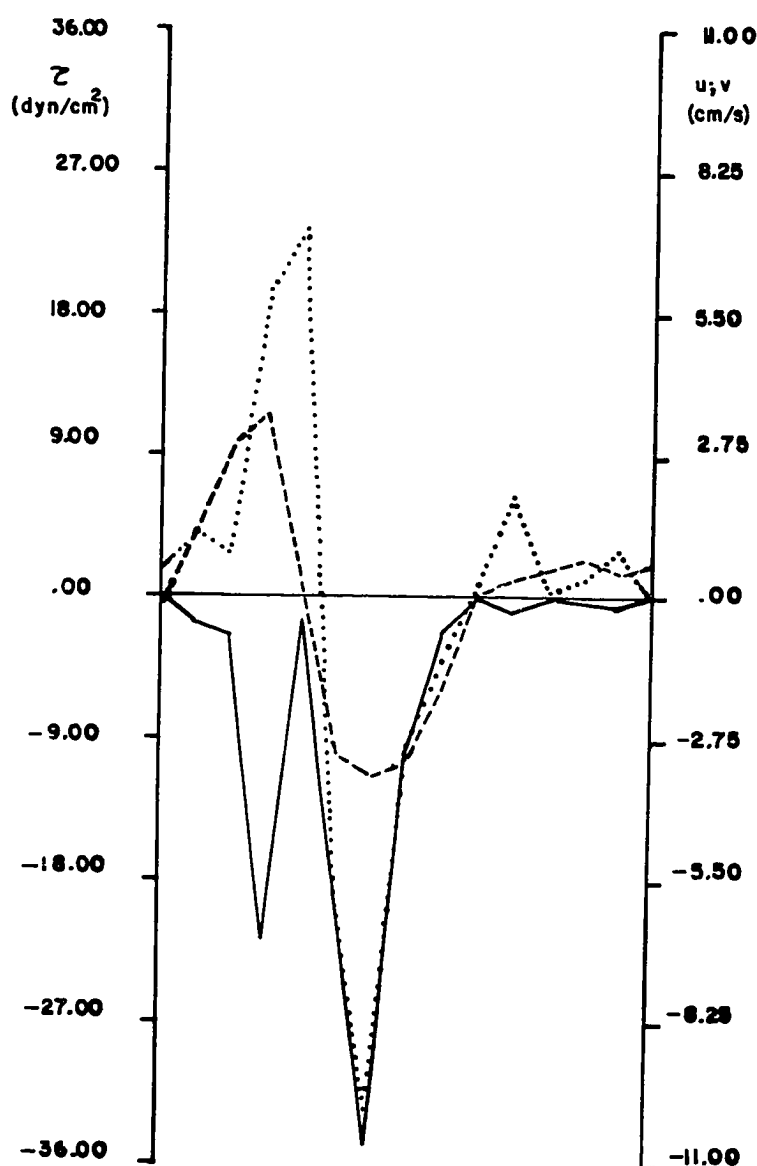
Fig. 75. Expanded spike for record 4-05
(Fig. 67). Time length between
zero crossings equals to 3.50
sec. Sum of the instantaneous shear
shear stresses between zero
crossings equals to -94. 15
dyn/cm^2. Percent contribution
to the value of $\mathcal{C}$ = 29.97%, $\mathcal{C}$ =———,
u = ————, w = ...
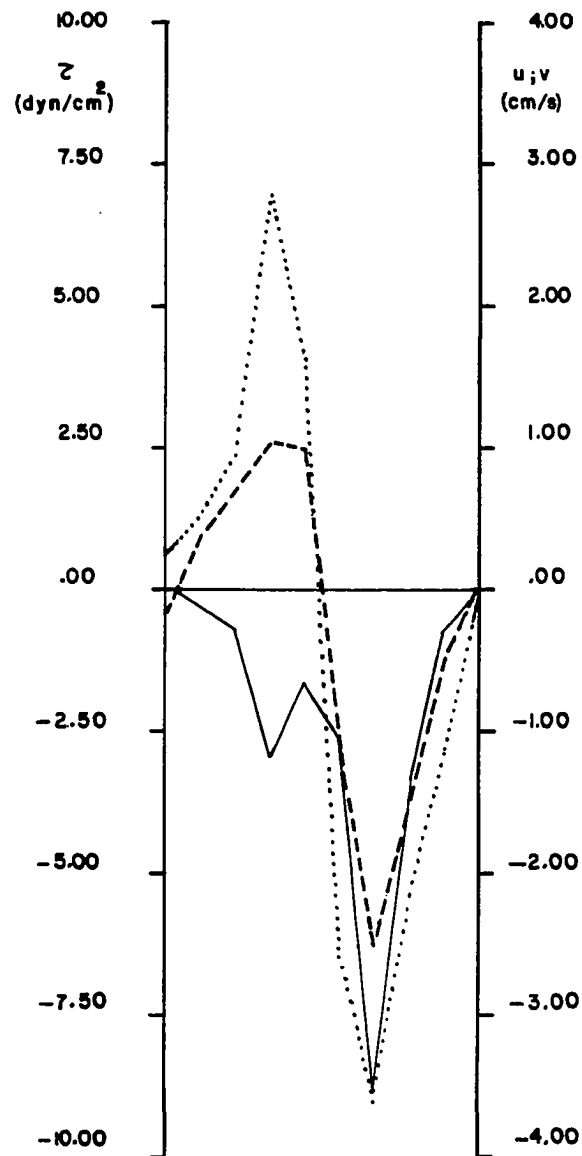
Fig. 76. Expanded spike for record 4-05
(Fig. 67). Time length between
zero crossings = 2.25 seconds.
Sum of the instantaneous shear
stresses between zero crossings
equals to -21.41 dyn/cm^2.
Percent contribution to the
value of $\overline{z}$ = 6.82%. z = ——— ,
u = ————, w = ...
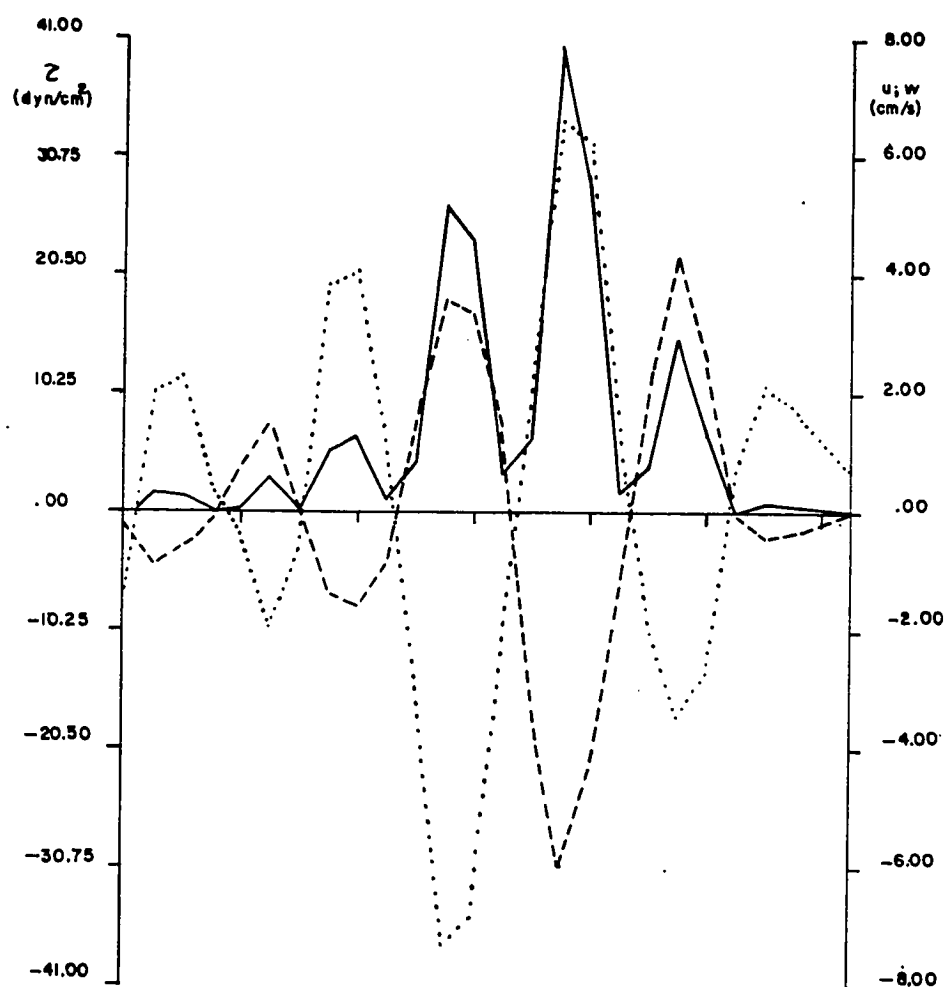
Fig. 77. Expanded spike for record 3-04 (Fig. 68). Time length between zero crossings = 6.25 seconds. Sum of the instantaneous shear stresses between zero crossings = 179.71 dyn/cm^2. Percent contribution to the value of τ = 18.85% τ = —— , u = ---- . w = ...

BIBLIOGRAPHY

Adams, C. E., and Weatherly, G. L., 1981. Suspended sediment transport and benthic boundary layer dynamics. Mar. Geol. 42:1-18.

Allen, G. P.; Castaing, P.; and Klingebiel, A., 1972. Distinction of elementary sand population in the Gironde Estuary (France) by R-mode factor analysis of grain size data. Sediment. 19:21-35.

Allen, J. R. L., 1968. Current ripples: Their relation to patterns of water and sediment motion. North-Holland Pub. Co., Amsterdam. 433 pp.

Allen, J. R. L., 1980. Sand waves: a model of the origin and internal structures. Sedim. Geol. 26:281-328.

Bagnold, R. A., 1966. An approach to the sediment transport problem from general physics. U.S. Geol. Surv. Prof. Paper 422 - I. 37 pp.

Bendat, J. S., and Piersol, A. G., 1971. Random data: analysis and measurement procedures. Wiley Interscience, New York. 407 pp.

Benjamin, T. B., 1959. Shearing flow over a wavy boundary. J. Fluid Mech. 6:161-205.

Bowden, K. F., 1962. Measurements of turbulence near the sea bed in a tidal current. J. Geophys. Res. 67: 3181-3186.

Bowden, K. F., and Proudman, J., 1949. Observations on the turbulence fluctuations of a tidal current. Proc. Roy. Soc. London A199:311-327.

Bowden, K. F., and Fairbairn, L. A., 1956. Measurements of the turbulent fluctuations and Reynolds stress in a tidal current. Proc. Roy. Soc. London A237: 422-438.

Bowden, K. F.; Fairbairn, L. A.; and Hughes, P., 1959. The distribution of shearing stresses in a tidal current. Geophs. J. Roy. Astr. Soc. 2:288-305.

Carruthers, J. N., 1967. An improved simple current-measuring bottle for fishermen. Fisherman News, 3 pp.

Chung, J. Y., 1979. Turbulence spectra in a well-mixed estuary. Ph.D. Dissertation, Dept. of Oceanography, Old Dominion University. 233 pp.

Corino, E. R., and Brodkey, R. S., 1969. A visual investigation of the wall region in turbulent flow. J. Fluid Mech. 37:1-30.

Cornish, V., 1901. On sand waves in tidal currents. Geogr. J. 18:170-202.

Davies, A. G., and Wilkinson, R. H., 1977. The movement of non-cohesive sediment by surface waves. Part I: Literature survey. Inst. Ocean. Sci. Rept. 45, 73 pp.

Daily, J. W., and Harleman, D. R. F., 1966. Fluid Dynamics. Addison-Wesley, Pub. 454 pp.

Darwin, G. H., 1884. On the formation of ripple-marks. Proc. Roy. Soc. London 36:18-43.

Davis, J. C., 1973. Statistical and data analysis in geology. Wiley-Interscience, New York. 550 pp.

Drapeau, G., 1973. Factor analysis: how it copes with complex geological problems. Math. Geol. 5:351-363.

Dyer, K. R., 1970. Current profiles in a tidal channel. Geophy. J. R. Astr. Soc. 22:153-161.

Dyer, K. R., 1972. Bed shear stresses and the sedimentation of sandy gravel. Mar. Geol. 13:M31-M36.

Fenchel, T. M., and Riedl, R. J., 1970. The sulfide system: a new biotic community underneath the oxydized layer of marine sand bottoms. Mar. Biol. 7:255-268.

Firek, F.; Shideler, G. L.; and Fleischer, P., 1972. Heavy-mineral variability in bottom sediments of lower Chesapeake Bay, Virginia. Mar. Geol. 23: 217-235.

Folk, R. L., 1974. Petrology of sedimentary rocks. Hemphill's, Austin, Texas. 170 pp.

Folk, R. L., and Ward, W. C., 1957. Brazos river bar: a study in the significance of grain size parameters. J. Sediment. Petrol. 27:3-26.

Friedman, G. M., 1961. Distinction between dune, beach and river sands from their textural characteristics. J. Sediment. Petrol. 31:514-529.

Friedman, G. M., 1967. Dynamic processes and statistical parameters compared for size frequency distribution of beach and river sands. J. Sediment. Petrol. 37: 327-354.

Goldsmith, V., and Sutton, C. H., 1977. Bathymetry of Chesapeake Bay. Virginia Inst. Mar. Sci. Bathy. Chart Ser. 2.

Gordon, C. M., 1974. Intermittent momentum transport in a geophysical boundary layer. Nature 248:392-394.

Gordon, C. M., and Witting, J., 1977. Turbulent structure in a benthic boundary layer. In Nihoul, J. C. J. (ed.): Bottom turbulence. Elsevier, Amsterdam. 59-81.

Granat, M. A., 1976. The dynamics and sedimentology of Inner Middle Ground-Nine Foot shoal, Chesapeake Bay entrance, Virginia. MS Thesis, Dept. of Oceanography, Old Dominion Univ. 110 pp.

Granat, M. A., and Ludwick, J. C., 1980. Perpetual shoals at the entrance to Chesapeake Bay: Flow-substrate interactions and mutually evasive net currents. Mar. Geol. 36:307-323.

Grosch, C. E., 1981. Lecture notes on statistical wave theory. Dept. of Oceanography, Old Dominion Univ. (unpublished) 100 pp.

Harms, J. C.; Southard, J. B; Spearing, D. R.; and Walker, R. G., 1975. Depositional environments as interpreted from primary sedimentary structures and stratification sequences. Soc. Est. Pet. Min. Short Course 2, 161 pp.

Heathershaw, A. D., 1974. Bursting phenomena in the sea. Nature 248:394-395.

Heathershaw, A. D., 1976. Measurements of turbulence in the Irish Sea benthic boundary layer. In: McCave, I. N. (ed.), The benthic boundary layer. Plenum Pub. Co., New York. 11-31.

Heathershaw, A. D., 1979. The turbulent structure of the bottom boundary layer in a tidal current. Geophys. J. Roy. Astr. Soc. 58:395-430.

Heathershaw, A. D., 1981. Comparisons of measured and predicted sediment transport rates in tidal currents. Mr. Geol. 42:75-104.

Heathershaw, A. D., and Simpson, J. H., 1978. The sampling variability of the Reynolds stress and its relation to boundary shear stress and drag coefficient measurements. Est. Coast. Mar. Sc. 6:263-274.

Hilder, F. A., 1980. Surface circulation and horizontal diffusion processes of the lower Chesapeake Bay. Ph.D. Dissertation, Dept. of Oceanography, Old Dominion Univ. 188 pp.

Hine, A. C., 1977. Lily Bank, Bahamas: history of an active oolite sand shoal. J. Sediment. Petrol. 47: 1554-1581.

Hinze, J. O., 1975. Turbulence. McGraw Hill, Inc., 2 ed. 790 pp.

Houbolt, J. J. H. C., 1968. Recent sediments in the southern bight of the North Sea. Geol. in Minj. 47:245-273.

Hsu, S. T., and Kennedy, J. F., 1971. Turbulent flow in wavy pipes. J. Fluid Mech. 47:481-502.

Hubbard, D. K.; Ortel, G.; and Nummedal, D., 1979. The role of waves and tidal currents in the development of tidal-inlet sedimentary structures and sand body geometry: Examples from North Carolina, South Carolina, and Georgia. J. Sediment. Petrol. 49:1073-1092.

Imbrie, J., and Purdy, E. G., 1962. Classification of modern Bahamian carbonate sediments. In: Hams, W. E. (ed.), Am. Assoc. Petrol. Geol. Mem. 1:253-272.

Imbrie, J., and van Andel, T. H., 1964. Vector analysis of heavy mineral data. Geol. Soc. Am. Bull. 75:1131-1156.

Johns, B., 1970. On the mass transport induced by oscillatory flow in a turbulent boundary layer. J. Fluid. Mech. 43:177-185.

Johns, B., 1975. The form of the velocity profile in a turbulent shear wave boundary layer. J. Geophys. Res. 80:5109-5112.

Jonsson, I. G., and Carlsen, N. A., 1976. Experimental and theoretical investigations in an oscillatory turbulent boundary layer. J. Hydr. Res. 14:45-60.

Jopling, A. V., 1965. Hydraulic factors controlling the shape of laminae in laboratory deltas. J. Sediment. Petrol. 35:777-791.

Jorgensen, B. B., 1977. The sulfide cycle of a coastal marine sediment (Limfjorden, Denmark). Limn. Ocean. 22:814-831.

Kajiura, K., 1968. A model of the bottom boundary layer in water waves. Bull. Earth. Res. Inst., Japan. 46:75-123.

Karahan, M. E., and Peterson, A. W., 1980. Visualization of separation over sand waves. ASCE-J. Hyd. Div. 106:1345-1352.

Kendall, J. M., 1970. The turbulent boundary layer over a wall with progressive surface waves. J. Fluid. Mech. 41:259-281.

Kim, H. T.; Kline, S. J.; and Reynolds, W. C., 1971. The production of turbulence near a smooth wall in a turbulent boundary layer. J. Fluid. Mech. 50:133-160.

Kinsman, B., 1965. Wind waves: their generation and propagation on the ocean surface. Prentice Hall, Inc., New Jersey. 676 pp.

Klovan, J. E., 1966. The use of factor analysis in determining depositional environments from grain-size distributions. J. Sediment. Petrol. 36:115-125.

Lu, S. S., and Willmarth, W. W., 1973. Measurements of the structure of the Reynolds stress in a turbulent boundary layer. J. Fluid. Mech. 60:481-511.

Ludwick, J. C., 1970. Sand waves in the tidal entrance to Chesapeake Bay. Chesapeake Sc. 11:98-110.

Ludwick, J. C., 1972. Migration of tidal sand waves in Chesapeake Bay entrance. In: Swift, D. J. P., Duane, D. B., and Pilkey, O. (eds.), Shelf sediment transport: process and pattern. Dowden, Hutchinson and Ross, Inc., Pennsylvania.

Ludiwick, J. C., 1973a. Tidal currents and zig-zag sand shoals in a wide estuary entrance. Dept. of Oceanography, Old Dominion Univ. Tech. Rept. 7, 109 pp.

Ludwick, J. C., 1973b. Tidal currents, sediment transport, and sand banks in Chesapeake Bay entrance, Va. Dept. of Oceanography, Old Dominion Univ. Tech. Rept. 16, 31 pp.

Ludwick, J. C., 1975. Variations in the boundary drag coefficient in the tidal entrance to Chesapeake Bay, Va. Mar. Geol. 19:19-25.

Ludwick, J. C., 1979. An analysis of bathymetric changes in lower Chesapeake Bay. Dept. of Oceanography, Old Dominion Univ. Tech. Rept. 39, 43 pp.

Ludwick, J. C., 1981. Bottom sediments and depositional rates near Thimble Shoal Channel, lower Chesapeake Bay, Virginia. Geol. Soc. Am. Bull. 92:496-506.

Ludwick, J. C., and Wells, J. T., 1974. Particle size distributions and small-scale bedforms on sand waves, Chesapeake Bay entrance, Va. Dept. of Oceanography, Old Dominion Univ. Tech. Rept. 12, 53 pp.

Lukasik, S. J., and Grosch, C. E., 1963. Pressure-velocity correlation in ocean swell. J. Geophys. Res. 68: 5689-5699.

Mason, C. C., and Folk, R. L., 1958. Differentiation of beach dunes and aeolian flat environments by size analysis, Mustang Is., Texas. J. Sediment. Petrol. 28:211-226.

McCave, I. N., 1971. Sand waves in the North Sea off the coast of Holland. Mar. Geol. 10:199-225.

McLean, S. R., and Smith, J. D., 1979. Turbulence measurements in the boundary layer over a sand wave field. J. Geophys. Res. 84:7791-7808.

Meisburger, E. P., 1972. Geomorphology and sediments of the Chesapeake Bay entrance. U.S. C.E.R.C., Tech. Mem. TM 38, 64 pp.

Middleton, G. V., 1976. Hydraulic interpretation of sand size distributions. J. Geol. 84:405-426.

Middleton, G. V., and Southard, J. B., 1978. Mechanics of sediment movement. SPEM, Short course no. 3 (2 ed.), 257 pp.

Miesch, A. T., 1976. Q-mode factor analysis of compositional data. Comp. Geosc. 1:147-159.

Moiola, R. J., and Weiser, D., 1968. Textural parameters: an evaluation. J. Sediment. Petrol. 38:45-53.

Monahan, D., 1976. Morphology and sediments of sand waves in the St. Lawrence estuary. Marit. Sed. 12:1-7.

National Ocean Survey (NOAA), 1972. Bathymetric map: Chesapeake Bay-Hampton Roads. Plate 14.

Nelsen, T. A., 1981. The application of Q-mode factor analysis of suspended particulate matter studies: an example from the New York bight apex. Mar. Geol. 39:15-31.

Ortel, G. F., 1973. Examination of textures and structures of mud in layered sediments at the entrance of a Georgia tidal inlet. J. Sediment. Petrol. 43:33-41.

Parker, G.; Perillo, G. M. E.; and Violante, R. A., 1978. Caracteristicas geologicas de los bancos alineados (linear shoals) frente a Punta Medanos, Provincia de Buenos Aires. Acta Ocean. Argent. 2:11-50.

Passega, R., 1957. Texture as characteristics of clastic deposition. Bull. A.A.P.G. 41:1952-1984.

Phillips, O. M., 1980. The dynamics of the upper ocean. Cambridge Univ. Press, 336 pp.

Pond, S., and Pickard, G. L., 1979. Introductory dynamic oceanography. Pergamon Press, New York. 241 pp.

Raudkivi, A. J., 1963. Study of sediment ripple formation. ASCE-J. Hyd. Div. 89:15-33.

Rao, K. N.; Nurashima, R.; and Badri Narayanan, M. A., 1971. The "bursting" phenomenon in a turbulent boundary layer. J. Fluid Mech. 48:339-352.

Reineck, H. E., and Singh, I. B., 1980. Depositional sedimentary environments. Springer -Verlag (2nd ed.). 549 pp.

Schlichting, H., 1968. Boundary layer theory. McGra Hill, New York.

Shideler, G. L., 1975. Physical parameters distribution patterns in bottom sediments of the lower Chesapeake Bay estuary, Va. J. Sediment. Petrol. 45:728-737.

Shields, A., 1936. Anwendung der Anhlichkeitsmechanik und
    der Turbulenzforschung auf du Geschiebebewegung.
    Mitteilungen der Preussischan. Versuchsanstalt fur
    Wasserbau und Schiffbau. Transl. by Ott, W. P., and
    van Uchelen, J. C. Cal. Inst. Tech. Pub. 167.

Simon, D. B.; Richardson, E. V.; and Nordin, C. F., 1965.
    Sedimentary structures generated by flow in alluvial
    channels. Soc. Econ. Paleo. Min. Spec. Pub. 12:34-52.

Smith, J. D. , 1969. Investigations of turbulent boundary
    layer and sediment-transport phenomena as related to
    shallow marine environments. Part 2: Studies of
    non-uniform boundary layer flows. Dept. of
    Oceanography, Univ. of Washington. Tech. Rept.
    A69-7.

Soulsby, R. L., 1980. Selecting record length and digit-
    ali. :ion rate for near-bed turbulence measurements.
    J. Phys. Ocean. 10:208-219.

Soulsby, R. L., 1981. Measurements of the Reynolds stress
    components close to a marine sand bank. Mar. Geol.
    42:35-47.

Soulsby, R. L., and Dyer, K. R., (in press). The form of
    the near-bed velocity profile in a tidally accelerat-
    ing flow. J. Geophys. Res.

Stenberg, R. W., 1968. Friction factors in tidal channels
    with differing bed roughness. Mar. Geol. 6:243-260.

Swift, D. J. P.; Stanley, D. J.; and Durray, J. R., 1971.
    Relict sediments on continental shelves: a reconsid-
    eration. J. Geol. 79:322-346.

Swift, D. J. P.; Parker, G.; Lanfredi, N. W.; Perillo,
    G. M. E.; and Figge, K., 1978. Shoreface-connected
    sand ridges on American and European shelves: a
    comparison. Est. Coast. Mar. Sci. 7:257-273.

Taylor, P. A., and Gent, P. R., 1974. A model of
    atmospheric boundary-layer flow above an isolated
    two-dimensional "hill," an example of flow above
    "gentle topography." Boundary-layer Met. 7:349-362.

Taylor, P. A.; Gent, P. R.; and Keen, J. M. 1976. Some
    numerical solutions for turbulent boundary-layer flow
    above rough wavy surfaces. Geophys. J. R. Astr. Soc.
    44:177-201.

Taylor, P. A., and Dyer, K. R., 1977. Theoretical models
    of flow near the bed and their implications for

sediment transport. In Goldberg, McCave and O'Brien (eds.) The Sea. Wiley Interscience, New York. Vol. 6, pp. 579-601.

Terwindt, J. H. J., 1971. Sand waves in the southern bight of the North Sea. Mar. Geol. 10:51-67.

Townsed, A. A., 1976. The structure of turbulent shear flow. Cambridge Univ. Press, London. 429 pp.

Visher, G. S., 1969. Grain size distributions and depositional processes. J. Sediment. Petrol. 39: 1074-1106.

Vanoni, V. A., 1946. Transportation of suspended sediment by water. Trans. ASCE 111:67-133.

Wells, J. T., 1973. Particle size distribution and small-scale bedforms on sand waves, Chesapeake Bay entrance, Va. MS Thesis, Dept. of Oceanography, Old Dominion Univ., 110 pp.

Wimbush, M., and Munk, W., 1970. The benthic boundary layer. In: Maxwell, A. E. (ed.) The Sea. Wiley-Interscience, New York, Vol. 4,

Yalin, M. S., 1977. Mechanics of sediment transport. Pergamon Press, (2nd ed.). 299 pp.

APPENDIX A

SELECTED COMPUTED PROGRAMS

```
ccccccccccccccccccccccc ccccccccccccccccccccccccccccccc ccccccccccccccc
c                                                                     c
c                        PROGRAM GSIZE.FOR                            c
c                                                                     c
c                        GERARDO M. E. PERILLO.                       c
c                                                                     c
c*********************************************************************c
c                                                                     c
c          PROGRAM GSIZE.FOR WAS DESIGNED FOR DETERMINATICN           c
c          OF STATISTICAL PARAMETERS OF SAND SAMPLES.                 c
c          NOTE : NO PIPPETE DATA WILL BE ANALYZED IN THE             c
c          PRESENT PROGRAM UNLESS THE NECESSARY MODIFICATION ARE       c
c          MADE TO IT.                                                c
c                                                                     c
c*********************************************************************c
c                                                                     c
c                        INPUT DATA                                   c
c                                                                     c
c          DATA MUST BE ENTERED BY A DATA FILE (FILENAME.DAT),        c
c          FILENAME CAN BE ANY UP TO 6 LETTER COMBINATICN             c
c          EXAMPLE : SAMPLE.DAT                                       c
c                                                                     c
c          DATA IN FILENAME.DAT ARE TC BE ARRANGED IN THE FOLLOWINGc
c          ORDER :                                                    c
c                                                                     c
c          LINE 1 : NUMBER OF SAMPLES TO BE ANALYSED.                 c
c          LINE 2 : SMALLEST SIEVE VALUE THRU WHICH ALL SEDIMENT      c
c                   HAVE PASSED, SIEVE INTERVAL USED                  c
c                   (I.E.: -1.25 0.25)                                c
c          LINE 3 : FIRST SAMPLE NUMBER. IT CAN BE ANY COMBINATION c
c                   OF UP TO 4 NUMBERS AND LETTERS (I.E.: G039)       c
c          LINE 4 : WEIGHT BEFORE WET SIEVE, WEIGHT AFTER WET SIEVEc
c                   WEIGHT BEFORE HCL, WEIGHT AFTER HCL, DEPTH,       c
c                   TYPE OF SAMPLE, MAXIMUN GRAIN.                    c
c                   (I.E.: 657.32 638.45 10.0 9.46 12.24 1 2.4)      c
c                   NOTE : IF CARBONATE ANALYSIS WAS NOT PERFORMED c
c                          ENTER 0. 0. IN THE PLACE WBHCL WAHCL       c
c                          DEPTH IS RECOMENDED IN METERS             c
c                          IF NO SAMPLE TYPE ENTER 0                 c
c                          IF NO MAXIMUN GRAIN, ENTER 0.             c
c          LINE 5 : WEIGHT FOR SIEVES 1 TO 8                         c
c          LINE 6 : WEIGHT FOR SIEVES 9 TO 13                        c
c          LINE 7 : WEIGHT FOR SIEVES 14 TO END                     c
c          LINE 8 AND SO ON : REPEAT LINES 3 TO 7 AS MANY TIMES AS c
c                   SAMPLES TO BE ANALYSED.                          c
c                                                                     c
c*********************************************************************c
c                                                                     c
c                        OUTPUT DATA                                  c
c                                                                     c
c          OUTPUT INFORMATION IS GIVEN IN A TABULATED SELF-EXPLANA-c
c          TORY FORM, FROM LINE PRINTER.                             c
c          AS AN OPTION THE SUBROUTINE CUMPLT.FOR PLOT A CUMULATIVEc
c          CURVE IN ARITHMETIC SCALE. WHEN RUNNING, THE PROGRAM      c
c          WILL ASK FOR PLOT.                                        c
c                                                                     c
c          INDIVIDUAL PERCENTAGE MAY BE OUTPUT IN FILE FERC.OUT       c
c                                                                     c
c          FOLK GRAPHIC PARAMETERS MAY BE OUTPUT IN FILE FOLK.OUT     c
c          THE DATA CAN BE USED TC PLOT IN THE VARIAN PLOTTER.        c
```

```
C                                                                   C
C          GENERAL PERCENTAGES (GRAVEL, ALL SIZES OF SANDS, AND     C
C          SILT/CLAY) ARE OUTPUT IN FILE GEPERC.TXT.                C
C                                                                   C
C*******************************************************************C
C                                                                   C
C              LIST VARIABLES                                       C
C                                                                   C
C          N : INTEGER, NUMBER OF SAMPLES.                          C
C          PHIMIN : REAL, PHI SIEVE VALUE THRU WHICH ALL SEDIMENT   C
C                   HAVE PASSED                                     C
C          DELPHI : REAL, PHI INTERVAL BETWEEN SIEVES              C
C          SIEVE : REAL, PHI SIEVE VALUES. PAN = 5.                C
C          SN : ALFANUMERIC (1A4), SAMPLE NUMBER                   C
C          DEPTH : REAL, DEPTH IN METERS AT WHICH SAMPLE WAS OBTAI-C
C                   NED. IF SAMPLE WAS OBTAINED ABOVE SEA LEVEL,EN- C
C                   TER 0.0.                                        C
C          WBWS : REAL, WEIGHT OF TOTAL SAMPLE BEFORE WET SIEVE    C
C          WAWS : REAL, WEIGHT OF TOTAL SAMPLE AFTER WET SIEVE     C
C          WBHCL : REAL, WEIGHT OF SAMPLE BEFORE HCL.              C
C          WAHCL : REAL, WEIGHT OF SAMPLE AFTER HCL.               C
C          WIND : REAL, WEIGHT OF SEDIMENT RETAINED IN EACH INDIVI-C
C                   DUAL SIEVE.                                     C
C          IPHI : INTEGER, TOTAL NUMBER OF SIEVES, INCLUDES PHIMIN C
C                   AND PAN.                                        C
C          WACC : REAL, ACCUMULATIVE WEIGHT.                       C
C          PIND : REAL, PERCENTAGE OF WIND.                        C
C          PACC : REAL, PERCENTAGE OF WACC.                        C
C          HALFI : REAL, MIDPOINT FOR EACH CLASS INTERVAL. PAN =   C
C                   4.5                                             C
C          XMME : REAL, MOMENT MEAN.                               C
C          SDEV : REAL, MOMENT STANDARD DEVIATION.                 C
C          SK : REAL, MOMENT SKEWNESS.                             C
C          KG : REAL, MOMENT KURTOSIS.                             C
C          FMZ : REAL, FOLK'S GRAPHIC MEAN.                        C
C          FSD : REAL, FOLK'S GRAPHIC STANDARD DEVIATION.          C
C          FSK : REAL, FOLK'S SKEWNESS.                            C
C          FKG : REAL, FOLK'S KURTOSIS.                            C
C          JTY : INTEGER, TYPE OF SAMPLE.                          C
C          GLEN : REAL, INTERMEDIATE DIAMETER OF MAXIMUM GRAIN, IN C
C                   MILLIMETERS.                                    C
C                                                                   C
CCCCCCCCCCCCCCCCCCCCCCCCCCCCCCCCCCCCCCCCCCCCCCCCCCCCCCCCCCCCCCCCCCCCC
C
          DIMENSION PHI(10), WIND (40), WACC(40), PIND(40),
       *           PACC(40), PFOL(10), HALFI(40), FW(40),
       *           SIEVE(40), SN(1)
          INTEGER OPT, OPT2, OPT3, OPT4
          REAL KG
          DATA PFOL /1.,5.,16.,25.,35.,50.,65.,75.,84.,95./
          JOUT1 = 23
          JOUT2 = 1
          JOUT3 = 24
C
C...      READ GENERAL INFORMATION
C
          TYPE 5
5         FORMAT(//5X,'ENTER OPTION FOR CUMULATIVE CURVE'/
       *  5X,'ENTER : 1 FOR YES, 0 FOR NO')
          ACCEPT *, OPT
```

```
           TYPE 10
   10      FORMAT (/5X,'ENTER OPTION FOR INDIVIDUAL PERCENTAGE'/
         * 5X,'OUTPUT. 0 = NO, 1 = YES')
           ACCEPT *, OPT2
           TYPE 15
   15      FORMAT (/5X,'ENTER OPTION FOR FOLK PARAMETERS'/
         * 5X,'OUTPUT. 0 = NO, 1 = YES')
           ACCEPT *, OPT3
           TYPE 20
   20      FORMAT (/5X,'ENTER OPTION FOR GENERAL PERCENTAGES'/
         * 5X,'0 = NO, 1 = YES')
           ACCEPT *, OPT4
           TYPE 25
   25     'FORMAT ('OFILE SPECS FOR DATA FILE (UNIT = 20,
         * EXAMPLE <SAMPLE.DAT>')
           OPEN (UNIT = 20, ACCESS = 'SEQIN', MODE = 'ASCII',
         * DIALOG)
           READ (20,*) N
           READ (20,*) PHIMIN,DELPHI
   C
   C...     CALCULATE PHI INTERVALS
   C
           DO 30 I = 1,40
           DEL = (I - 1) * DELPHI
           SIEVE(I) = PHIMIN + DEL
           IF (SIEVE(I) .EQ. 4.) GO TO 35
   30      CONTINUE
           GO TO 50
   35      IPHI = I + 1
           SIEVE(IPHI) = 5.
   C
   C...     READ INDIVIDUAL SAMPLE INFORMATION
   C
           IF (OPT2 .EQ. 0) GO TO 40
           OPEN (UNIT = JOUT1, ACCESS = 'APPEND', FILE = 'PERC.TXT')
   40      IF (OPT3 .EQ. 0) GO TO 45
           OPEN (UNIT = JOUT2, ACCESS = 'APPEND', FILE = 'FOLK.TXT')
           WRITE (JOUT2,*) N
   45      IF (OPT4 .EQ. 0) GO TO 50
           OPEN (UNIT = JOUT3, ACCESS = 'APPEND', FILE = 'GENPRC.TXT')
   C
   50      SUMPE = 0.0
           SUSD = 0.0
           DO 595 NN = 1,N
           READ (20,55) SN
   55      FORMAT (1A4)
           READ (20,*) ARNS, WINS, W3HCL, WAHCL,DEPTH, JTN,CLEN
           READ (20,*) (WIND(I), I = 1,8)
           IF (IPHI .EQ. 8) GO TO 60
           READ (20,*) (WIND(I), I = 9,13)
           IF (IPHI .EQ. 13) GO TO 60
           READ (20,*) (WIND(I), I=14,IPHI)
   C
   C...     CALCULATE ACCUMULATIVE AND TOTAL WEIGHT
   C
   60      WACC(1) = 0.0
           DO 65 I = 2,IPHI
           WACC(I) = WACC(I-1) + WIND(I)
   65      CONTINUE
           TOTAL = WACC(IPHI)
```

```
C
C...      CALCULATE INDIVIDUAL AND ACCUMULATIVE
C...      PERCENTAGES
C
          PACC(1) = 0.0
          PIND(1) = 0.0
          DO 70 I = 2,IPHI
          PINP(I) = (WIND(I) * 100.)/TOTAL
          PACC(I) = PACC(I-1) + PIND(I)
70        CONTINUE
C
C...      HALF POINT AND MOMENT MEAN CALCULATION
C
          HALFI(1) = 0.0
          SUMFW = 0.0
          DO 75 I = 2,IPHI
          HALFI(I) = (SIEVE(I) + SIEVE(I-1))/2.
          FW(I) = HALFI(I) * WIND(I)
          SUMFW = SUMFW + FW(I)
75        CONTINUE
          XMME = SUMFW/TOTAL
          SUMME = SUMME + XMHE
C
C...      PRINT GENERAL INFORMATION AND
C...      TABLE OF WEIGTHS AND PERCENTAGES
C
          WRITE (3,80)
80        FORMAT ('1',//,9X,'OLD DOMINION UNIVERSITY'/
     *    8X,'DEPARTMENT OF OCEANOGRAPHY'/5X,'GRAIN-SIZE
     *    ANALYSIS (STATISTICS)')
          WRITE (3,85) SN,DEPTH,GLEN
85        FORMAT(//5X,'SAMPLE : ',I14,5X,'DEPTH = ',F6.2,2X,'M',
     *    4X,'MAXIMUM GRAIN = ',F5.2,2X,'MM')
          WRITE (3,90)
90        FORMAT (//25X,'SIEVE DATA ONLY'//
     *    12X,'PHI CLASS',15X,'WEIGHT',13X,'PERCENTAGE')
          WRITE (3,95)
95        FORMAT (/3X,'N',5X,'SIEVE',3X,'MIDPOINT',2(6X,'INDIV.',
     *    4X,'ACCUM.'))
          DO 105 I = 1,IPHI
          WRITE (3,100) I, SIEVE(I),HALFI(I),WIND(I),WACC(I),
     *    PIND(I),PACC(I)
100       FORMAT (2X,I2,2(4X,F6.3),2(6X,F6.3,4X,F7.3))
105       CONTINUE
C
C...      OUTPUT INDIVIDUAL PERCENTAGE IN FILE PERC.TXT
C...      IF OPTION OF I2 = 1
C
          IF (OPT2 .EQ. 0) GO TO 115
          II = IPHI - 1
          WRITE (JOUT1,110) JTY,SN, (PIND(I), I = 2,II)
110       FORMAT (1X,I1,A4,21F6.3)
C
C...      PLOT CUMULATIVE PERCENT CURVE IN
C...      ARITHMETIC SCALE IF OPTION = 1
C
115       IF (OPT .EQ. 0) GO TO 120
          CALL CUMPLT (PACC,IPHI,SN,SIEVE)
C
C...      INTERPOLATION OF PHI VALUES FOR
```

```
C...      FOLK PARAMETEPS
C
120       DO 135 I = 1,10
          DO 125 J = 1,IPHI
          IF (PACC(J) .LE. PFOL(I)) NJ = J
          IF (PACC(J+1) .GT. PFOL(I)) GO TO 130
125       CONTINUE
130       NJ1 = NJ + 1
          DELY1 = PACC(NJ1) - PACC(NJ)
          DELY2 = (PACC(NJ1) - PFOL(I)) * SIEVE(NJ)
          DELY3 = (PFOL(I) - PACC(NJ)) * SIEVE(NJ1)
          PHI(I) = (DELY2 + DELY3)/DELY1
135       CONTINUE
C
C...      PRINT PHI VALUES
C
          WRITE (3,140)
140       FORMAT (//5X,'PHI VALUES FOR GRAPHIC MEASURES')
          WRITE (3,145)
145       FORMAT (//7X,'PHI',5X,'PERCENTAGE'/)
          DO 155 I = 1,10
          WRITE (3,150) PFOL(I), PHI(I)
150       FORMAT (7X,F3.0,6X,F7.4)
155       CONTINUE
C
C...      CALCULATE FOLK INCLUSIVE GRAPHIC
C...      STATISTICAL PARAMETERS
C
          FMZ = (PHI(3) + PHI(6) + PHI(9))/3.
          D8416 = PHI(9) - PHI(3)
          D955 = PHI(10) - PHI(2)
          D7525 = PHI(8) - PHI(4)
          FSD = (D8416/4.) + (D955/6.6)
          DPHI = PHI(6) * 2.
          SK1 = PHI(3) + PHI(9) - DPHI
          SK2 = PHI(2) + PHI(10) - DPHI
          FSK = SK1/(2. * D8416) + SK2 /(2. * D955)
          FKG = D955/(2.44 * D7525)
          QD = D7525 /2.
C
C...      CALCULATE MOMENT STATISTIC PARAMETERS
C
          SUMDE2 = 0.0
          SUMSK = 0.0
          SUMKG = 0.0
          DO 160 I = 1,IPHI
          DELTA = HALFI(I) - XMME
          DEL2 = DELTA * DELTA
          DEL3 = DELTA * DEL2
          DEL4 = DELTA * DEL3
          SUMDE2 = SUMDE2 + DEL2 * WIND(I)
          SUMSK = SUMSK + DEL3 * WIND(I)
          SUMKG = SUMKG + DEL4 * WIND(I)
160       CONTINUE
          SDEV1 = SUMDE2/TOTAL
          SDEV = SQRT(SDEV1)
          SDEV3 = SDEV1 * SDEV
          SDEV4 = SDEV1 * SDEV1
          SK = SUMSK/(TOTAL * SDEV3)
          KG = SUMKG/(TOTAL * SDEV4)
```

```
               SUSD = SUSD + SDEV
C
C...      PRINT GRAPHIC AND MOMENT STATISTIC PARAMETERS
C
          WRITE (3,165) SN
165       FORMAT ('1',////5X,'SAMPLE = ',1A4)
          WRITE (3,170)
170       FORMAT (/////16X,'STATISTIC PARAMETERS (SIEVE DATA)')
          WRITE (3,175)
175       FORMAT (/12X,'GRAPHIC',3X,'MOMENT',9X,'GENERAL')
          WRITE (3,180) FMZ, XMME, PHI(6)
180       FORMAT (/2X,'MEAN',6X,F7.4,2X,F7.4,5X,'MEDIAN',5X,
         *  F7.4)
          WRITE (3,185) FSD, SDEV, QD
185       FORMAT (/2X,'STD. DEV.',F8.4,2X,F7.4,5X,'QUAR. DEV.',
         *  F8.4)
          WRITE (3,190) FSK, SK
190       FORMAT (/,2X,'SKEWNESS',2(2X,F7.4))
          WRITE (3,195) FKG, KG
195       FORMAT (/2X,'KURTOSIS',2(2X,F7.4))
C
C...      OUTPUT FOLK STATISTIC PARAMETERS IN FILE
C...      FOLK.TXT, IF OPTION OPT3 = 1
C
          IF (OPT3 .EQ. 0) GO TO 205
C
          WRITE (JOUT2,200) JTY,SN,FMZ,FSD,FSK,FKG,XMME,CD,GLEN
200       FORMAT (1X,I1,1X,A4,7(1X,F8.4))
C
C...      CALCULATE SEDIMENT CHARACTERISTICS
C
C...      PERCENTAGE OF GRAVEL, SAND AND SILT-CLAY (MUD) OF
C...      TOTAL SAMPLE
C
205       WPER = 100./WFWS
          WSC1 = WBWS - WAWS
          WSC2 = (WIND(IPHI) * WAWS)/TOTAL
          WSC = WSC1 + WSC2
          PSC = WSC * WPER
          WGR = 0.0
          WVCS = 0.0
          WCS = 0.0
          WMS = 0.0
          WFS = 0.0
          WVFS = 0.0
          III = IPHI - 1
          DO 265 I = 1, III
          IF (SIEVE(I) + 1.) 210,210,215
210       WGR = WGR + WIND(I)
          GO TO 265
215       IF (SIEVE(I)) 220,220,225
220       WVCS = WVCS + WIND(I)
          GO TO 265
225       IF (SIEVE(I) - 1.) 230,230,235
230       WCS = WCS + WIND(I)
          GO TO 265
235       IF (SIEVE(I) - 2.) 240,240,245
240       WMS = WMS + WIND(I)
          GO TO 265
245       IF (SIEVE(I) - 3.) 250,250,255
```

```
250       WFS = WFS + WIND(I)
          GO TO 265
255       IF (SIEVE(I) - 4.) 260,260,270
260       WVFS = WVFS + WIND(I)
265       CONTINUE
270       WGRS = (WGR * WAWS)/TOTAL
          PGR = WGRS * WPER
          WSAND = WVCS + WCS + WMS + WFS + WVFS
          WSA2 = (WSAND * WAWS)/TOTAL
          PSAND = WSA2 * WPER
          PPSA = 100./WSAND
          PVCS = WVCS * PPSA
          PCS = WCS * PPSA
          PMS = WMS * PPSA
          PFS = WFS * PPSA
          PVFS = WVFS * PPSA
          WRITE (3,275)
275       FORMAT (//12X,'SAND SIZE PERCENTAGES'/2X,'V. COARSE',
         * 2X,'COARSE',2X,'MEDIUM',3X,'FINE',3X,'V. FINE')
          WRITE (3,280) PVCS, PCS, PMS, PFS, PVFS
280       FORMAT (/1X,2(3X,F6.3),3(2X,F6.3))
          WRITE (3,285)
285       FORMAT (///6X,'GRAPHIC-STATISTIC VALUES INDICATE
         * THAT THE SAMPLE IS :')
C
C...      DETERMINATION OF STANDARD DEVIATION
C
          IF (FSD - .35) 315,320,290
290       IF (FSD - .50) 320,325,295
295       IF (FSD - .71) 325,330,300
300       IF (FSD - 1.0) 330,335,305
305       IF (FSD - 2.0) 335,340,310
310       IF (FSD - 4.0) 340,345,345
315       WRITE (3,355)
          GO TO 350
320       WRITE (3,360)
          GO TO 350
325       WRITE (3,365)
          GO TO 350
330       WRITE (3,370)
          GO TO 350
335       WRITE (3,375)
          GO TO 350
340       WRITE (3,380)
          GO TO 350
345       WRITE (3,385)
350       CONTINUE
C
355       FORMAT (/10X,'VERY WELL SORTED')
360       FORMAT (/10X,'WELL SORTED')
365       FORMAT (/10X,'MODERATELY WELL SORTED')
370       FORMAT (/10X,'MODERATELY SORTED')
375       FORMAT (/10X,'POORLY SORTED')
380       FORMAT (/10X,'VERY POORLY SORTED')
385       FORMAT (/10X,'EXTREMELY POORLY SORTED')
C
C...      DETERMINATION OF SKEWNESS
C
          IF (FSK - 1.0) 390,435,440
390       IF (FSK - 0.3) 395,430,435
```

```
395     IF (FSK - 0.10) 400,425,430
400     IF (FSK + 0.10) 405,420,425
405     IF (FSK + 0.30) 410,415,420
410     IF (FSK + 1.0) 440,415,415
415     WRITE (3,450)
        GO TO 445
420     WRITE (3,455)
        GO TO 445
425     WRITE (3,460)
        GO TO 445
430     WRITE (3,465)
        GO TO 445
435     WRITE (3,470)
        GO TO 445
440     WRITE (3,475)
445     CONTINUE
C
450     FORMAT (/10X,'STRONGLY COARSE SKEWED')
455     FORMAT (/10X,'COARSE SKEWED')
460     FORMAT (/10X,'NEAR SYMMETRICAL')
465     FORMAT (/10X,'FINE SKEWED')
470     FORMAT (/10X,'STRONGLY FINE SKEWED')
475     FORMAT (/10X,'VERY STRONGLY SKEWED, SOME ERROR IN DATA')
C
C...    DETERMINATION OF KURTOSIS
C
        IF (FKG - .67) 500,505,480
480     IF (FKG - .90) 505,505,485
485     IF (FKG - 1.11)510,510,490
490     IF (FKG - 1.50) 515,515,495
495     IF (FKG - 3.0) 520,520,525
500     WRITE (3,535)
        GO TO 530
505     WRITE (3,540)
        GO TO 530
510     WRITE (3,545)
        GO TO 530
515     WRITE (3,550)
        GO TO 530
520     WRITE (3,555)
        GO TO 530
525     WRITE (3,560)
530     CONTINUE
C
535     FORMAT (/10X,'VERY PLATYKURTIC ')
540     FORMAT (/10X,'FLATYKURTIC ')
545     FORMAT (/10X,'MESOKURTIC ')
550     FORMAT (/10X,'LEPTOKURTIC ')
555     FORMAT (/10X,'VERY LEPTOKURTIC ')
560     FORMAT (/10X,'EXTREMELY LEPTOKURTIC ')
C
C...    CALCULATE AND PRINT PERCENTAGE OF CARBONATE (AS CALCIUM
C...    CARBONATE) IN SAND
C
        IF (WRHCL .EQ. 0.) GO TO 570
        PCAR = ((WRHCL - WAHCL) * 100.)/WRHCL
        WRITE (3,565) PCAR
565     FORMAT (/2X,'% CARBONATE (AS CALCIUM
       * CARBONATE) IN SAND = ',F7.3)
C
```

```
C...      PRINT GRAVEL, SAND AND MUD PERCENTAGES
C
570       WRITE (3,575)
575       FORMAT (///25X,'TOTAL SAMPLE')
          WRITE (3,580) PGR, PSAND, PSC
580       FORMAT (/5X,'% GRAVEL = ',F7.3,3X,'% SAND = ',
     *    F7.3,3X,'% SILT-CLAY = ',F7.3)
C
C...      CALCULATE GENERAL PERCENTAGES IF OPT4 = 1
C
          IF (OPT4 .EQ. 0) GO TO 595
          TS = PSAND/WSAND
          TVCS = WVCS * TS
          TCS = WCS * TS
          TMS = WMS * TS
          TFS = WFS * TS
          TVFS = WVFS * TS
          WRITE (JOUT3,*) PGR,TVCS,TCS,TMS,TFS,TVFS,PSC
          WRITE (3,585)
585       FORMAT (//2X,'GRAVEL',2X,'V. COARSE',2X,'COARSE',2X,'MEDIUM',
     *    3X,'FINE',2X,'V. FINE',2X,'SILT-CLAY')
          WRITE (3,590) PGR,TVCS,TCS,TMS,TFS,TVFS,PSC
590       FORMAT (//2X,F6.3,1X,2(3X,F6.3),2(2X,F6.3),2X,F6.3,3X,F6.3)
595       CONTINUE
C
C...      CALCULATE AND PRINT AVERAGE MOMENT MEAN AND
C...      STANDARD DEVIATION OF TOTAL SAMPLES ANALYZED
C
          AVME = SUMME/N
          AVSD = SUSD/N
          WRITE (3,600) N, AVME, AVSD
600       FORMAT (//5X,'NUMBER OF SAMPLES = ',I9/5X,'AVERAGE OF
     *    MEANS = ',F13.3,/5X,'AVERAGE OF STD. DEVIATIONS = ',F7.3)
          STOP
          END
```

```
          SUBROUTINE CUMPLT (A,NN,AN,PHO)
          DIMENSICN A(30), PHC(30),FREY(30),
      *            PHIX(30), AN(2)
          CALL PLOTS (IJK)
          CALL PLOT (0.,-11.,-3)
          CALL PLOT (0.,2.,-3)
C
C...   START AXIS
C
          CALL PLOT (0.,6.5,3)
          CALL PLCT (0.,0.,2)
          CALL PLOT (7.5,0.,2)
          CALL PLOT (0.,0.,3)
C
C...   GRAPHIC THE TICK MARKS IN X-AXIS
C
          DO 5 I = 1,6
          X = I * 1.1667
          Y = -0.1
          CALL PLCT (X,0.,3)
          CALL PLOT (X,Y,2)
5         CONTINUE
C
C...   GRAPH TICK MARKS IN Y - AXIS
C
          CALL PLOT (0.,0.,3)
          DO 10 I = 1,10
          Y = I * .6
          X = -0.1
          CALL PLOT (0.,Y,3)
          CALL PLOT (X,Y,2)
10        CONTINUE
C
C...   GRAPH NUMBERS IN X AND Y AXIS
C
          CALL PLOT (0.,0.,3)
          DO 15 I = 1,6
          PRRY = 20. * I - 20.
          X = -0.5
          Y = 1.2 * (I - 1)
          CALL PLOT (X,Y,3)
          CALL NUMBER (X,Y,0.125,PRRY,0.,-1)
15        CONTINUE
          CALL PLOT (0.,0.,3)
          DO 20 I = 1,7
          PHI = I - 3.
          Y = -0.375
          X = (I - 1) * 1.1667
          CALL PLOT (X,Y,3)
          CALL NUMBER (X,Y,0.125,PHI,0.,-1)
20        CONTINUE
          CALL SYMBOL (.5,5.8,.17,7HSAMPLE ,0.,7)
          CALL SYMBOL (1.8,5.8,.17,AN,0.,4)
          CALL SYMBOL (2.5,6.7,.2,18HCUMULATIVE PERCENT,0.,18)
          CALL SYMBOL (3.5,6.4,.12,12H(SIEVE DATA),0.,12)
          CALL SYMBOL (-.65,6.35,.2,3HPCT,0.,3)
          CALL SYMBOL (7.25,-.5,.2,3HPHI,0.,3)
C
C...   SCALE FACTORS
C
```

```
        NT = NN - 1
        DO 25 I = 2,NT
        PREY(I) = A(I) * .06
        PHIX(I) = PHC(I) * 1.1667 + 2.3334
25      CONTINUE
C
C
        CALL PLOT (0.,0.,3)
        DO 35 I = 2,NT
        CALL PLOT (PHIX(I),PREY(I),2)
35      CONTINUE
        CALL PLOT (0.,0.,3)
        CALL PLOT (10.,0.,-3)
        RETURN
        END
```

AUTOBIOGRAPHICAL STATEMENT

GERARDO MIGUEL EDUARDO PERILLO

BORN:

29 January 1951, Buenos Aires, Argentina.

EDUCATION:

Bachiller, Colegio Nacional Julio A. Roca, Buenos
Aires, Argentina, December 1967.

Licenciado en Ciencias Geologicas, Universidad de
Buenos Aires, Buenos Aires, Argentina, August 1975.

APPOINTMENTS AND POSITIONS:

Teaching and Research Assistant, Departamento de
Geologia, Universidad de Buenos Aires, Argentina,
1972-1973.

Assistant Investigator, Servicio de Hidrografia Naval,
Buenos Aires, Argentina, 1974 to present.

Pro-Secretary, National Advising Committee of Inter-
national Association for Physical Science of the
Ocean (IAPSO), 1976-1978.

Editor of Acta Oceanographica Argentina, 1978.

Teaching Assistant, Departmento de Geologia,
Universidad de Buenos Aires, Argentina, 1978.

SELECTED PUBLICATIONS:

Perillo, G.M.E., 1975. Rasgos geologicos y geomor-
fologicos de los sectores continental, litoral y
maritimo del area comprendida entre Mar de Ajo y
Pinamar, Provincia de Buenos Aires. Thesis,
Universidad de Buenos Aires.

Swift, D.J.P.; Parker, G.; Lanfredi, N.W.; Perillo,
G.M.E.; and Figge, K., 1978. Shoreface-connected
sandridges on American and European shelves: a
comparison. Est. Coast. Mar. Sc. 7:257-273.

Parker, G.; Perillo, G.M.E.; and Violante, R.A., 1978.
Caracteristicas geologicas de los bancos alineados

(linear shoals) frente a Punta Medanos, Provincia de Buenos Aires. Acta Ocean. Arg. 2:11-50.

Perillo, G. (in press). Calculo del volumen de sedimentos de la playa frontal en el area de Punta Medanos, Provincia de Buenos Aires. Acta Ocean. Arg. 2.

MEMBERSHIP IN PROFESSIONAL SOCIETIES:

Asociacion Geologica Argentina
Consejo Profesional de Geologia
International Association for Physical Sciences
of the Ocean
American Geophysical Union
Sigma Xi
International Association of Mathematical Geology